GA-A--21203

DE93 010836

INERTIAL CONFINEMENT FUSION TARGET COMPONENT FABRICATION AND TECHNOLOGY DEVELOPMENT SUPPORT

ANNUAL REPORT TO THE U.S. DEPARTMENT OF ENERGY

JANUARY 1, 1991 THROUGH SEPTEMBER 30, 1992

by

PROJECT STAFF
David Steinman, editor

Work prepared under
Department of Energy
Contract No. DE-AC03-91SF18601

GENERAL ATOMICS PROJECT 3896
DATE PUBLISHED: MARCH 1993

GENERAL ATOMICS

DISCLAIMER

This report has been reproduced
directly from the best available copy.

Available to DOE and DOE contractors from the
Office of Scientific and Technical Information
P.O. Box 62
Oak Ridge, TN 37831
Prices available from (615) 576-8401,
FTS 626-8401.

Available to the public from the
National Technical Information Service
U.S. Department of Commerce
5285 Port Royal Rd.
Springfield, VA 22161

The 1992 Target Fabrication and Target Technology Development Team

General Atomics
San Diego, California

Neil Alexander, Jan Ankney, Wes Baugh, Chuck Beal, Donald Beighley, Gary Bentley, Gottfried Besenbruch, Bob Bourque, Lloyd Brown, Sharon Considine, Bob Fagaly, Kett Gifford, Ileese Glatter-Schneir, Jose Gomez, Martin Hoppe, David Husband, James Kaae, James Lindgren, Tu Luong, Barry McQuillan, Wayne Miller, Joe Pontelandolfo, John Ruppe, Chuck Schneidmuller, Ken Schultz, Clyde Shearer, John Simpson, David Steinman, Rich Stephens, Don Wall.

W. J. Schafer Associates
Livermore, California

Thomas Alberts, Don Bittner, Frank Carey, Andrea Denton, Barbara Lane, David Diffenderfer, Illes Faron, Charles Hendricks, Cynthia Keller, Michael McClellan, Michael Monsler, Craig Rivers, James Sater, Diana Schroen-Carey, Keith Shillito.

Soane Technologies Inc.
Hayward, California

Emil Asadulla, Sue Bernard, Eben Lilley, Donald Nelson, David Soane, Zoya Soane.

ABSTRACT

On December 31, 1990, the U.S. Department of Energy entered into a contract with General Atomics (GA) to be the Inertial Confinement Fusion (ICF) Target Component Fabrication and Technology Development Support contractor. This report documents the technical activities of the period January 1, 1991 through September 30, 1992. During this period, GA was assigned 15 tasks in support of the Inertial Confinement Fusion program and its laboratories. These tasks included Facilities Activation, Staff Development, and Capabilities Validation to establish facilities and equipment, and demonstrate capability to perform ICF target fabrication research, development and production activities. The capabilities developed and demonstrated are those needed for fabrication and precise characterization of polymer shells and polymer coatings. We made progress toward production capability for glass shells, barrier layer coatings, and gas filling of shells.

We also were asked to provide direct onsite technical and scientific support at Lawrence Livermore National Laboratory (LLNL) and Los Alamos National Laboratory (LANL). We fabricated over 1000 beam diagnostic foil targets for Sandia National Laboratory Albuquerque (SNLA) and provided full-time on-site engineering support for target fabrication and characterization.

We initiated development of methods to fabricate polymer shells by a controlled mass microencapsulation technique, and performed chemical syntheses of several chlorine- and silicon-doped polymer materials for the University of Rochester's Laboratory for Laser Energetics (UR/LLE). We performed the conceptual design of a cryogenic target handling system for UR/LLE that will fill, transport, layer, and characterize targets filled with cryogenic deuterium (DD) or deuterium-tritium (DT) fuel, and insert these cryogenic targets into the OMEGA-Upgrade target chamber for laser implosion experiments.

This report summarizes and documents the technical progress made on these tasks.

TABLE OF CONTENTS

TABLE OF CONTENTS

LIST OF FIGURES

LIST OF TABLES

SECTION 1

TARGET FABRICATION PROGRAM OVERVIEW

1. TARGET FABRICATION PROGRAM OVERVIEW

On December 31, 1990, the U.S. Department of Energy entered into a contract with General Atomics (GA) to be the Inertial Confinement Fusion (ICF) Target Component Fabrication and Technology Development Support contractor. This report documents the technical activities of the period January 1, 1991 through September 30, 1992. GA was assisted by W.J. Schafer Associates (WJSA) and Soane Technologies Inc. (STI) and we have carried out the ICF Target Fabrication tasks as a fully integrated team effort.

1.1. INTRODUCTION

Although GA was assigned responsibility for ICF Target Component Fabrication Support at the end of December 1990, difficulties associated with the protest of this award delayed initiation of work until May 9, 1991. Further contractual and, eventually, legal difficulties between Department of Energy (DOE) and the prior contractor prevented transfer of the government-owned equipment associated with the target fabrication tasks. Thus, FY91 activities were limited to preparation of facilities, development and training of staff, and planning.

FY92 was a transition year for the GA/WJSA/STI team. In December we, in concert with DOE and the ICF laboratories, decided to proceed immediately to achieve full target production capability without the government-owned equipment held by the prior contractor. Through the generous support of the nation's ICF laboratories, we met this goal and we are now poised to fabricate and deliver the majority of the types of targets and target components desired by the ICF program.

This report was prepared using a format meant to highlight the technical achievements of the GA/WJSA/STI team as well as to show compliance with the task descriptions specified by the contract. The first section presents a task-by-task summary and briefly describes task accomplishments and status. The remaining sections provide the technical details of the work undertaken to fulfill the task statements and are organized by technical topic rather than by task.

1.2. FY92 TASKS SUMMARY

During FY92 the GA/WJSA/STI team was assigned 12 formal tasks.

1.2.1. GA01 FACILITIES ACTIVATION AND GA03 CAPABILITIES VALIDATION

The Facilities Activation and Capabilities Validation Tasks were carried out to acquire equipment and demonstrate target fabrication capability in each of the key technical areas: shells, coatings, films and filters, characterization, and tritium and gas fill.

1.2.1.1. SHELL FABRICATION

The ultimate objective of the facility activation and capabilities validation tasks (GA01 and GA03) was to enable the GA/WJSA team to fabricate ICF targets and target components for the National Laboratories. The ability to produce glass and plastic shells is of paramount importance to the fulfillment of this objective. To bring shell production capability on-line, we obtained shell fabrication equipment from a number of sources. Lawrence Livermore National Laboratory (LLNL) provided us with furnaces for use in a glass shell drop tower and a spray dryer for the production of monosized glass precursor particles. The spray dryer may also be used for polyvinyl alcohol (PVA) coating of shells. We fabricated and installed a polystyrene (PS) drop tower based on the design of the LLNL drop tower. We used a new "hot box" design for the PVA coating tower. Additional facilities were dedicated to complex emulsion and controlled mass microencapsulation processing of polymer shells.

Glass Shells. We borrowed three furnaces and a multipoint programmable temperature controller from LLNL and used them to set up a glass shell drop tower. The drop tower is limited to low-temperature melting point glass compositions by the 1500°C temperature limit of the silicon carbide heating elements and, further, by the temperature-dependent life of the quartz process tube. We have purchased ceramic process tubes to permit 1500°C operation at a later date. The glass drop tower is not yet operational, primarily due to problems with the programmable temperature controller. When the controller is fixed, we intend to install a particle feed device we fabricated, which will deliver uniformly sized glass precursor particles one at a time into the glass shell drop tower.

We also borrowed from LLNL a spray dryer to use in the preparation of monosized glass precursor particles. The dryer is fully operational using the stock droplet nozzle; however, this nozzle forms particles too small for use in glass shell production. To overcome this limitation, we designed and fabricated a drop-on-demand generator which will supply the correct sized drops to the spray dryer. The spray dryer has also been used for a proof-of-principle experiment in which PVA has been coated on small metal spheres.

Polymer Shells. We modified the PS drop tower from the LLNL design to reduce thermal convection at the top of the hot tower. The droplet generation region is separated from the hot tower by an insulated 2 in. diameter tube. The tower is operated with a slight temperature gradient, decreasing from top to bottom, so as to further minimize thermal convection.

The PS drop tower is fully operational, routinely producing high quality shells made from either pure polystyrene or a blend of polystyrene with polychlorostyrene. These shells have passed capabilities validation as required by the task description.

The complex emulsion microencapsulation (CEME) process uses standard laboratory equipment. We have set up laboratories for both the production of shells and the development of the CEME process. We now routinely produce target-quality shells using the CEME process, and this capability has been validated by the University of Rochester's Laboratory for Laser Energetics (UR/LLE).

A large part of the CEME effort was spent in identifying the PVA content inside the shells. We reduced the PVA content in the shells by reducing the quantity of PVA in the bath from 5 % down to 0.05 %. We optimized the process temperature by ramping it up from 70° to 78.6°C during the process. This temperature ramp regime gave a steadily increasing temperature (to limit vacuole formation via temperature fluctuations), while seeking to remain below the boiling point of the solvents (which also may cause vacuoles). We found the process could be used with a combination of benzene plus 1,2-dichloroethane solvents for polystyrene (the UR/LLE solvent system), or by a single solvent of fluorobenzene. Fluorobenzene has a boiling point near that of benzene or 1,2-dichloroethane and has a matching density of 1.02 g/cc. We found no significant difference between spheres made from fluorobenzene, as opposed to those made with benzene plus 1,2-dichloroethane.

We built additional facilities dedicated to the development of the controlled mass microencapsulation (CMME) process and constructed a CMME test apparatus for use in studying the process. This is described further under Task GA05.

Barrier Layer Coating. We designed the PVA coating tower using a "hot box" concept. Each vertical zone of the tower is in a separate electrically heated box containing a fan to ensure that the air temperature is uniform. This design prevents hot spots on the wall which lead to thermal convection and loss of product to the walls of the process tube. Completion of the PVA tower awaits delivery of the process tube.

1.2.1.2. COATINGS, FILMS AND FILTERS

GDP Coatings. The objective of this task was to develop the capability to deposit glow discharge polymerization (GDP) coatings and then to coat shells and submit them to LLNL for validation of this capability. To this end, Jan Ankney spent four months at LLNL becoming familiar with the GDP process. At GA, she and Clyde Shearer assembled a coater that was an exact copy of the LLNL design. We were helped in this effort by the loan of unused coater components from Los Alamos National Laboratory (LANL) and a helical resonator from LLNL.

Parylene Coatings. The objective of this task was to design and build a parylene coating system that can be routinely used to coat various types of targets with specified thicknesses of parylene of specified compositions. An additional goal was to validate the operation of the parylene coater by depositing coatings on flat substrates. In progressing toward these objectives, we completed and costed a design of a coater with the basic capabilities to deposit parylene coatings. The required components for this coater were either purchased, obtained on loan from the National Laboratories, or acquired from the limited government furnished equipment (GFE) released from the prior contractor. Assembly of the coater was completed in the new WJSA laboratory in early September and shake down experiments were concluded with the deposition of parylene on flat substrates.

Films and Filters. The objective of this task was to utilize existing GA capabilities to fabricate films and filters of the types employed by Sandia National Laboratory (SNL) and to supply samples to SNL for validation. Previously, vacuum evaporation had been employed for this application. The GA equipment employs cathodic sputtering, but this was not expected to make any difference in the quality of the deposited films. Tom Alberts, a

WJSA scientist/engineer who worked on films and filters for the prior contractor, spent several weeks at GA transferring expertise in handling and mounting of films to GA. Mylar-backed gold foils were submitted to SNL for validation in September 1991; free-standing gold foils were submitted to SNL for validation in January 1992; and free-standing aluminum foils were submitted to SNL for validation in June 1992. SNL validated the first two of these foils in FY92, but validation of free-standing aluminum foils was not completed before the end of the fiscal year.

Work was also carried out on the deposition of free-standing titanium foils, but this effort did not reach the stage where foils could be submitted for validation. We had also planned to work on the fabrication of parylene-backed tin foils, but no work was done in this area, mainly because the coater was not available for three months and because fabrication of Mylar-backed gold foils was given a higher priority at SNL's request.

During 1992, Tom Alberts was relocated to SNL to supply fabrication support. This support consisted of coordinating deliveries and specifications between experiments at SNL and the production facilities at GA as well as fabricating and characterizing additional films and filters using resources available at SNL.

1.2.1.3. CHARACTERIZATION

The objective of the facility activation task with respect to characterization was to set up work stations to perform target selection and assembly activities; to set up characterization systems (i.e., optical microscopy, SEM, EDXS, micro-Raman and IR spectroscopy, X–ray radiography, XRF, and α-particle spectroscopy); and to write procedures both for calibration against standards and for characterization of desired materials.

A major impediment to this goal was the lack of access to most of the GFE from the prior contractor. However, by making use of the limited GFE, purchasing several high-quality compound microscopes, and borrowing equipment from the National Laboratories we have been able to meet this goal.

Characterization Equipment. We have set up five stereozoom microscopes and a compound microscope for noncritical shell inspections and manipulations. Handling and washing jigs, and shipping containers have been acquired.

We have set up five optical characterization work stations capable of detailed shell analysis. Three of these stations include interference microscopes for dimensional and uniformity measurements. Two of the stations have phase contrast microscopes for inspecting wall and surface defects. All have either polaroid film or CCD cameras attached for documentation. The GA microscope cameras are also linked to networked computers for ease of data collection and access. We have NIST-traceable magnification standards and have verified the band pass of all the interference filters. We have two Nikon microscopes, one of which has long working distance objectives to enable focusing on the bottom of large shells (up to 2000 μm in diameter). We have a Jenavert interference microscope that can measure shell walls up to 15 μm thick and a Zeiss "Universal" which can measure walls up to 70 μm thick. The microscopes at the GA facility will be installed in Class 100 clean work areas; the hoods have been ordered but have not yet arrived.

We have two Cambridge scanning electron microscopes (SEMs), one belonging to GA with elemental analysis capability and one at WJSA borrowed from LLNL, for high resolution characterization of shell surfaces. The LLNL SEM was moved to temporary storage while the WJSA laboratory was being built; reassembly has begun, but was not finished in FY92.

We have used a micro-Raman spectrometer belonging to GA to identify chemical deposits inside microencapsulation shells. It was moved to temporary storage while the GA laboratory was being built; reassembly was begun but not finished in FY92.

A GA-owned atomic force microscope (AFM) was installed in GA's SEM lab, and ICF personnel have been trained in its use. It gives quantitative roughness measurements of small patches of shell surfaces with nanometer resolution.

Characterization Procedures. The lack of access to the GFE required creative solutions to develop and verify measurement procedures to satisfy the statement of work. WJSA personnel working with the Zeiss interference microscope were trained in o.d., non-concentricity, and wall thickness measurements by experienced operators. GA personnel, working on quite different instruments, developed similar procedures to provide process development feedback to the shell fabrication groups.

Early in the year, we selected and characterized a delivery of small glass shells for LLNL. By the end of the year, we had developed, codified, and tested procedures. These

procedures were used to select and characterize shells for microencapsulation, drop tower, and GDP coating capability validation, and for characterization capability validation. Our measurements on all the shells delivered were acceptable to the recipients and met the requirements of the statement of work. We are awaiting the evaluation of the shells we measured for characterization capability validation. Characterization procedures used for deliverables are summarized below.

We measure shell diameters by analyzing the image of the shell observed in transmission on our Nikon microscope, on a computer screen calibrated with an NIST-certified magnification standard. This has proven to be operator independent and reproducible to less than ±1%. We have a systematic difference with LLNL measurements of 0.8% and a systematic difference in the other direction with UR/LLE measurements of 0.7%.

We use the Jenavert in reflection mode to measure the wall thickness of small and large glass shells and bare plastic shells. This instrument and the procedures we use have proven to be operator independent and reproducible to less than ±0.05 μm. Our measurements are within tolerance of those of the National Laboratories.

To measure the coating thickness of composite shells, we immerse the shell in index matching fluid so that we can directly see the inner and outer surfaces of the coating. Measuring the coating thickness at selected points around the circumference and rotating the shell gives coating uniformity. These measurements are reproducible and agree with SEM measurements to within 1 μm.

We use the Zeiss "Universal" in transmission mode to measure the total wall thickness of composite shells. The technique is the same as that for the Jenavert, except that if thicknesses from 35 to 70 μm are to be measured, we have to extend the measurement range of the microscope. This was done by butting together, in the field of view, two cover slips with a thickness difference of about 35 μm and placing the shell on the thinner of the two cover slips. The reproducibility of this technique has not been tested; the phase shifting linkage slips, and it cannot be used for precise measurements until that has been fixed.

We use the Jenavert in reflection mode to measure the nonconcentricity of small and large glass shells and bare plastic shells. For deliverables, we either measure two random views or rotate the shell to the worst view. Our measurements agree with those of the National Laboratories.

We use the Zeiss "Universal" in transmission mode to measure the nonconcentricity of composite shells. We measure the offset of the interference rings in the shell relative to the geometric center of the shell. The coefficient which gives nonconcentricity from offset is being determined from ray-tracing calculations with help from UR/LLE.

The Nikon phase contrast microscope is used to identify shell defects down to submicron sizes. We use GA's Cambridge SEM for overall views of smaller debris, and GA's AFM for quantitative roughness measurements on small areas. All deliverables are examined under the Nikon. We have built jigs and developed techniques for looking at uncoated, unattached deliverables in the SEM, but the hazards and dirt associated with excess handling have made use of witness shells in the SEM and AFM preferable.

1.2.1.4. TRITIUM AND GAS FILL

While GA is currently licensed and has a work authorization to receive and store the tritium and tritium fill equipment in a dedicated room in the Hot Cell facility, the tritium fill equipment will eventually be moved and set up in Room 114, Building 27 (the Radiochemistry Lab). This will be necessary when the Hot Cell is shut down for decontamination and decommissioning. In anticipation of this action, we applied for a license amendment to allow use of 20,300 ci of tritium at any location at GA. The license amendment was granted on October 20, 1992. Authorization for actual operation will be granted in four phases as follows:

- Receipt and storage of the tritium and equipment.
- One or more test runs for deuterium in both glass and plastic microshells.
- One or more test runs for tritium/deuterium application.
- Full operation authorization.

A dedicated room in the Hot Cell facility has been ready for receipt and storage of the tritium and the tritium fill equipment since early in FY92. Modifications made in Room 114 in Building 27 (Radiochemistry Lab) to make it suitable for tritium work included installing a wide door to allow putting the tritium fill equipment into the room without disassembly and upgrading the room's exhaust system.

We estimated the amount of tritiated waste that will be generated after the tritium and tritium fill equipment is received at GA. If the tritium and equipment are received and stored, the amount of waste per year would be in the range of one-half barrel per year for wipes from surveys. If the equipment were to be set up and operated, the amount of waste generated would be increased to one barrel per year.

At DOE's request, GA looked into the types and availability of shipping containers for shipping the four uranium bed tritium containing traps from the prior contractor to GA. The tritium shipping package which seems most suitable is USA/9932/B, Model No. UC-609 designed by LLNL for packaging large quantities of tritium.

Training sessions on the "Safe Handling of Tritium" conducted by Rolin Jalbert of LANL were attended by personnel who will be involved in the tritium and tritium fill station receipt and storage at GA.

In addition to the tritium fill system work, we designed a system for filling polymer shells with up to 200 atmospheres of deuterium at 25°C and glass shells with up to 400 atmospheres of deuterium at 360°C. Components for this system were ordered, most were received, and system assembly has begun. Receipt of the remaining components, assembly of the D_2 fill system, leak testing, proof pressure testing, and a demonstration fill of shells will be completed in early FY93.

1.2.2. GA02 STAFF DEVELOPMENT

The objectives of this task are summarized below:

- To enhance our understanding of current laboratory programs, priorities, capabilities, and requirements through management visits to ICF Laboratories and DOE Headquarters.
- To assign contractor technical personnel to visit ICF Laboratories to obtain technical training and orientation.
- To conduct extended training and development activities as appropriate in preparation for ICF task assignments.

One of our first major activities was to conduct a major recruiting campaign in Ann Arbor, Michigan, in May and June 1991 to capture some expertise and Q-clearances of

personnel from the former contractor. This was successful as we hired ten mid-level scientists and engineers, all of whom had Q clearances.

Our management visits to ICF Laboratories commenced on July 16, 1991, with a trip to the University of Rochester's Laboratory for Laser Energetics. The attendees for the GA/WJSA team were Dr. D. Overskei, Dr. M. Monsler, Dr. K. Schultz, and Dr. C. Hendricks. The meetings were also attended by Mr. D. Neely of DOE-San Francisco and Dr. L. Coleman and Dr. W. Hatcher of LLNL as the lead lab representatives. On the next day, the group traveled to Washington, D.C., to meet with Dr. M. Sluyter and his staff at DOE Headquarters in the morning and with scientists at the Naval Research Laboratory in the afternoon. A second management visit was conducted in August when we visited LANL and Sandia National Laboratory, Albuquerque (SNLA). The trip to LLNL was postponed until June 1992. These management visits were an invaluable introduction into the plans, programs, and current issues of the ICF programs and their target fabrication needs.

Between May and September, 1991, we arranged for several experts to hold technical seminars at GA and WJSA. Experts included Dr. C. Hendricks of WJSA, Prof. Hyo-gun Kim of the University of Rochester, Prof. Kevin Kim of the University of Illinois, and Dr. L. Foreman of LANL. These lectures on target fabrication techniques and the materials science problems that have been addressed and solved were invaluable.

In conjunction with the seminars, directed study and reading assignments were made to the scientists and engineers in the technical areas appropriate to their backgrounds. These assignments culminated in presentations to the rest of the staff on what was learned in each technical area. Also, in August 1991, ICF target fabrication report libraries were created in both the San Diego and Livermore sites.

The Eighth Target Fabrication Specialist Meeting was held at SNLA at the end of September 1991 and was attended by over 20 GA/WJSA staff members. This was a profitable time to learn more detailed techniques from the experts at the ICF Laboratories. Furthermore, many of our staff had their Q-clearances re-established in time to attend the classified sessions. In addition, the few days of meetings were valuable time for our and the ICF laboratories' scientists and engineers to get to know one another and build technical relationships for the future.

There were about 20 individual assignments of GA/WJSA personnel to ICF Laboratories performed from August 1991 through the end of January 1992. During this time, scientists

from our staff visited the University of Rochester to discuss optical characterization techniques and the science and art of microencapsulation. They visited LANL to learn state-of-the-art micromachining, coating technology, cryogenic layering techniques, and the use of spherical interferometry to measure target surfaces. Our scientists and engineers visited LLNL to examine glass drop towers and PVA drying towers, to learn characterization techniques, to evaluate SEM techniques, to learn about computed proton tomography, and proton-induced X–ray emission. At SNLA, we learned techniques to fabricate and use films and filters for PBFA II.

Three of the assignments were of a longer term nature and two of these three turned into technical tasks in their own right in FY92 and FY93. Dr. J. Sater worked at LLNL from October through January 1992 on cryogenic characterization techniques, such as microcalorimetry. Ms. J. Ankney worked October through February 1992 at LLNL to learn the art of GDP coatings. Mr. T. Alberts worked at SNLA from December through January to learn how to fabricate and characterize Mylar-backed gold foils.

In conclusion, we would like to thank the ICF Laboratories for their hospitality and support. The management visits were absolutely essential for learning the plans and programs of laboratories and in building trusting relationships at the management level. The group leaders at the laboratories were extremely helpful in giving of their time for orientation and teaching of our technical staff. Finally, the long-term assignments were productive to both parties in that they provided for a more in-depth learning experience for our staff and were significant in assisting the laboratories in the performance of their tasks.

1.2.3. GA04 CHARACTERIZATION DEVELOPMENT

This task description required that Dr. J. Sater of the GA/WJSA team collaborate with LLNL physicists in the development and characterization of cryogenic layering technology and the use of cryogenics for characterization of Nova targets. He was also to lead the effort to complete LLNL's automatic capsule sorter.

Deliverables for this task included: (1) an analytical model to evaluate the feasibility of using calorimetry to diagnose the fills of opaque Nova targets, (2) definition of system and equipment for calorimetry, (3) a review and rescoping of the automatic capsule sorter project, and (4) provide technical oversight.

Calorimeter. The characterization development task was composed of two parts. Part one involved the study of possible characterization techniques for Nova targets. Specifically, we investigated methods to measure fill pressures of opaque targets. After this study, we decided that a method involving calorimetric measurements on the targets at very low temperatures offered a good probability of success. We decided to proceed with the development of the hardware needed to do this measurement.

We have made good progress towards producing a working calorimeter this year. A cryogenic insert was ordered. It arrived late in the year. A prototype sample holder is currently being fabricated. The necessary vacuum hardware for a cryogenic experiment has been gathered and so has the electronic equipment we will need. This hardware is being assembled and tested. We anticipate that we will complete the calorimeter next year.

Automatic Target Selector (ATS). The ATS project was reviewed, and a clearly defined set of objectives was established. A schedule was established for the completion of the ATS. The conclusions were reviewed by LLNL management, and approval was given to go ahead with the ATS. Dr. Sater started supplying technical oversight to the project and has concluded that it is currently on schedule and will be completed in FY93.

The ATS is now capable of scanning a substrate with shells randomly placed upon it and selecting shells according to size and circularity. It can load the selected shells directly into a capillary. This is ideal since shells are typically placed in a capillary for the next coating step. We will implement the methods for measuring wall thickness and concentricity of the inner and outer surfaces of the shell in the coming fiscal year. We will also do a series of validation runs to define measurement tolerances.

1.2.4. GA05 MICROENCAPSULATION PROCESS DEVELOPMENT

The objective of this task was to improve the microencapsulation technique of polymer shell production through three efforts. The first was to further understand the fundamental processes of sphere formation. The second was to use statistical process analysis to identify the most important process variables. The third was to construct a triple-orifice droplet generator and develop the controlled-mass method of microencapsulation.

Fundamental studies of polymer solution phase behavior and phase separation kinetics were carried out via optical techniques. Polymer solution phase behavior was measured using

the method of Thermal Optical Analysis. As a result, a complete phase diagram of the methyl ethyl ketone (MEK)/polystyrene/water system was obtained. At 40°C, the limiting concentration of water in the system before two phases form (indicating the development of vacuoles) is approximately 4%. In addition to equilibrium thermodynamic measurements, phase separation kinetics were measured by light scattering (turbidity) measurements. Measurements on MEK/1,2-dichloroethane/polystyrene contacted with water show phase separation occurring in approximately 1 to 2 sec.

Statistical process analysis of the complex-emulsion microencapsulation technique has identified the major variables that control shell diameter, wall thickness, aspect ratio, uniformity, and vacuole density. Using a Fold-Over Plackett-Burnam experiment design, 16 variables were screened for their effects on production of polymer shells. At least two significant process variables were found for each of the above responses. The average diameter of the shell batches ranged from 0.11 to 1.8 mm with the largest shell being 6.1 mm. To gain quantitative knowledge of the effects of the process variables, more detailed optimization experiments are required.

To allow independent control of shell diameter and wall thickness, which the other techniques lack, a triple-orifice droplet generator was constructed for development. Using this controlled-mass approach to shell production, shell size and wall thickness can be predetermined. The goals for this year were to construct the triple-orifice, demonstrate microencapsulation, and to cure polymer shells. Microencapsulation was demonstrated using a vegetable dye in the inner water phase to indicate successful shell formation. Shells, which were not target quality, were produced in the size range of 0.5 to 1.2 mm.

1.2.5. GA06 MICROMACHINING TRANSITION PLANNING

The GA/WJSA team was tasked to develop a comprehensive draft plan for the transition of ICF micromachining capability for hohlraums and other target components from Rocky Flats to an appropriate DOE contractor site. A principal objective of the plan was to maintain the continuity of supply of components during the transition period. The task activities included fact finding at the Rocky Flats facility and at LANL, an initial assessment describing the urgency and options related to ensuring the continuity of micromachining support to meet laboratory requirements, and the development of a formal draft transition plan which served as the basis for a potential FY93 Task Assignment to implement the transition.

GA/WJSA visited Rocky Flats and coordinated with LANL, LLNL, and DOE to gather information needed to make an initial assessment and to develop the detailed transition plan. Items that were evaluated included Rocky Flats' plans and schedules, availability of Government-owned equipment from Rocky Flats and elsewhere, estimated ICF program component requirements for FY93 and FY94 and the equipment required to produce these components, the possibility of stockpiling, the potential for interim micromachining support by LANL and LLNL, facility security requirements, etc.

A comprehensive transition plan was drafted and formally submitted to DOE. The plan addressed facility planning for the micromachining facility, including recommended location, facility upgrades as required, facility and security plans and estimated costs, and equipment relocation plans and estimated costs. Consideration was given to staff planning to provide qualified staff to operate the micromachining facility, which included assessment of personnel needs, planning to obtain the needed staff, and provision for necessary staff training. Consideration was given for maintaining continuity of production and supply during the transition by relying on limited production at Rocky Flats and requesting interim production support from LANL.

Seven transition options were evaluated, ranging from maintaining operations at Rocky Flats unperturbed, to moving the facility off-site in the local Denver area, to transitioning completely to a California location. The GA/WJSA recommendation was to transition the micromachining and support equipment from Rocky Flats to GA/WJSA facilities in California as quickly as practically possible. Limited production was recommended to continue at Rocky Flats while the hohlraum production capability was relocated immediately, with the capability to machine witness plates, physics packages, discs, etc. following. LANL would be requested to provide a "bridge" in production while the transition ensued and GA/WJSA validated capability to accept production orders. The schedule for completion of the transition to the point of being fully ready to accept production orders is an aggressive six months.

1.2.6. LL01 ONSITE SUPPORT AT LAWRENCE LIVERMORE NATIONAL LABORATORY

Our onsite team at LLNL emphasized activities in micromachining of target components, assembling target components into complete targets, and characterizing target components and complete targets to assure their quality for use in Nova ICF experiments.

In micromachining, Craig Rivers, our micromachinist, developed a "kit" approach to target assembly by which machined target components travel as an integral kit for subsequent assembly out of "bins." The kit approach alleviated problems of missing (misplaced), lost, or out-of-stock parts which caused time delays in completing target assembly. John Ruppe, our target assembler, assembled nearly 100 classified hohlraum targets, and about half as many unclassified targets of many designs. In characterization, Andrea Denton determined the key properties of targets and target assemblies by a variety of techniques including: radiography with image analysis, interferometry, optical microscopy, and Energy Dispersive X–ray Spectroscopy (EDXS).

1.2.7. LA01 ONSITE CRYOGENIC SUPPORT AT LOS ALAMOS NATIONAL LABORATORY

This work enabled LANL to produce high-quality images for analysis during the performance of two beta-layering experiments. The work consisted primarily of the setup and testing of experimental apparatus, optimization of data acquisition setup parameters, and performance of 75 and 250 μm beta-layering experiments. Setup work included the design of imaging system mounting and positioning hardware, determination of an appropriate illumination system configuration, and the set-up and testing of the CCD imaging system and beta-layering cell cryostat. Testing of the imaging system was done using precision image analysis software obtained from LLNL. Optimization work determined how to find best image focus and determined optimal camera exposure times and optimal number of image frames to average to produce the best image quality.

Beta-Layering experiments were performed with 75 and 250 μm DT solid layers, and analysis performed on the 75 μm data. This analysis examined the surface quality of the DT layer and determined the size of modal defects out to Mode 512. Overall layer quality was measured to about 4 μm, and individual modal defects were measured to about 0.2 μm. There were no significant surface defects above Mode 20, and lower order modal defects were less than 0.6 μm with the exception of a 1.4 μm P1 (offset). The layer offset was expected because the experiment was not run to completion due to the very long equilibration time constant for the DT cell geometry used.

1.2.8. LA02 ONSITE SUPPORT AT LLNL FOR LANL

Task LA02 directed us to "provide the services of one full-time Q-cleared person onsite at the LLNL Nova target assembly area to perform final assembly of LANL targets for the Nova laser." We found recruiting a person to be difficult due to the Q-clearance requirement. An interview was held in May for a well-qualified individual. We made him an offer in June, but the offer was turned down. We expanded our search, making inquiries at other DOE facilities and placing advertisements in key newspapers near those facilities.

At the same time, John Ruppe, our target assembler at Livermore working on LLNL targets, began working overtime to assemble targets for LANL. During July, August, and September, John assembled or assisted in the assembly of 23 hohlraums for LANL and helped in other ways by cutting patches, providing formvar films, and drilling out and assembling target posts.

Our recruiting efforts eventually paid off. Kett Gifford was hired and started work in October 1992.

1.2.9. SL01 FABRICATION OF FILMS AND FILTERS

The objective of this task was to deliver well-characterized foil targets or filters mounted on frames as specified by SNL. These targets or filters were to have fiducial holes or, for some mylar-backed films, uncoated fiducial regions. In addition, the fabrication effort was to be supported by an engineer assigned to SNL.

Although we were validated to fabricate free-standing gold films and free-standing aluminum films had been submitted for validation, SNL requests for targets were confined to Mylar-backed gold films. In FY92, we fabricated 360 targets of four different designs at the GA/WJSA facility, and 162 targets of three different designs were fabricated at SNL by our engineer, Tom Alberts, who was assigned to support the fabrication effort. Using SNL resources, Alberts also was responsible for the acquisition, fabrication, characterization, and assembly of 366 X-ray filters.

1.2.10. UR01 OMEGA-UPGRADE CRYOGENIC TARGET DELIVERY SYSTEM

The upgrade of the OMEGA laser at UR/LLE will result in a need for millimeter size targets filled with D_2 or DT and maintained at cryogenic temperatures. This mandates a

cryogenic target delivery system capable of filling, layering, characterizing, and delivering cryogenic targets to the OMEGA-Upgrade target chamber. The program goal is to design, construct, and test the entire target delivery system by June 1997. When completed (including an operational demonstration), the system will be shipped to Rochester for reassembly and commissioning in time for the OMEGA-Upgrade cryogenic campaign scheduled to start in 1998.

The GA/WJSA team was tasked with developing a conceptual design in FY92. To develop the conceptual design, we hosted a series of cryogenic working group meetings. The first, in January, brought together cryogenic experts in the ICF community. These included personnel from LLNL, LANL, the UR/LLE, the University of Illinois and Syracuse University, along with members of the GA/WJSA team. The focus of the first meeting was to determine the current state of knowledge as it pertained to cryogenic targets and delivery systems. On the basis of these discussions (and a number of meetings with Rochester target designers, fabricators, and system operators), a design requirements report was drawn up. This report (issued in April), defining the minimum requirements that a cryogenic target delivery system must meet, was circulated among the ICF cryogenics community for comment.

Once the design requirements were defined, a number of design concepts were considered. Another cryogenic working group meeting was held in June to consider and prioritize the design concepts felt most likely to lead to a successful design. Once the concepts were selected, detailed work on the conceptual design commenced. A draft report was circulated to LLE and the National Laboratories in August and the actual conceptual design report was issued in September. In conjunction with the DOE Target Support Contractor Review in October, a third cryogenic working group meeting was held to review the conceptual design. Based on the comments received at that meeting, minor revisions are being made to the design. Additional details are described in Section 6 (OMEGA-Upgrade Cryogenic Target Delivery System) of this report and in the OMEGA-Upgrade cryogenic target delivery system conceptual design report itself.

1.2.11. UR02 DOPED POLYMER SYNTHESIS

This task sought to obtain 50 g of each of five doped polystyrene polymers. Ten gram quantities of two doped styrene polymers were supplied to UR/LLE on time. The polymers supplied were polychlorostyrene and poly(trimethylsilylstyrene), with molecular weights

in the neighborhood of 150–250K. The polymers were free of obvious impurities (by NMR), gel, and crosslinked material. Shells were made by microencapsulation from each polymer.

We did not produce the deuterated materials during FY92 due to several constraints involving material availability. The only material commercially available, at reasonable cost, was perdeuterostyrene. We obtained this material and are proceeding with the syntheses.

SECTION 2

CAPABILITIES ACTIVATION

2. CAPABILITIES ACTIVATION

A significant portion of our initial activities were devoted to acquiring equipment and demonstrating the capability to produce ICF target components.

2.1. SHELL FABRICATION

Fabrication of plastic and glass shells is the first step in ICF capsule target production.

2.1.1. POLYSTYRENE SHELL TOWER

We are now routinely producing polystyrene shells and chlorinated polystyrene shells that meet the specifications of the task statement (180 to 550 μm o.d. and 2 to 4 μm wall). We are using the systems and methods previously employed in the field, the current methods used by Lawrence Livermore National Laboratory (LLNL), and techniques developed at GA.

The drop tower system is composed of a frequency driven shaker, direct drive solution injector, a custom press fit injection needle, a low-temperature viewing zone, and a 6 in. by 22 ft tube with a well-defined temperature gradient. The top of the tower is shown in Fig. 2-1 and details of the heating system are given in Table 2-1.

The first step in polystyrene shell production is to introduce droplets of polymer/solvent solution into the top of the heated portion of the tower. If the droplet injection system is too hot, solvent will flash in the injection needle preventing the formation of uniform-sized droplets. Heat in the viewing section is also a symptom of thermal convection currents between the heated portion of the tower and the viewing section. Since thermal convection currents are a major cause of loss of shells to the wall, they must be minimized. To reduce the heat transfer from the hot tower, we reduced the tower diameter from 6 in. to 2 in. through the 7 in. from the heated tower to the viewing section and droplet generator. We also installed a cool cap on top of the

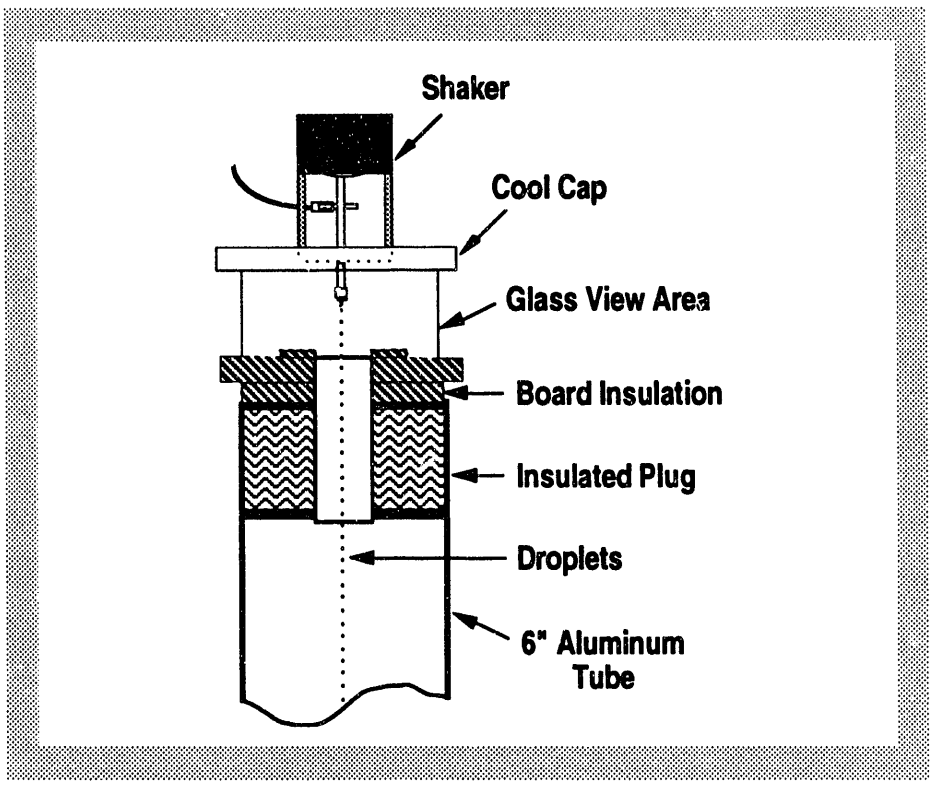

Fig. 2-1. PS tower droplet injection system.

viewing chamber. We found that the restricted diameter reduced the heat transfer such that the cooling water flow to the cool cap is not normally required.

Previous work at LLNL and elsewhere has shown that a constant tower wall temperature is the preferred mode of operation. We introduce a slight temperature gradient, hotter at the top and lower at the bottom, to suppress thermal convection and increase yield. The tower temperature is controlled in nine temperature-controlled axial zones followed by a long unheated zone. The process tube in each zone is wrapped with from one to four glass-insulated, laboratory heating tapes. The temperature of the top zone is selected based on the solution composition and the desired shell size. Thereafter, temperature is decreased by 2°C per zone. The transition zone is operated at an intermediate temperature and the bottom zone at ambient.

There is a distinct range of temperatures that creates different product. The maximum and minimum temperatures may vary with the type of injector used, but the effect of temperature change on product is consistent. If the tower is too cool, the solvent will not evaporate and the droplet will "splat" in the collection plate. As the temperature increases, the next phase is solid beads. The assumption is that the droplet of solvent and polymer

TABLE 2-1

HEATING SYSTEM FOR PS TOWER

Zone	1	2	3	4	5	6	7	8	9	10
Heaters	1	2	3	3	3	4	4	4	4	0
Zone length (in.)	5	10	15	15	15	20	20	20	20	124
Total length (in.)	5	15	30	45	60	80	100	120	140	264
Temperature (°C)	224	222	220	218	216	214	212	210	180	Ambient

needs to be heated to a point where vapor bubbles are formed within the drop. Too low a temperature will evaporate solvent without nucleating a vapor bubble with the result that the droplet will not blow into a shell. The next type of product produced is "gravel." Gravel is a polymer mass containing multiple bubbles. The assumption is that the temperature was high enough to nucleate the bubbles but not enough to expand the bubbly mass into a shell. When the proper temperature is reached, the majority of product is shells. Continue to increase the temperature and thicker walled shells will be formed. Eventually beads will be produced again. The assumption is that the shells melted back down into beads or the surface of the droplet quickly skinned over causing the walls to be too thick to blow into a shell. The tower temperature range that produces good polystyrene shells is only 10° to 15°C.

The wall uniformity of the shells we have produced is equivalent to that of state-of-the-art drop tower shells, 10% to 20% non-concentricity (NC). There is some concern that the use of a chlorinated polymer has an adverse affect on uniformity. Although shell NC is not affected, a visible distortion or "fuzziness" is apparent in the fringe pattern of shells viewed under an interferometric microscope. The best chlorinated

shells to date have been made with a particular batch of technical grade polychlorostyrene (PCS) with a broad molecular weight distribution peaking around 80K.

For additional information, please contact D. Husband (GA).

2.1.2. FRIT PRECURSOR

The generation of a spherical, hollow glass shell, whose dimensions are suitable for ICF targets, depends critically on several factors. If the spheres are to be produced in a high-temperature vertical furnace, liquid or solid precursors carrying the correct masses of glass-forming chemicals are introduced to fall vertically through the hot zones of the furnace. The shell diameter and wall thickness will dictate the mass of the precursors, and the desired chemical composition of the shell will dictate the compounds to be used in the precursors. In order to ensure that the shells will all have the same characteristics, the precursors must be uniform. In the 1970s, liquid drop techniques were developed at LLNL to produce very uniform glass shells. Aqueous solutions of glass-forming chemicals were formed into uniform drops and passed vertically through high-temperature furnaces in which the solvent evaporated. The remaining solute melted and formed exceptionally high-quality glass shells. If the solution of glass-forming materials is dried, pulverized, sieved, and the resulting particles dropped through the furnace, glass shells may also be produced. However, these shells will have a wide distribution of sizes and wall thicknesses because of the variation in size of the frit particles introduced into the vertical furnace. To circumvent the variations in size of the frit precursors used for glass shell formation, an intermediate step has been introduced during the past year. An atomizer spray dryer has been activated for use as a tool to be used in the production of dry frit particles for glass shell production.

A spray dryer made in Denmark under the name "NIRO ATOMIZER" was transferred from LLNL to GA/WJSA. Figure 2-2 is a schematic diagram of the spray dryer. Liquid drops to be dried to precursor frit particles can be introduced into the spray dryer through an opening in the top of the dryer. Heated air enters the dryer body and circulates inside carrying the particles around and downward toward the bottom center of the chamber. The dried particles are extracted from the flowing air by means of a cyclone separator in the air exit line of the dryer. The temperature of the air in the dryer can be controlled to temperatures between ambient and about 400°C by the electric heater in the inlet line for the airflow. The airflow velocity can be controlled by the fan speed and by baffles at the air exit.

Several means can be employed to form and introduce the liquid drops into the dryer. A standard spray nozzle produces particles which are normally too small to be useful and a size distribution which is too broad to be very interesting. A better choice is a Rayleigh drop generator, which breaks up a liquid jet into a stream of very uniform liquid drops. Because of aerodynamic drag forces, many of the drops collide and coalesce producing some larger drops and broadening the size distribution. To avoid the coalescence problem, the drops can be separated by electrostatic means or another drop generator, the drop-on-demand (D-o-D) generator, can be used. Figure 2-3 shows a schematic diagram of a generic D-o-D drop generator. In response to a single, short high-voltage pulse into the D-o-D generator, a single drop of liquid can be produced. The pulse amplitude and duration, the orifice size, and the fluid pressure in the fluid feed system all combine to determine the drop size and exit velocity from a given drop generator. The use of the D-o-D generator allows the introduction of single drops at predetermined times into the dryer. Thus, coalescence of the drops is avoided and a set of uniform precursor particles results. We designed a D-o-D generator which will be built in FY93.

To drop dried precursor particles one by one into the high-temperature furnace, a device was designed and fabricated. Figure 2-4 shows, schematically, the general features of the

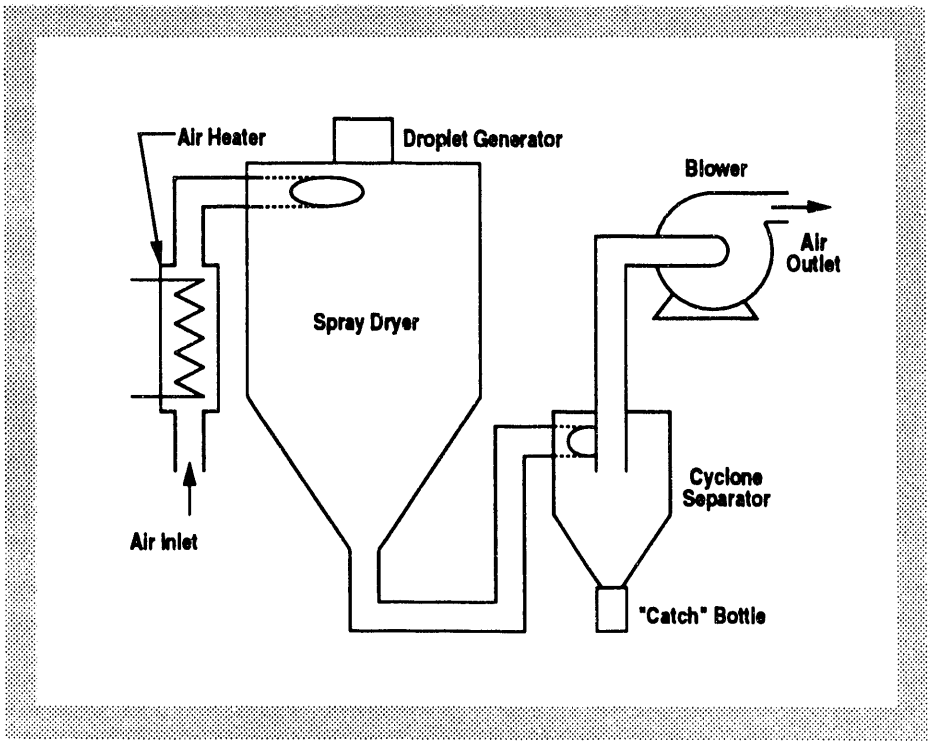

Fig. 2-2. Spray dryer.

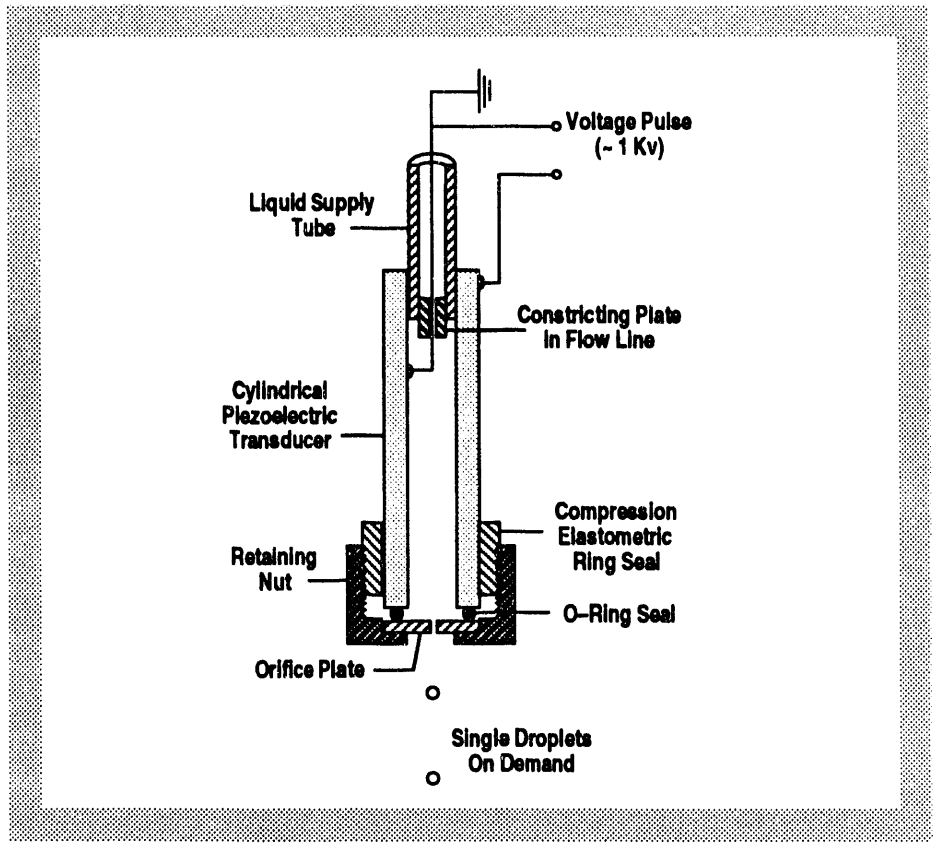

Fig. 2-3. Drop-on-demand droplet generator.

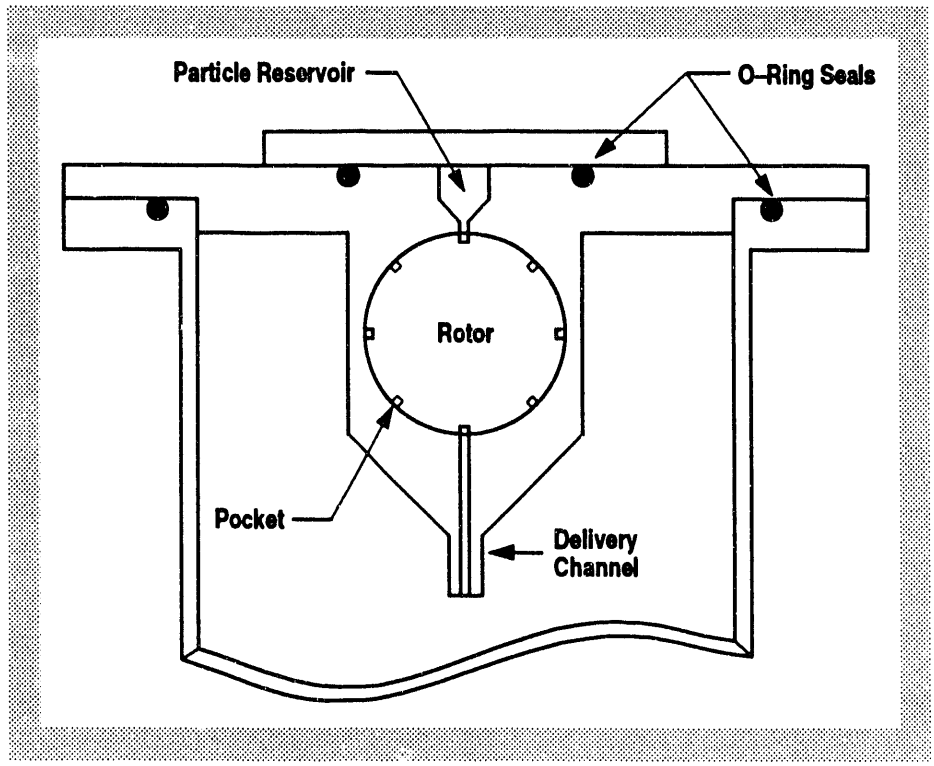

Fig. 2-4. Single particle feeder.

dropper and its mode of operation. The design permits the dropper to operate in a high vacuum system, or at normal atmospheric pressures without undesirable air flows in the system. The single particle feeder allows the introduction of successive single particles into the high temperature furnace at a demand rate determined by the motor speed.

For additional information, please contact Dr. C. Hendricks (WJSA).

2.1.3. GLASS SHELL TOWER

Formation of glass shells is done in two stages. In the first stage, precursor particles are fabricated of the desired chemical composition, each particle containing material sufficient to form a glass shell of the desired dimensions. In the second stage, after a low-temperature heat treatment required to establish a uniform level of volatiles in all particles the precursor particles are dropped through a long furnace, the glass shell drop tower.

We fabricated our glass shell tower from three 3-zone furnaces and a multipoint temperature control system borrowed from LLNL. These furnaces were last used in the mid-80s and were in generally good shape but many of the silicon carbide heating elements were broken. We assembled the three furnaces into a single glass shell tower enclosing a quartz process tube. The total heated length of the tower is 11 ft. This is 3 ft longer than the LLNL tower but 1 ft shorter and 150°C less in maximum temperature than the tower used by the prior contractor. The 3 in. diameter quartz process tube extends 4 ft below the hot zone to a collection chamber. The main support for the process tube is at the top of the tower. The tube is also supported at the bottom of the tower by a vertical traveling fixture. This fixture is counterweighted such that approximately half the weight of the quartz tube is carried from each end.

When we attempted to reprogram the temperature controller to control the third furnace, we discovered that the temperature controller was being upgraded at the time LLNL ceased production of glass shells. The result was a system which could be operated as previously programmed but which could not be reprogrammed. Upgrading the software permitted the system to be reprogrammed at the factory but it cannot yet be user programmed.

The furnaces had lost some heating elements through breakage before and during removal from LLNL. The replacement silicon carbide heating elements apparently have a slightly lower resistance than the original elements. The Silicon Controlled Rectifier (SCR)

final control elements were being operated very close to their current limit resulting in four of the SCR controllers failing. The SCR's failed by shorting through rather than burning out with the result that a failure causes an uncontrolled thermal excursion. The failures were detected before any damage could be done, but since the failure mode precludes unattended operation of the furnaces, we have ordered higher rated SCR modules for installation in the temperature controllers.

The glass shell drop tower is awaiting delivery of the replacement SCR temperature controllers before we complete shakedown and glass shell fabrication validation.

For additional information, please contact Dr. L. Brown (GA).

2.1.4. PVA COATING

A polyvinyl alcohol (PVA) shell coating tower was designed with a goal of improving the process yield. The two primary mechanisms responsible for shell loss in this process are the thermal convection currents which carry the shells to the tower wall and the variable thermal histories for different particles resulting in both over-heated and under-dried coatings in a single batch. These loss mechanisms can be minimized by eliminating the thermal gradients induced through localized contact of the tower wall with heating elements. We designed our tower based on the "hot box" concept. Each of the ten, 2 ft high axial zones of the tower is in an individual "oven." The temperature in each zone is independently controlled and an internal fan ensures that the air temperature in each zone is uniform. When operated with temperature setpoints, which decrease slightly with distance down the tower, thermal convection should be minimized and all particles should undergo the same thermal history as they fall through the tower. The design of the PVA tower is shown in Fig. 2-5.

A second small tower is included in the hot box for experimental work and possibly as an improved polystyrene shell tower.

The PVA tower is awaiting delivery of the process tubes and completion of the wiring at the time of this writing.

For additional information, please contact Dr. L. Brown (GA).

2.1.5. MICROENCAPSULATION

Our charter was to learn the complex emulsion ("shake and toss") microencapsulation process and to produce high-quality polystyrene spheres for capability validation by University of Rochester's Laboratory for Laser Energetics (UR/LLE). For much of the period, we struggled to produce appropriate spheres. Ultimately, we produced target quality spheres on a regular basis, within the specifications set in the task description, and were validated by UR/LLE.

Several technical issues were identified and resolved along the path to producing target quality spheres. The predominant issues pertained to vacuoles in the shell walls, and debris inside the spheres. The most significant issue is the debris on the inside of the shell. Several sources of this debris were found. First, round bead-like strings of debris were discovered in many spheres when they were broken open and examined under an electron microscope. By energy dispersive X-ray analysis, the debris was found to contain oxygen, which pointed toward it being PVA. Infrared spectroscopy confirmed the identification. The PVA was coming from the bath into which the precursor polystyrene shell droplets were being tossed and was somehow getting into the interior of the spheres. By lowering

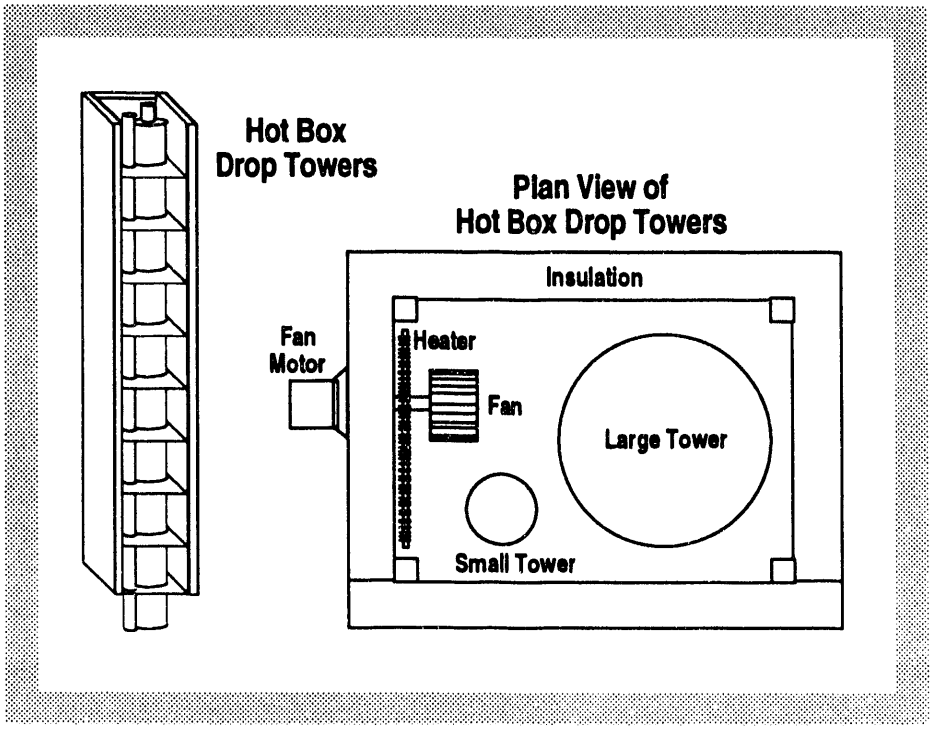

Fig. 2-5. Design of the PVA tower.

the PVA content in the bath, from 5% to 0.05%, this debris problem was dramatically reduced and now few isolated beads are found inside the spheres.

A second debris source occurred when the polystyrene solution was not adequately filtered. Gel present in broad molecular weight polystyrene was being trapped within the spheres, giving a foamy appearance to the resulting spheres. By going to a narrow molecular weight polystyrene, and passing the polystyrene in solution through a 0.2 μm filter, the foamy looking material was eliminated.

The second major target flaw is the presence of vacuoles (bubbles) in the shell wall. We presume that vacuoles result from a "precipitation" of water (or low polymer concentration fluid), within the shell wall as it forms. There may be several mechanisms by which this bubble is formed (see Section 4 – Microencapsulation Process Development for more details). One mechanism could be for the organic phase to become supersaturated with water. In the solvent system benzene and 1,2 dichloroethane (1,2), the (1,2) is more soluble in water, so one would anticipate it would enter the PVA bath more rapidly initially and evaporate from the surface. This rapid removal of (1,2) would leave a benzene-rich polymer phase behind to form the shell wall. Since (1,2) also dissolves in water better than benzene, the removal of (1,2) might leave the resulting benzene solution supersaturated with water, so water balls would nucleate in the wall and harden in place to form the vacuoles. To mitigate this nucleation, we sought to find a single solvent system, the constant removal of which may prevent supersaturation. We chose fluorobenzene because it has properties similar to the mixed solvent. Its boiling point is near 80°C, its density is 1.02g/cc at room temperature, and it is a good solvent for polystyrene. Our current findings are that spheres made from fluorobenzene are as good as those made from the mixture benzene and (1,2), but there is not a dramatic improvement in target quality. (For modeling purposes, simplicity of phase diagram studies, and simplicity of lab operation, fluorobenzene has advantages over the dual solvent system.)

A second mechanism for vacuole formation could be boiling of the solvent. All the individual solvents considered to date boil near 80°C: benzene at 80.1°C, (1,2) at 83.5°C, fluorobenzene at 84.7°C, and MEK at 79.6°C. We noted a much more vigorous boiling solution when the temperature rose above 80° to 85°C. We rationalize that if the sphere wall solution was boiling, the nucleated bubbles of gas may be trapped in the viscous wall solution and form vacuoles. We found that by limiting the maximum solution temperature to 78.6°C,

that larger "vacuole" defects seemed to be limited, regardless of the solvent system, fluorobenzene or benzene and (1,2).

In conversations with Clare Vinton, a process engineer experienced with microencapsulation, we learned that having a positive temperature gradient throughout the process reduced the vacuole problem. He explained that temperature fluctuations in a saturated solvent system may lead to nucleation of second-phase material, which could cause the formation of vacuoles. We have thus sought to maintain an increasing temperature throughout most of our runs, rather than a constant temperature.

As a result of combining the above issues, we now toss the solution from the vial when the temperature reaches 70°C, as the temperature is ramping toward 78.6°C. This profile gives an increasing temperature during the critical first 15 to 30 minutes, a rapid removal of solvent, and yet remains below the boiling point of the solvents. We toss into a solution of 0.05% PVA, which has been filtered to 0.1 μm.

We found several other processing conditions affected the spheres:

1. Going to higher molecular weight polystyrene (400K) gave greater strength to the spheres, and less cracking, by producing thicker walled shells on average. Lower molecular weight (90K) gave more cracking but a higher average shell diameter.

2. Increasing either the percent polystyrene concentration, or the amount of polymer solution in the vial, increased the average o.d. and average wall thickness of the spheres in the batch.

3. There was some correlation of polystyrene molecular weight and the resulting wall thickness. Using the same procedure, and the same percent polystyrene in the vial, higher molecular weight (400K) gave thicker walls than lower molecular weight (152K).

For additional information, contact Dr. B. McQuillan or I. Glatter-Schneir (GA).

2.2. COATINGS FABRICATION

A polymer coating must be applied to the shells to serve as an ablator.

2.2.1. GDP COATINGS

From late October 1991 through February 1992, we placed one person on-site at LLNL to learn the state-of-the-art of glow-discharge polymerization (GDP) coating. The following are some of the observations which were made using the coating station at LLNL, which consisted of a helical resonator and associated radio-frequency (rf) input, feed gas flow control channels supplied with hydrogen and trans-2-butene, and a vacuum system.

1. Increasing the power input causes the coating rate to increase up to a certain power level, after which, the coating rate levels off and then begins to fall as the power input is increased further.

2. The coating rate falls with increasing chamber pressure within the pressure range of 65 to 135 mtorr.

3. Increasing the trans-2-butene flow rate increases the coating rate for flows from 0.03 to 0.8 sccm, inclusive.

4. The coating rate falls as the hydrogen flow rate is increased.

5. The coating rate falls and the region of brightest glow moves up in the plasma tube (away from the substrates) as the helical resonator drive frequency is increased from 45 to 48 MHz.

The data for the first observation are shown in Fig. 2-6. The power levels given are the differences between the forward and reflected power measured at a point between the rf amplifier and the matching network. Power dissipated in the matching network is not taken into account with this arrangement, which was typical of all the GDP coaters in use at LLNL. Parameter Set 1 for Fig. 2-6 was a chamber pressure of 75 mtorr, a trans-2-butene flow rate of 0.7 sccm, a hydrogen flow rate of 6.9 sccm, and a frequency of 45.0 MHz. For parameter Set 2, the chamber pressure was again 75 mtorr, but the frequency was 50.4 MHz and the trans-2-butene and hydrogen flow rates were 0.18 and 10 sccm, respectively.

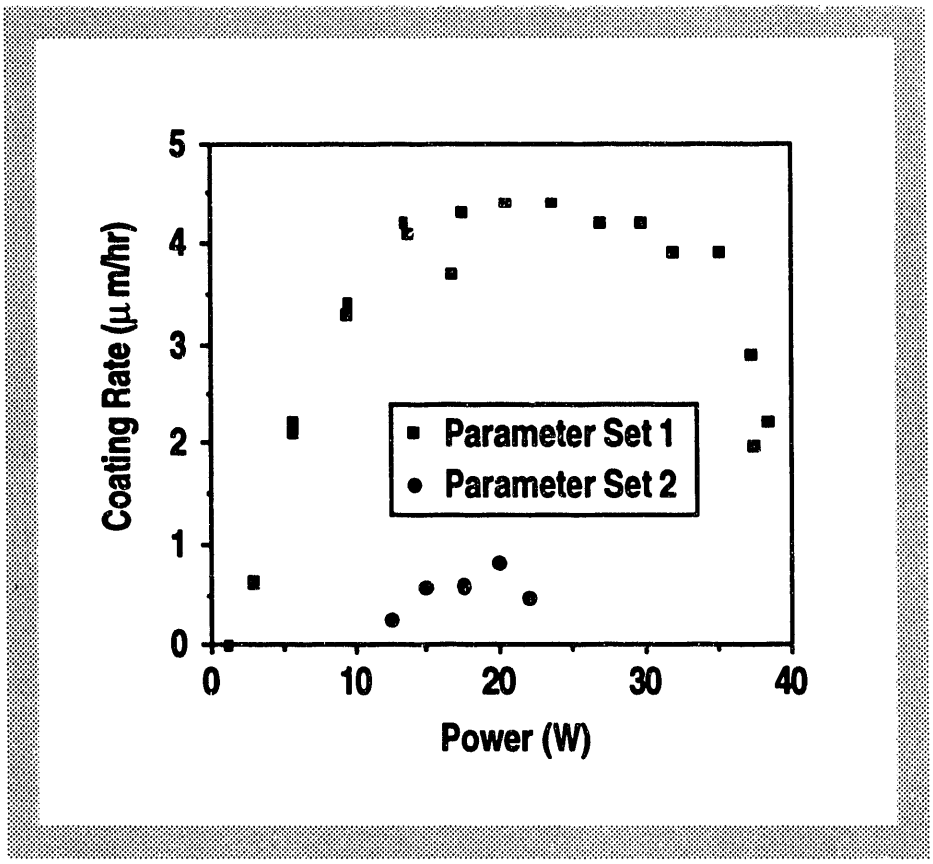

Fig. 2-6. Coating rates as functions of power for two different sets of coating parameters.

The second observation, that the coating rate is inversely related to pressure, was obtained with trans-2-butene and hydrogen flow rates of 0.3 and 10 sccm, respectively, a frequency of 45 MHz and 16.4 to 16.8 W power. The coating rate for a flat substrate was empirically determined to be:

$$r = 9.4 - 0.037\ p \quad ,$$

where r is the coating rate in μm/hr and p is the pressure in mtorr, which was measured with a capacitance manometer and controlled via a feedback loop between the manometer and the chamber outlet valve.

A coating rate rise with increasing trans-2-butene flow rate is an intuitively obvious result, which in this case was borne out by our observations (see Fig. 2-7). However, this behavior is restricted to a specific region of the operating parameter space of a plasma polymerization device. At higher flow rates, the deposition rate levels off as power, rather

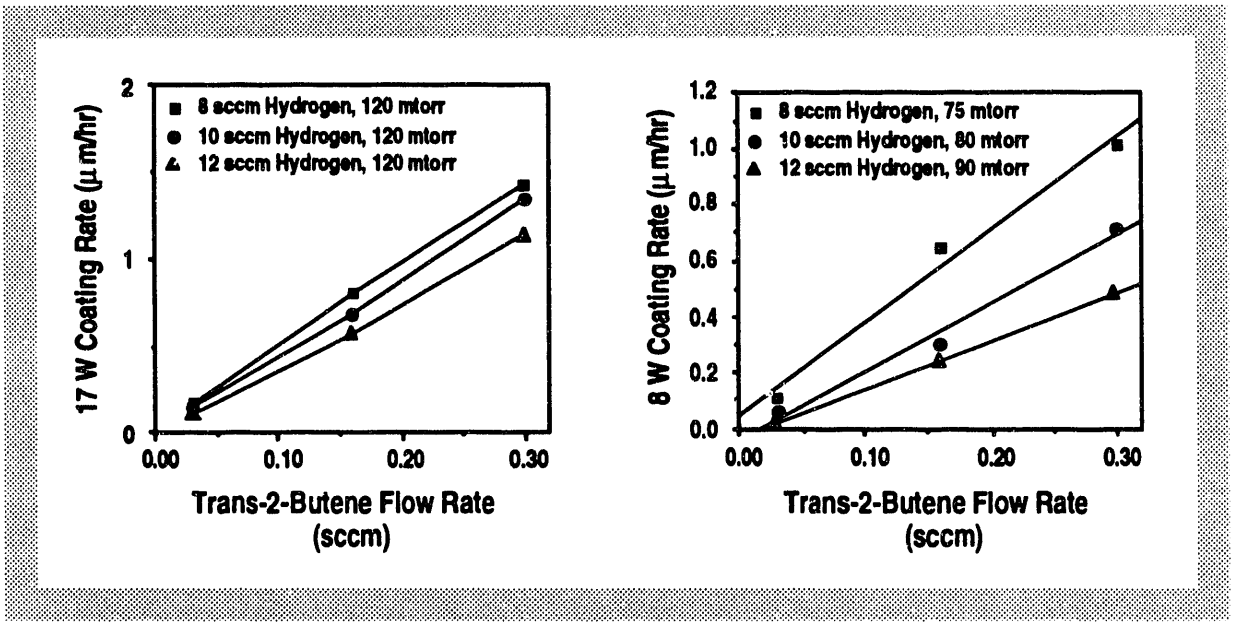

Fig. 2-7. Coating rates as functions of trans-2-butene flow rate for various sets of coating parameters at 45 MHz.

than feed gas flow rate, becomes the dominant parameter [2-1]. Thus, this observation verifies that we are operating in the flow-dependent regime.

The fourth observation, decreasing deposition rate with increased hydrogen flow, was found with trans-2-butene flow rates of 0.3 and 0.8 sccm. In both cases, the frequency was 45 MHz with 8 W power and 120 mtorr chamber pressure. While increased hydrogen flow lowers the coating rate, it has been associated with decreased stress in coatings and increased coating smoothness [2-2].

The fifth observation depends on the rf circuitry of the LLNL helical resonator, which we have also elected to use at GA. Since the magnitudes of current flow in the various regions of the helical resonator are frequency-dependent, the magnetic field strengths in these regions should also vary with frequency. Because the magnetic fields sustain the plasma, the locations (and perhaps the types) of chemical reactions which occur should also depend on frequency [2-3]. These observations of plasma brightness (made by means of a densitometric video camera) and coating rate support this hypothesis. The utility of these observations is in determining the best frequency to use for coating production.

Using the experience gained at LLNL, we began to assemble a similar coating apparatus at GA in March 1992. A helical resonator was loaned by LLNL. Since each of the helical resonators is slightly different, it was helpful that this was the same helical resonator that we had been using during our training, so that the benefit of our work at LLNL was maximized. Los Alamos National Laboratory (LANL) sent the components for an entire coating system. The loaned equipment, along with GA-owned and purchased equipment, was assembled along the lines of the LLNL systems incorporating modifications suggested by LLNL coating personnel. The first coating, deposited on a flat substrate, was made in early July. Our first coating rates were low and coatings exceeding a few micrometers in thickness were rough [see Fig. 2-8(a)]. Coating smoothness was improved by lowering the trans-2-butene flow rate, but the coating rate fell to an unacceptable 0.2 μm/hr.

At first, our matching network did not work well in the 45 MHz region. However, changing the length of the cable between the matching network and the helical resonator allows impedance matching at different frequencies [2-4, 2-5] and we were able to run at 45 MHz, the frequency which we had found to give the highest coating rate while at LLNL. The result of the frequency change was a smooth coating [see Fig. 2-8(b)] and a deposition rate on flat substrates of 0.42 μm/hr.

The shell bouncer pan was then installed, and shells were first coated in August 1992. We found that we could now double the trans-2-butene flow rate and still get an acceptably smooth background surface finish. The problem now was the appearance of mounds or "corns" on the coated shells. We began introducing new procedures intended to reduce the number of mounds. These procedures included: plasma cleaning the shells and pan for 4 hrs prior to coating, careful cleaning of the plasma tube prior to each run, coating the bouncer pan with a thin layer of polystyrene, and reducing the bouncer voltage to the minimum value necessary to move the shells. In addition, we cleaned the inside surface of the coating chamber and started keeping the pan covered until seconds before beginning evacuation. As a result, the total number of mounds on each shell was reduced, and we were able to produce shells which appeared to have no mounds at all.

In September 1992, shells from two runs were sent to LLNL for GDP coating capability validation. LLNL confirmed that both runs met the task requirements for validation of GDP coatings. One run was done in the course of our mound-reduction

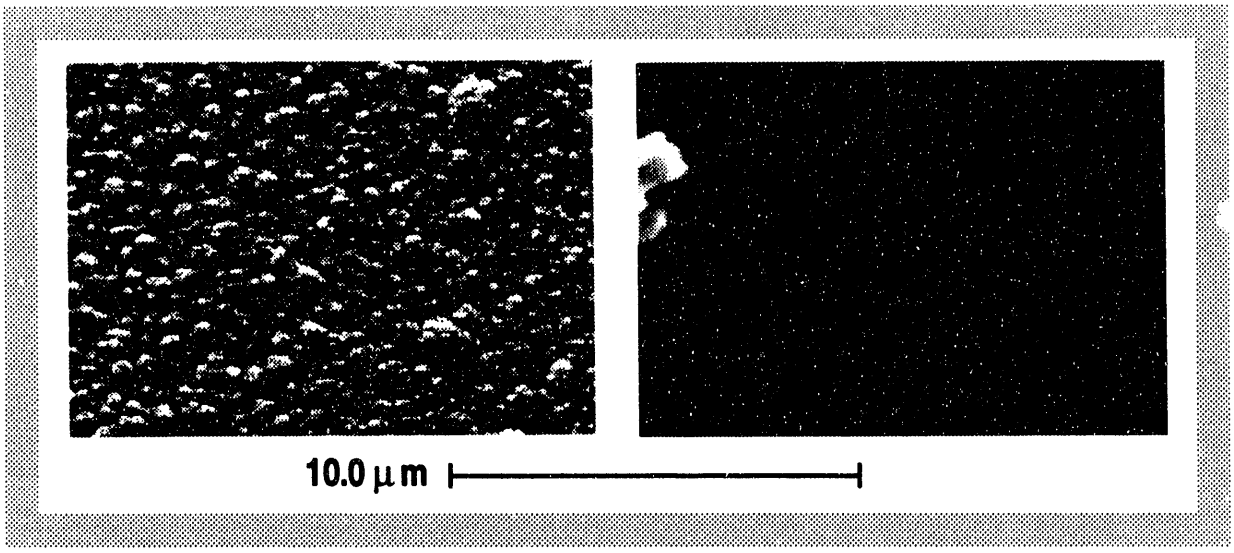

Fig. 2-8 (a). SEM micrograph of the surface of a 13 μm thick GDP film on a flat substrate which was obtained at 50.4 MHz with 10 sccm hydrogen and 0.18 sccm trans-2-butene.

Fig. 2-8 (b). SEM micrograph of the surface of a 10 μm thick GDP film on a flat substrate which was obtained at 45.0 MHz with 10 sccm hydrogen and 0.09 sccm trans-2-butene.

activities and shells from it had a low density of small mounds. The other run produced coated shells judged to be of high quality with few if any mounds. The validation task requirements and the values measured at LLNL on Batch (CH091092) were as follows:

Validation Requirements	Measured Values
• Thickness > 25 μm	Total wall = 30 to 31 μm (measured at LLNL), minus PS average wall of 4 μm (measured at GA), gives 26 to 27 μm coating thickness
• Thickness variation ≤ 5%	Percentage concentricity $(wall_{max} - wall_{min}) / wall_{avg}$ = 2.0 to 2.8%
• Surface finish (P/V) ≤ 2500 Å	RMS avg. surface finish = 94 Å (133 Å P/V)

Figure 2-9 is a scanning electron micrograph of the surface finish of one of the shells from Batch CH091092.

For additional information, please contact J. Ankney (GA).

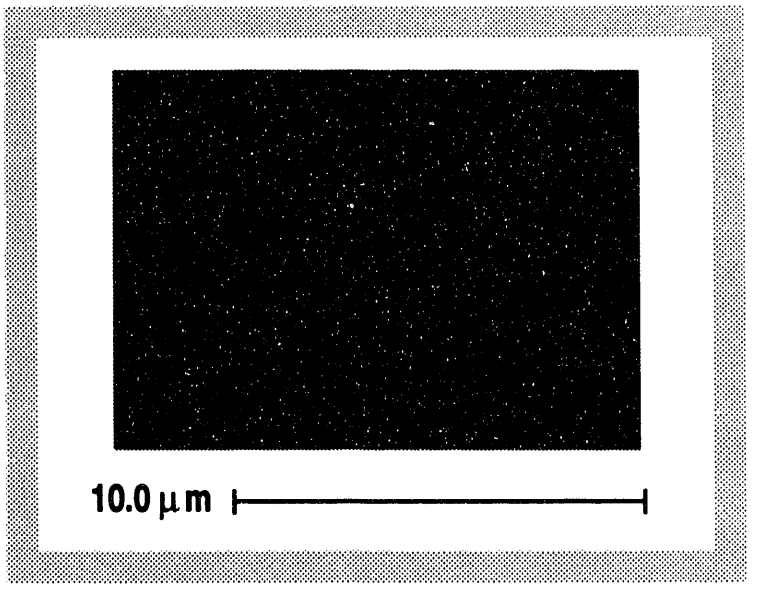

Fig. 2-9. Scanning electron micrograph of the surface finish of a shell from coating run CH091092. Coating parameters: frequency, 45 MHz; hydrogen, 10 sccm; trans-2-butene, 0.18 sccm; power, 16W.

2.2.2. PARYLENE COATINGS

To support the need in the ICF community for CH coatings of high quality, we have designed and activated a parylene coating system in the W.J. Schafer Associates (WJSA) laboratory. With this system, we can uniformly coat samples with parylene in the thickness range of a few microns to many tens of microns. The design is based on similar systems already in existence throughout the ICF community and is schematically shown in Fig. 2-10. In brief, solid di-para-xylylene is sublimed and flows through a high-temperature furnace causing it to break into a diradical that uniformly coats out of the gas phase onto any relatively cool surface.

The following describes some characteristics of the system:

- To achieve sublimator temperature uniformity in the ±1°C range, a fluidized sand bed is used.
- To ensure temperature uniformity throughout the pyrolysis region, a three-zone furnace is used.
- To increase the quality of the coatings, the pyrolysis region is lined with a quartz tube [2-6].

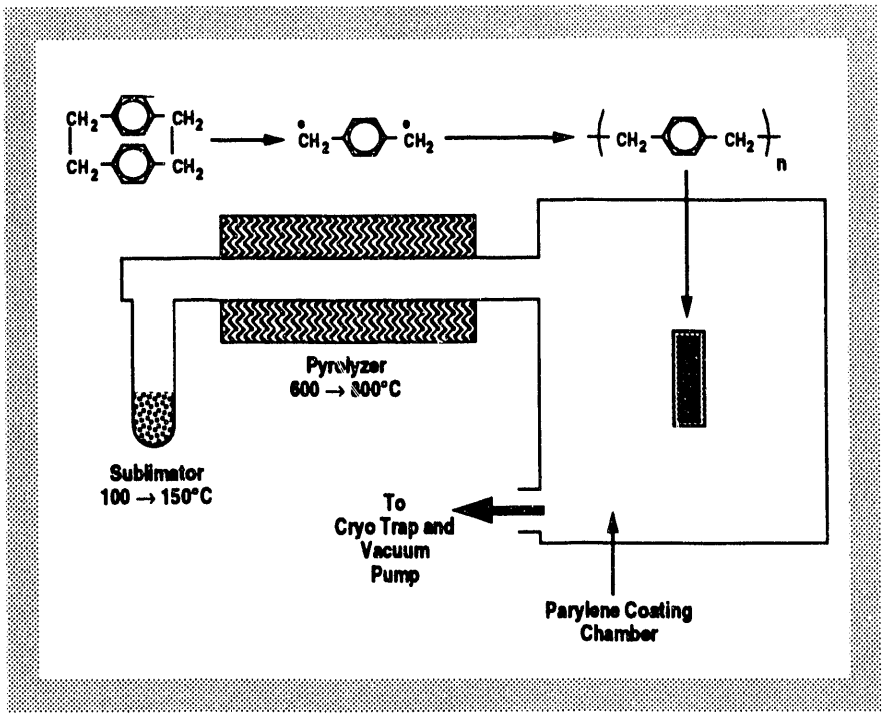

Fig. 2-10. Schematic of the parylene coating system.

- To ensure the complete break down of the di-para-xylylene in the pyrolysis region, quartz wool is loosely packed into the quartz tube.

- To minimize coating deposition onto the downstream system components, they are made of stainless steel and kept hot (150° to 200°C).

- To help achieve consistent coatings, we have a high vacuum pump installed on the system to initially pump out the system to ~10^{-6} torr.

- To provide the pumping while coating, we use a 12 CFM dual-stage rotary vane pump with its own molecular sieve trap to prevent oil contamination of the system.

For additional information, please contact Dr. M. McClellan (WJSA).

2.3. CHARACTERIZATION

A key part of target fabrication is precise characterization. We have made several improvements in characterization techniques.

2.3.1. INDEX MATCHING WALL THICKNESS

It has proved possible to directly examine the GDP coating of a composite plastic shell by immersing it in an index-matched liquid. Using this technique, one can measure coating thickness and thickness uniformity, see cracks growing through the coating, and observe delaminations. The technique is sensitive enough to show strata in the coating caused by abrupt changes in deposition conditions; they are thought to be the result of chemical changes in the deposited layer, and generally are not delaminations.

The experimental setup is as shown in Fig. 2-11. The shell floats in index matching fluid under a coverslip, so the microscope looks through a flat interface. Fluid with an index n = 1.548 has been a good match to the coatings produced at GA (the index depends on coating conditions and age).

When the fluid exactly matches the index of refraction of the surface of the coating, the microscope image shows an abrupt change in color at the interface. If there is a mismatch, there is also a bright band near the liquid/coating interface whose position moves as the focus is changed and whose intensity grows as the mismatch increases. Figure 2-12(a) shows an acceptable match. A good match is important to avoid lensing effects which will distort the apparent thickness of the interface. There are also two bright lines at the inside of the GDP layer. They are the result of the index mismatches between the GDP coating, the PS mandrel, and the air core. Their existence is a result of the strong distortion caused by the different index of the PS; their position is not a direct indication of the mandrel interfaces and cannot be used to measure the mandrel thickness.

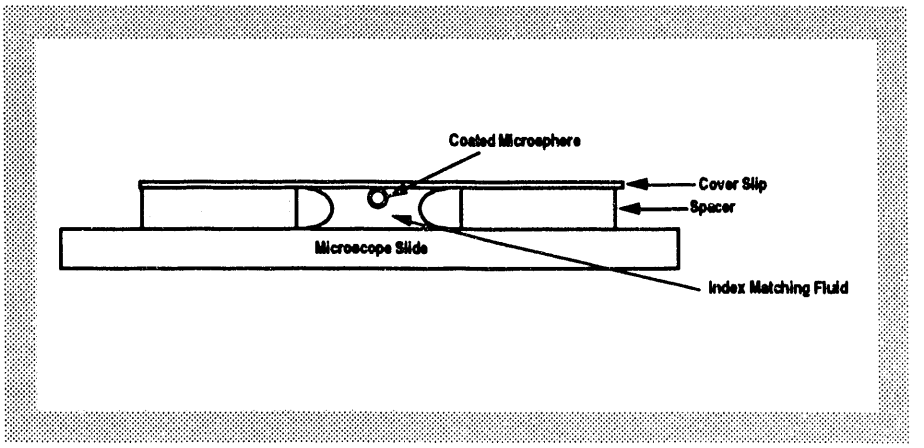

Fig. 2-11. GDP coated shell floating in index matching fluid for microscopic examination of shell wall.

The 4π coating uniformity can be determined by rolling the shell 90° so that its orthogonal orientation can also be measured. Since the shell rolls against the underside of the coverslip, that is easily done by tilting the slide until the shell has rotated the required amount; we tilt the entire microscope, thereby keeping the shell in view and in focus as it rolls to its new orientation at which point the microscope is returned to level.

Flaws or changes in coating composition are easily seen. Figure 2-12(a) shows a crack growing into an otherwise uniform coating from the mandrel. Figure 2-12(b) shows a coating deposited during a run in which the deposition conditions fluctuated; at one point, the plasma went out for some hours. The darkest line there corresponds to a coating delamination seen in SEM images of a broken shell.

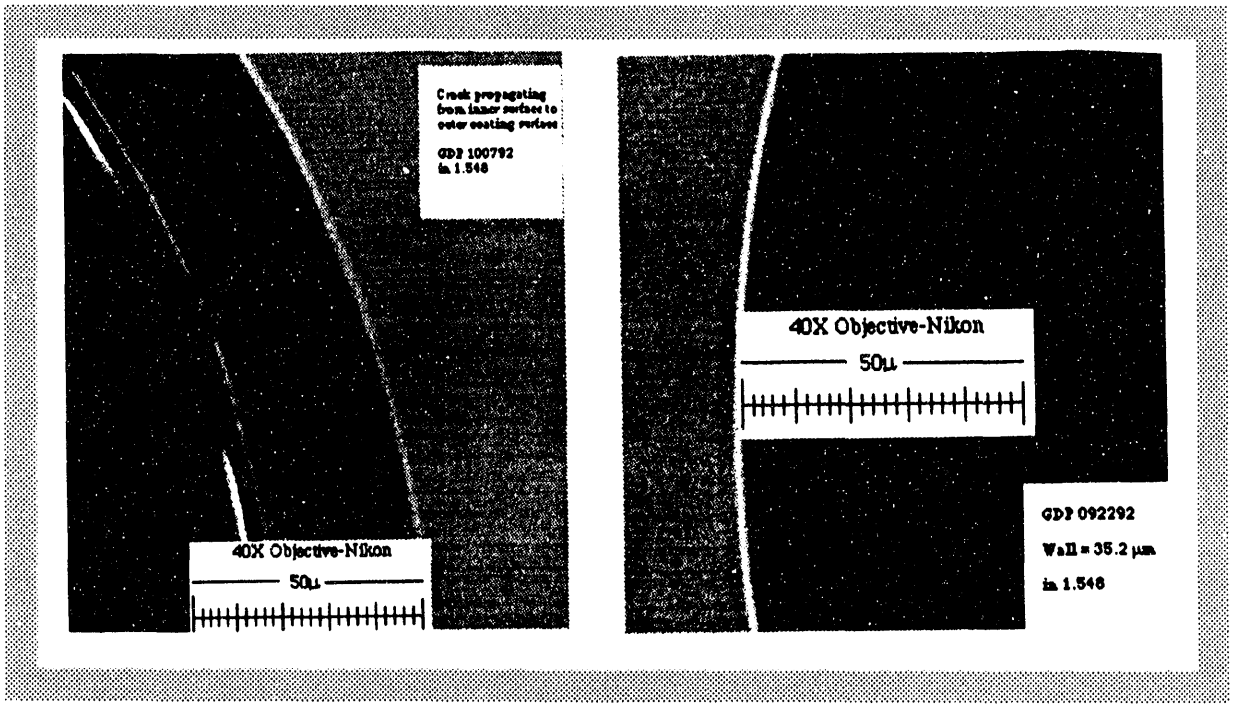

Fig. 2-12. GDP coating as viewed through 1.548 index matching fluid. (a) Crack growing into GDP coating from surface flaw in otherwise uniform coating. (b) Color and index changes within coating caused by fluctuations of and interruptions in plasma during deposition; the most prominent line corresponds to a delamination.

For additional information, please contact D. Steinman (GA).

2.3.2. COMPUTERIZATION

Coupling computers and image processing programs to our microscopes has considerably enhanced our efficiency by facilitating information transfer. With the current generation of equipment, stand-alone commercial systems bring most of the benefits of an integrated custom setup but without a long development time.

Our limited equipment base gave us the freedom to utilize recent advances in computing for image analysis, data collection, and data storage. We had to be rapidly productive, so we took advantage of the ease of data transfer (images and numbers) between stand-alone commercial programs on Macintosh computers rather than designing an integrated, custom program. This approach has worked well in the last year.

The microscope images are transferred to the computers using a Pulnix 745E CCD camera connected to a Macintosh computer through a Data Translation frame grabber. The camera is also connected to a monitor. Two stereozooms, two interference microscopes, and a phase contrast microscope are set up in this way.

The images are displayed and manipulated using freeware from National Institute of Health (NIH Image). It can display live images at four frames per second and can select among up to four potential inputs. The computer images are calibrated using a magnification standard (Geller-traceable to NIST if need be, or to an ordinary microscope stage reticule if not). Brightness and contrast can be manipulated and background subtraction or image averaging enabled to improve the image.

Data from the images are stored on prefabricated spreadsheets in Microsoft Excel. The spread sheets are designed to accommodate all types of shell measurements. They are modified as requested measurements and equipment change. The spreadsheets have entries for calibration for each individual type of measurement. Cells are set up to calculate the desired value from the measurement (e.g., wall thickness in microns from fringe shift in dial turns). Included in the spreadsheet are summary data: wall thickness average and standard deviation, o.d., nonconcentricity, and a graph of wall thickness versus o.d. Figure 2-13 shows a typical shell image from which measurements are taken and the spread sheet for recording the data as they appear on the Macintosh computer monitor.

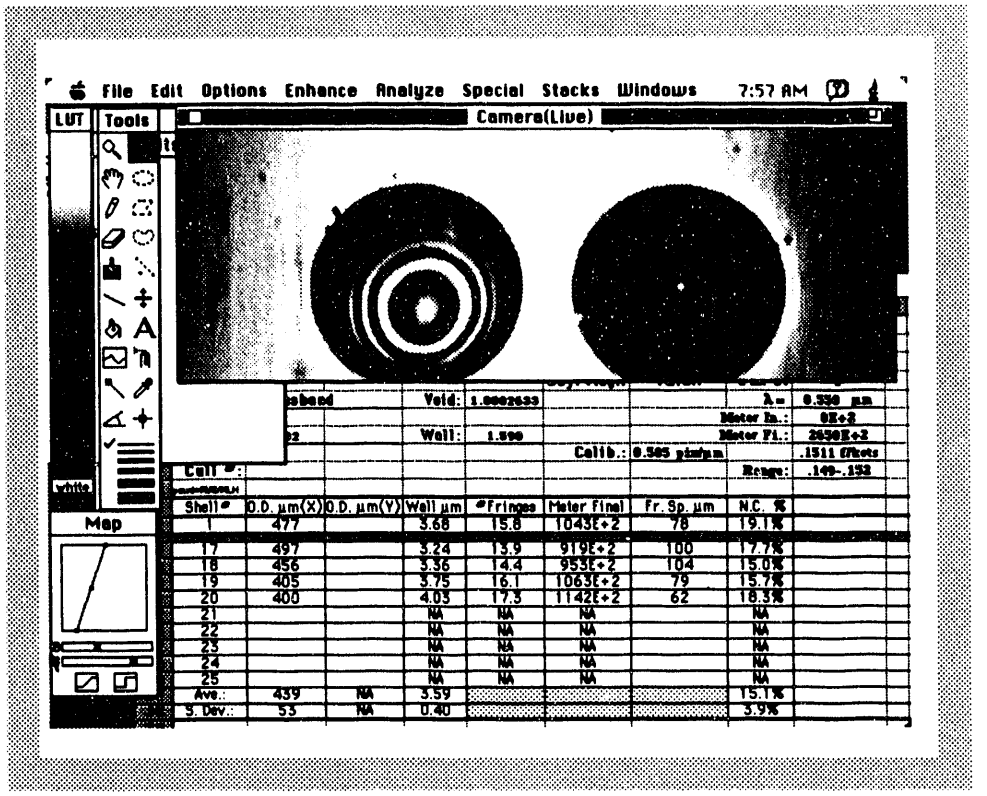

Fig. 2-13. Typical shell image and spread sheet appearing on Macintosh computer monitor used at GA.

The images and data sheets are stored together on a 220 MByte hard disk partitioned into two areas. The data is transferred to them over Appletalk links between the computers. When the first area is filled, its contents are transferred to the second, and an archive tape made of its contents. Under present use, we constantly have the last two month's data on our drive; earlier data is available from the tape archive. The first drive is backed up on a regular basis between transfers.

This system is designed to improve the speed and accuracy of data transfer. Because it is a collection of stand-alone parts, it takes some discipline to make sure data forms are behaving properly, backups are done regularly, and files are adequately labeled and transferred into the archive.

For additional information, please contact Dr. R. Stephens (GA).

2.3.3. JENAVERT AUTOMATION

We have automated the phase shifting knob of an interference microscope to ease data taking both by moving the control out to the operator and by calibrating its movement. This was

accomplished using a 12 mm o.d. motor, gear train, and shaft encoder which could be easily hung on the side of the microscope. This controller is small enough to be mounted virtually anywhere.

The Jenavert Interphako interference microscope was originally purchased by the previous contractor for use in an automated shell selection system which was never completed. It was never intended for its current use: routine measurement of shell wall thickness. The knob which shifts the relative phase of the interfering beams is uncalibrated, and is located high on the side, toward the back of the microscope (there is a calibrated control, but it only has a range of 0.1 μm).

Initially, we left this knob in a fixed position and simply measured the phase shift of fringes across the screen. We found this method to be unacceptable because the relative phase between the paths changed across the screen. The error was large enough to change or make ambiguous the selection of the appropriate fringe, with an attendant error of 0.3 μm. As a first correction, we mounted a ten-turn dial indicator to the phase shifter. This proved accurate, but because of its location and size, reading the dial was quite difficult and prone to error.

Finally, we found a line of small gear motors marketed by MicroMo which had an o.d. of 12 mm. Also available were gear heads able to reduce speed to <1 rpm; shaft encoders which give 10 pulses per motor revolution; and controllers able to change speed over a range of nearly 10:1. With this motor, we were able to motorize the phase shifting knob. The shaft rotation is shown on an LCD display directly on the motor controller and can be accurately positioned and read. The reading for each fringe shift is typed into a preconfigured spreadsheet which automatically does the conversion into wall thickness.

For additional information, please contact Dr. M. Hoppe (GA).

2.3.4. SIMPLIFIED FRINGE ANALYSIS

We have developed a simple fringe analysis technique which uses a small number of measurements to give an unambiguous shell wall thickness to within 1% [2-7]. It uses monochromatic light and is a spin-off of an analysis of the retardation of light passing through a perfect shell relative to a planar reference beam. The analysis uses an expansion in terms of shell aspect ratio (wall/radius) and location (distance from center/radius). This analysis has been put on the automated analysis system at UR/LLE and is undergoing tests of its reliability.

Presently, shell wall thickness is measured at UR/LLE by overlaying the shell interference fringes seen in monochromatic light with those calculated by a template program, and then modifying the program parameters until the overlay matches the observed pattern. This is done off-line and takes some operator assistance. The program gives wall thickness and non-concentricity with an uncertainty at the 1% level.

When we developed an analytic form of the phase shift (relative to a planar reference beam) as a function of position for a perfectly concentric shell, we found that the wall thickness could be unambiguously calculated from a simple measurement of fringe separation (see Fig. 2-14). The equation is in the form of an infinite expansion in powers of the aspect ratio and location and was carried out sufficiently far that the results had less than 1% termination error for typical shell dimensions.

A manual check of the accuracy of this procedure showed that these calculations (measured from Polaroid photographs) and the template results agreed within the limit of our ability to measure from the photos. This measurement scheme has recently been installed on the UR/LLE

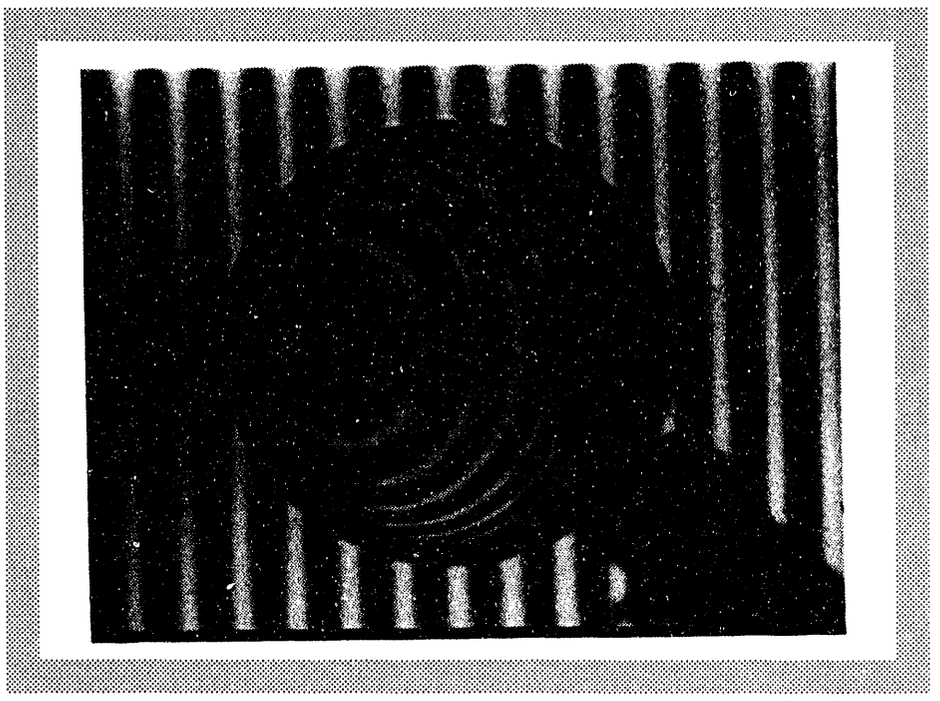

Fig. 2-14. Typical interference image of plastic shell in monochromatic light of wavelength λ. The phase has been adjusted so that there is a black fringe centered on the geometric center of the shell. The thickness of the shell wall, d, is calculated from this image using the equation below where δ is the aspect ratio (wall/radius) of the shell, n the index of refraction of its wall, and f is the distance from the shell center parallel to the background fringes to the center of the next fringe divided by the shell radius.

$$d = \frac{n\lambda}{(n-1)f^2}\left\{1 - \frac{(n^2+n+1)f^2}{4n^2} - \frac{(n^4+2n^3+2n+1)f^4}{16n^4} - \frac{(4n^6+n^5+2n^4-n^3+2n^2+n+4)f^6}{32n^6} - \delta\left[1 - \frac{(5n^4+2n^3+8n^2+2n+5)f^4}{16n^4}\right]\right\}$$

automated measurement system, so that the system can automatically find the fringe centers and separations and is being tested for agreement and reliability

For additional information, please contact Dr. R Stephens (GA).

2.3.5. "WORST VIEW" NONCONCENTRICITY

We have built a rotating vacuum chuck to enable a quantitative measurement of shell nonconcentricity from a single view.

Standard techniques for quantitative measurements of shell nonconcentricity involve analysis of several random views or of orthogonal views. The former leaves doubt whether the true nonconcentricity has been measured, and the latter requires a jig for obtaining orthogonal shell views, which is very hard to use with our sheared image interference microscope (Jenavert).

We have designed a simple rotating vacuum chuck using a 12 mm o.d. gear motor and stainless steel tubing and mounted it on a micromanipulator (see Fig. 2-15). The chuck is compact enough to fit under our microscope objectives and has sufficiently smooth motion to allow us to watch the fringes change as it rotates.

The micromanipulator is used to position the tip to hold and raise the selected shell slightly off the mirror surface. The shell is rotated at 1 to 10 rpm. Since the rotation axis of the chuck is nearly in the plane of view, the displacement vector of the shell's nonconcentricity defect (Type P1) will eventually be rotated into the viewing plane. Any localized wall thickness fluctuations are revealed during such rotations. Then analysis can proceed with the confidence that the true nonconcentricity is being measured.

For additional information, please contact Dr. M. Hoppe (GA)

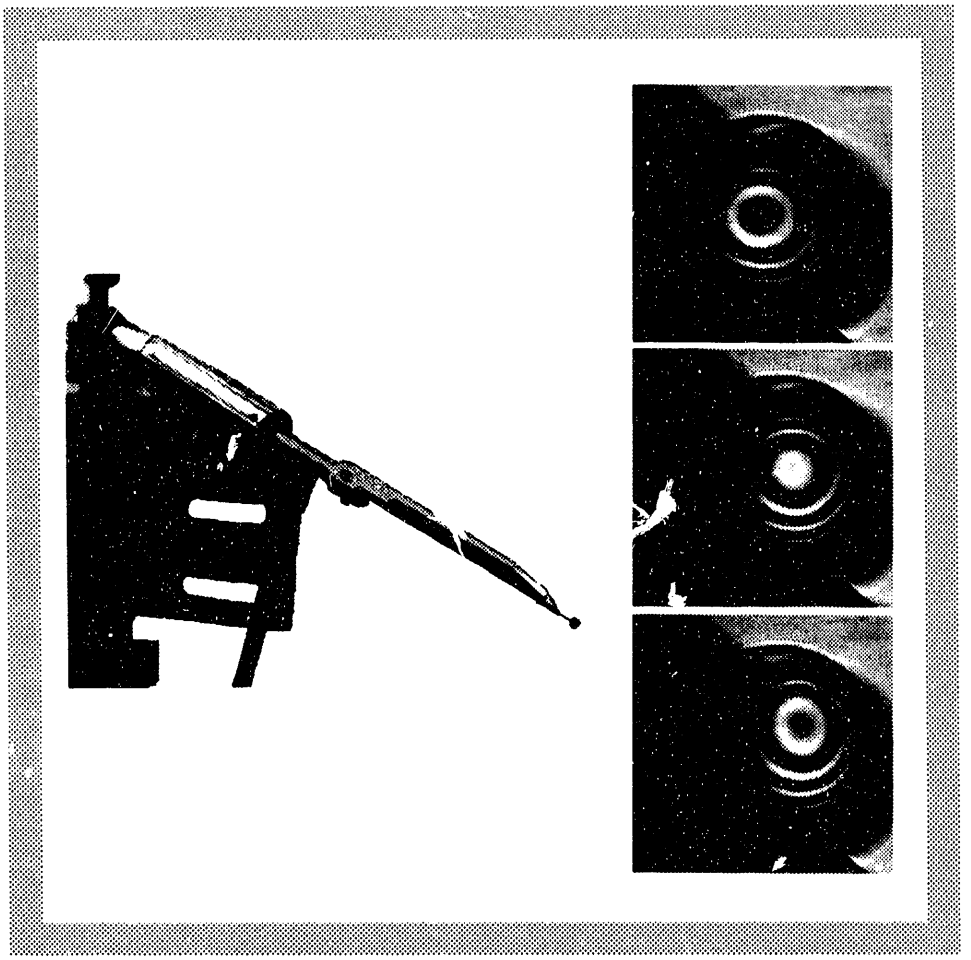

Fig. 2-15. Rotating vacuum chuck mounted on a micromanipulator. Second picture shows appearance of a sphere in several orientations.

2.4. REFERENCES

[2-1] Yasuda, H., Plasma Polymerization, Academic Press, Inc., (1985) pp. 301–313.

[2-2] Letts, S.A., D.W. Myers, and L.A. Witt, *J. Vac. Sci. Technol.* **19(3)** (1981) 739–742.

[2-3] Brusasco, R., "Status Update on Helical Resonator Coater Studies," Lawrence Livermore National Laboratory Report TST 92–029 (1992).

[2-4] Hayward, W.H., *Introduction to Radio Frequency Design,* Prentice-Hall, Inc., (1982) pp. 109–118.

[2-5] Brusasco, R. and G. Devine, "Reduction of HRA Coating Rate Variability," Lawrence Livermore National Laboratory Report TST 92–114 (1992).

[2-6] Williams, J.M. and J.T. Rowen, *J. Vac. Sci. Technol. A* **5** (1987) 2760.

[2-7] Stephens, R.B., "Shell Wall Thickness by Fringe Position Measurement," General Atomics Internal Memorandum ICFT91/087 (1991).

SECTION 3

LABORATORY RESEARCH SUPPORT

3. LABORATORY RESEARCH SUPPORT

An important part of our activities is to provide technical and scientific support at the ICF laboratories.

3.1. CRYOGENIC TRITIUM RESEARCH AT LANL

John Simpson of General Atomics (GA) performed on-site cryogenic tritium research activities at Los Alamos National Laboratory (LANL).

3.1.1. INTRODUCTION

The cryogenics program at LANL during 1992 focused on the measurement of the surface quality of solid deuterium-tritium (DT), layered through a process known as beta layering [3-1 through 3-3]. Using this process, a nonuniform layer of solid DT can be driven to uniformity by radioactively-induced sublimation in which tritium beta decay produces temperature gradients across the solid fuel. These gradients drive the sublimation of solid DT from thicker to thinner layer sections, which produces layer uniformity over time. The process has been demonstrated to be very effective at producing highly uniform solid DT layers in both cylindrical and spherical geometries, inside vessels having both high and low thermal conductivities.

Previous experiments examined the rate of symmetrization [3-2 through 3-4], effects of helium exchange gas pressure [3-4] on rate constant and final symmetry, and the effects of DT aging on rate constant [3-4]. In order to determine how well this technique will meet the highly exacting design requirements for the uniformity of DT layers inside ICF targets, we conducted an experiment to examine the actual surface quality of the DT solid layer, down to the sub-μm level, using high resolution CCD imaging, a long range (LR) microscope, and very precise image analysis tools. This experiment was performed inside a cylindrical copper DT cell and produced a final DT layer thickness of 75 μm. The overall surface uniformity was measured to about 4 μm, and the individual surface defect modes were measured to about 0.2 μm using precise edge tracing software and Fast Fourier Transform (FFT) analysis tools.

3.1.2. EXPERIMENTAL SETUP

The configuration of the experimental apparatus and imaging system is shown schematically in Fig. 3-1. All of the components, except the Macintosh computer and electronics for the Photometrics CCD camera, are contained in a specially designed glove box that functions as a hood. This allows reasonable access to the internal apparatus when needed and provides a fourth level of tritium containment in case of failure of the primary containment of the DT cell.

The internal dimensions of the cylindrical DT cell are 2×2 mm for the inner bore, and 3 mm diameter $\times$ 1 mm deep for the counterbore shown at each end of the primary cylinder. This re-entrant design allows a clear view of the DT solid edge, unobscured by solid DT wrapping around from the cylinder to the sapphire window. The cell is copper sealed with sapphire windows and indium O–rings, providing a tightly sealed isothermal container for the DT charge.

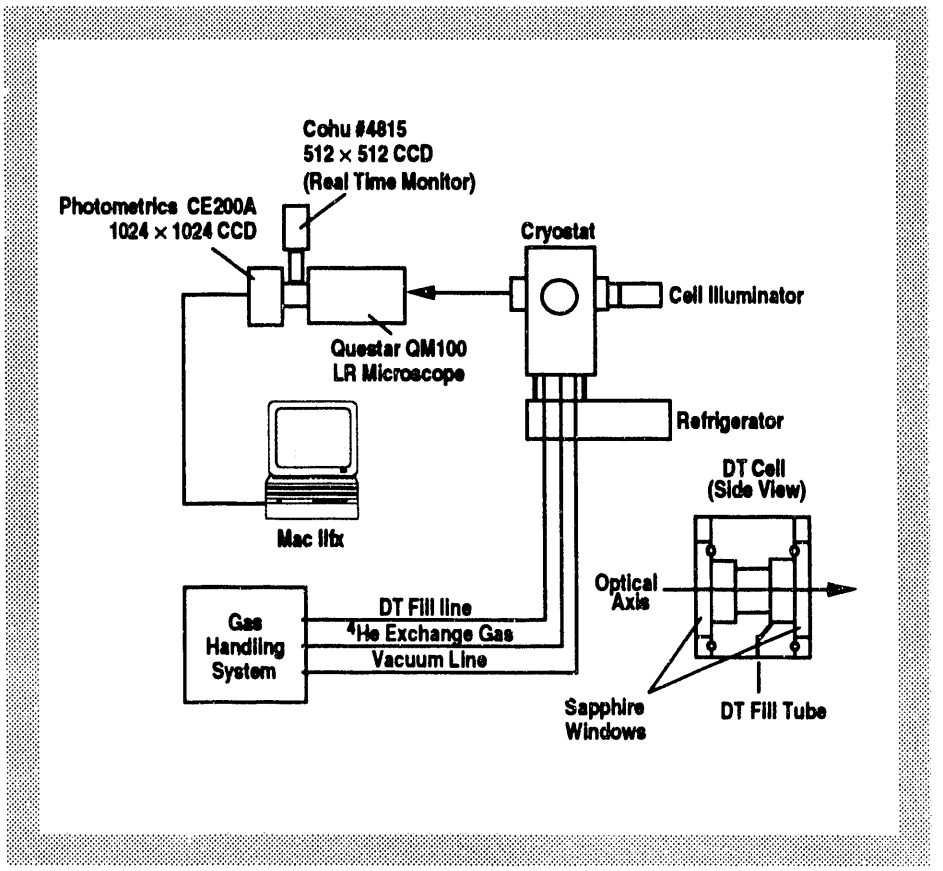

Fig. 3-1. β-layering experimental setup.

The optical system makes use of a Questar QM100 LR microscope coupled to a Photometrics CE200A CCD camera system, interfaced to a Mac II fx. The combination provides the equivalent of about an f/4 optical system with the cell image nearly filling the 1024 × 1024 pixel CCD array, giving a spatial resolution (1 pixel) of 2.5 μm. Using analysis software provide by Mapoles [3-5] of LLNL, we can measure solid layer uniformity to subpixel resolution. The Cohu camera allows real-time monitoring of the DT cell for camera focusing and to monitor the DT fills.

3.1.3. OPTIMIZATION OF IMAGE ACQUISITION PARAMETERS

To produce high quality images (and thereby best resolution), we examined the effect of several image acquisition setup parameters on image quality as determined by data scatter. Image quality was determined by the scatter (standard deviation) of the empty cell (or DT layer) radius, as it rotated over 2π. Data scatter decreases as image quality improves and is a function of image contrast, quality of focus, and image noise. The acquisition setup parameters that control these characteristics are camera exposure time, camera focus, and image frame averaging, respectively, so it was necessary to optimize them for best image quality.

The cryostat is cooled with a CT Cryogenics Model 22 refrigerator which causes periodic DT cell motion of about 30 μm (peak to peak) and which is another factor affecting image quality. The amount of cell motion that occurs during a single image exposure will smear the image and, consequently, the DT layer edge. Data scatter will increase accordingly. Additionally, averaging several image frames that were captured at different points on this motion cycle tend to smear the image and edges. These factors were considered when doing our acquisition parameter optimizations.

Figures 3-2 and 3-3 show results of image acquisition parameter optimization with respect to camera focus and exposure time, as well as multiple-image frame averaging. Figure 3-2 shows it is possible to find the best focus by examining the data scatter as the focus micropositioner is moved through that focus. The graph also shows that the best focus shifts slightly when the cryostat is cold, thus making it necessary to optimize focus after the cryostat is running at 21K. Six image frames were averaged for each of these curves, and the data set for the cold (moving) cryostat shows slightly more data scatter. Six-frame averaging was chosen as a result of earlier optimization experiments that showed that minimum data scatter occurred at about six frames averaged.

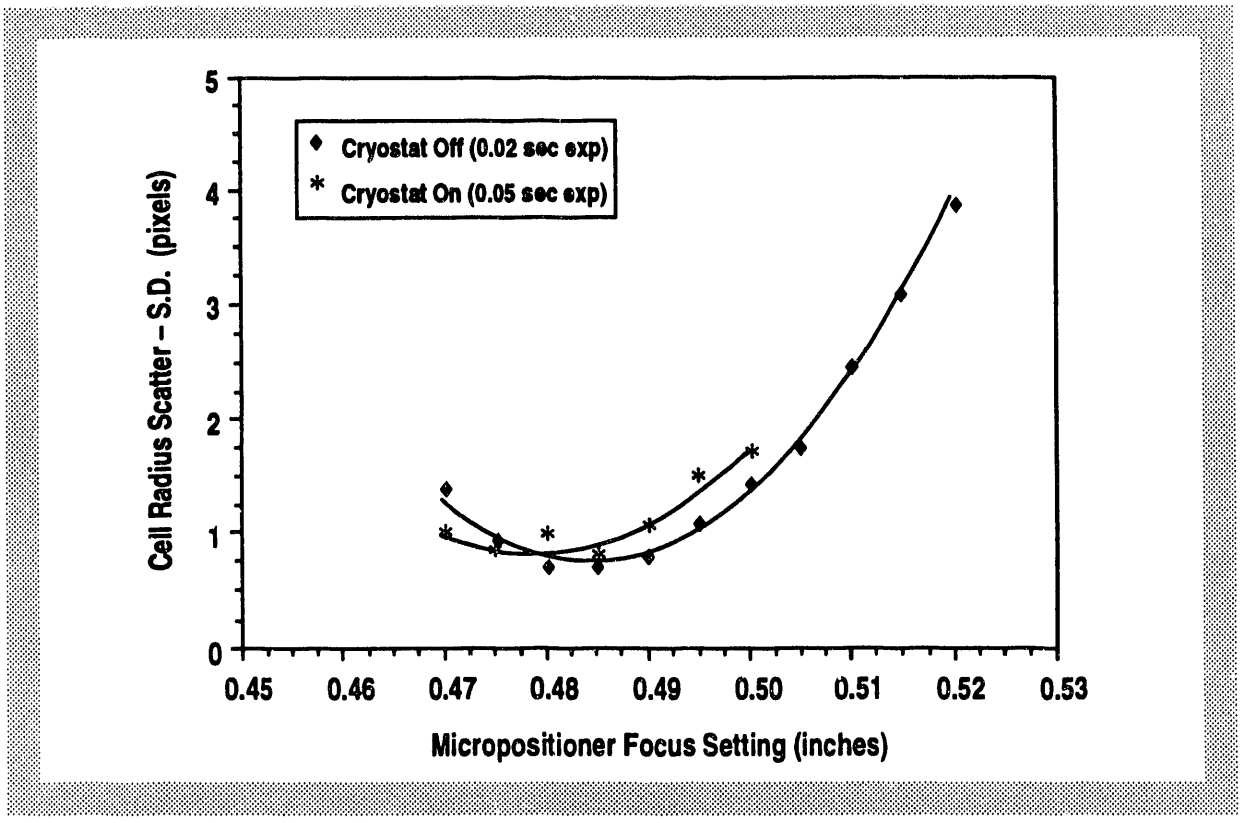

Fig. 3-2. Layering cell imaging system focus optimization (six frames averaged to determine scatter).

Figure 3-3 shows how camera exposure time and frame averaging affect image quality for both warm and cold (moving) cryostats. This graph shows that averaging six image frames with exposure times between 80 and 100 msec will optimize image quality to a resolution of about 0.6 pixels (1.5 μm). (The 120 msec exposure was actually saturating the entire central part of the image, although the DT layer edge was still clearly visible.) The lower curve shows that the resolution limit of just over 0.4 pixels (1.0 μm) is achieved only with the cryostat off. In order to achieve this limit of resolution, it may be necessary to trigger the camera shutter at the peak of the cryostat excursion (peak detection) or at the maximum rate of excursion (zero crossing detection).

3.1.4. EXPERIMENTAL RESULTS

The goal was to produce and analyze a 100 μm thick DT solid layer for symmetry and surface quality; we actually achieved 75 μm. Analysis tools included the MAC II fx with 32 MB of RAM running System 7, precision edge locator and analysis software provide by

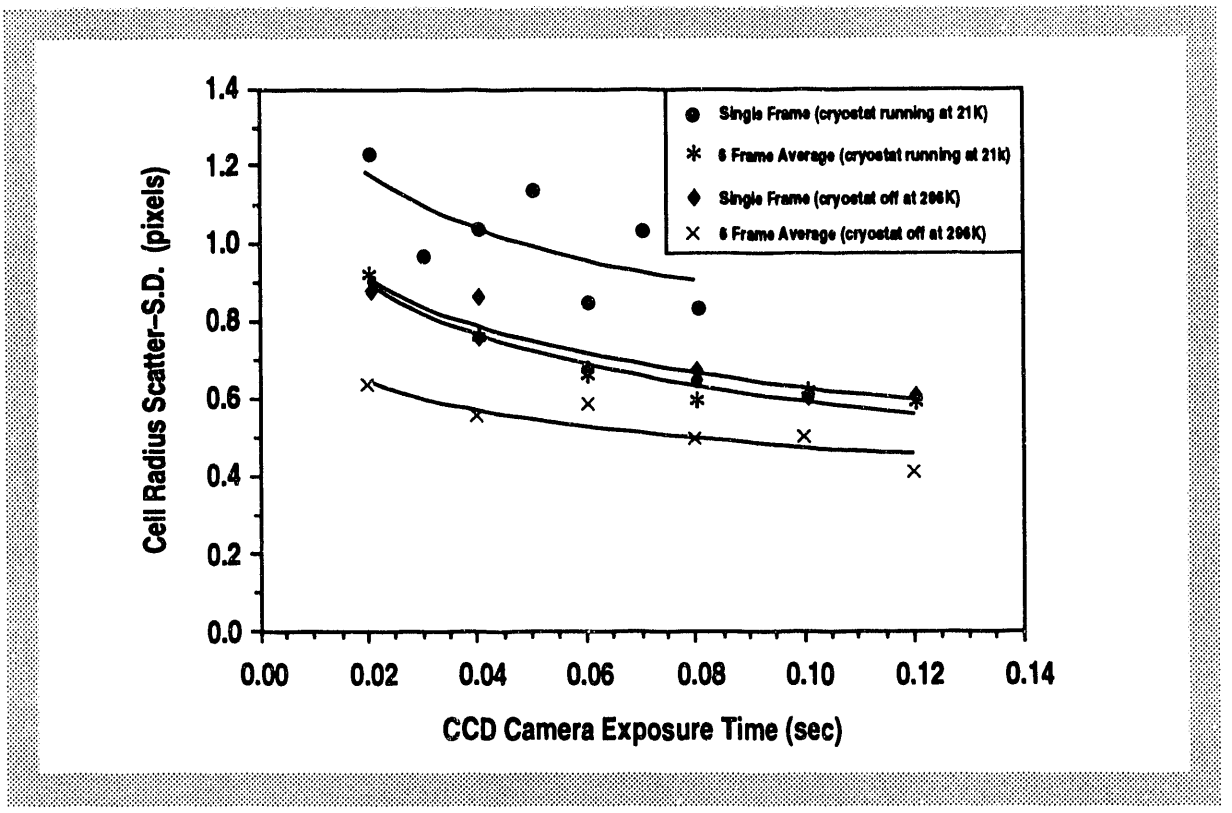

Fig. 3-3. Empty DT cell exposure optimization (single frame and averaged multiple image frames).

Mapoles of LLNL, an FFT analysis tool found in the Microsoft Excel 4.0 software package, and graphing tools found in DeltaGraph Professional.

Figure 3-4 shows the CCD image of the final layer as well as a polar plot of the DT layer inner edge and empty cell edge. The empty cell edge was chosen because the layering process had not been completed when we decided to stop the experiment, and it was difficult to accurately locate the edge of the cell with nonequilibrated DT solid covering that edge. Additionally, we wanted to accurately portray the relative data scatter of the cell edge and DT solid edge. The scatter in the average radius of the empty cell as shown in this figure is about 2.5 μm, whereas the scatter in the layer data is just over 4 μm, or about 5% of the solid layer thickness. We should be able to reduce the data scatter for our next experiments by using the optimal acquisition settings described above and synchronizing the camera shutter with the cryostat motion.

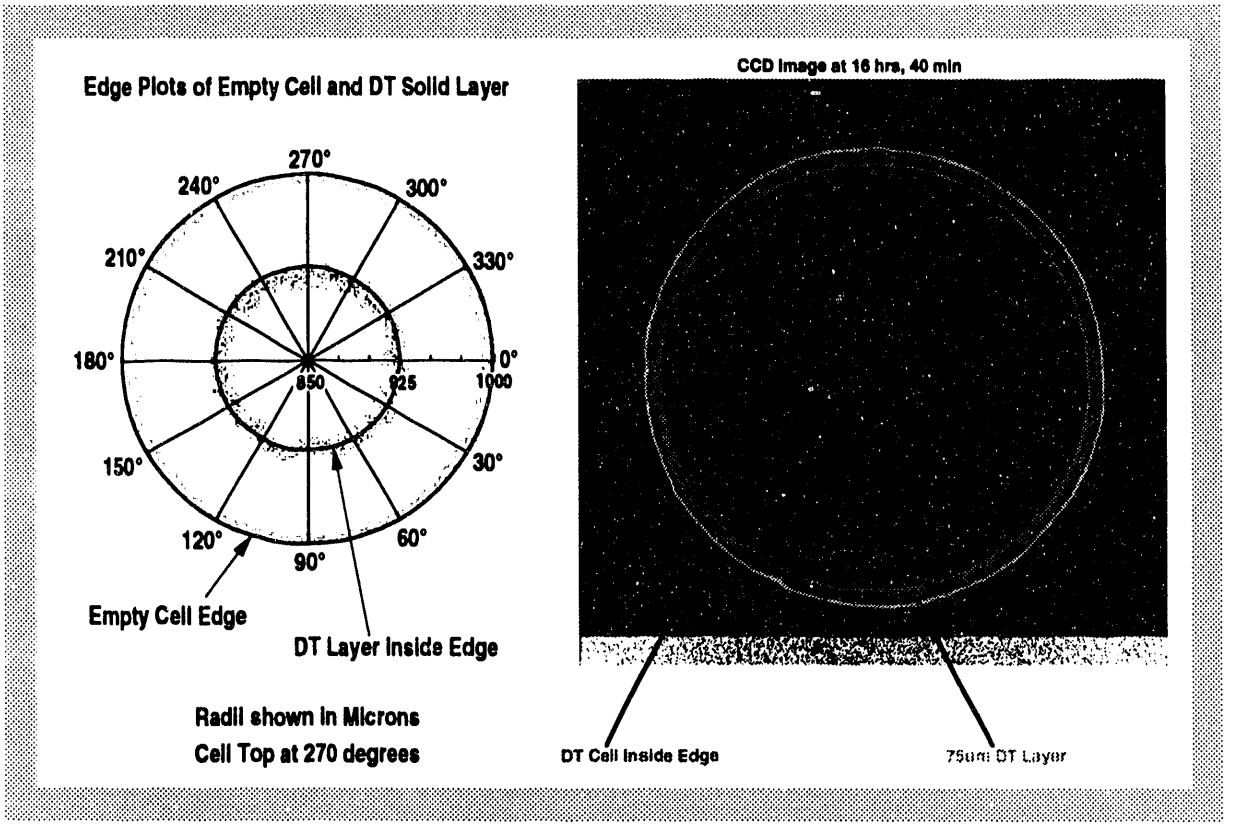

Fig. 3-4. Beta layering cell with DT solid layer.

The time constant for the layering process is normally about 30 minutes, with final equilibrium occurring after about 3 hr. For this cell geometry, however, the time constant and the time to reach equilibrium were much longer. This is the result of the re-entrant nature of the cell for which the view factor is not identical in all regions of this volume and, in fact, there are some regions that cannot "see" one another at all. Consequently, the DT layer did not reach equilibrium even after 16 hr, leaving a residual P1 (offset) defect for this layer.

We used a FFT algorithm to examine the modal surface quality or "finish" of this DT layer. The image analysis software, provided by Mapoles [3-5] of LLNL, sampled the layer edge at 1024 points, all of which were included in the FFT analysis. This analysis was done on an edge slice of the DT layer (i.e., the edge closest to the imaging camera at the interface of the front counterbore and the primary cylinder). The results of the first 128 modes of this analysis are shown in Fig. 3-5 with the empty cell data plotted along with the DT layer edge data. At all modes above 128, the data fell within an apparent 0.2 μm noise level and so are not shown. We were particularly interested in the higher mode defects, since they are most likely to induce implosion instabilities

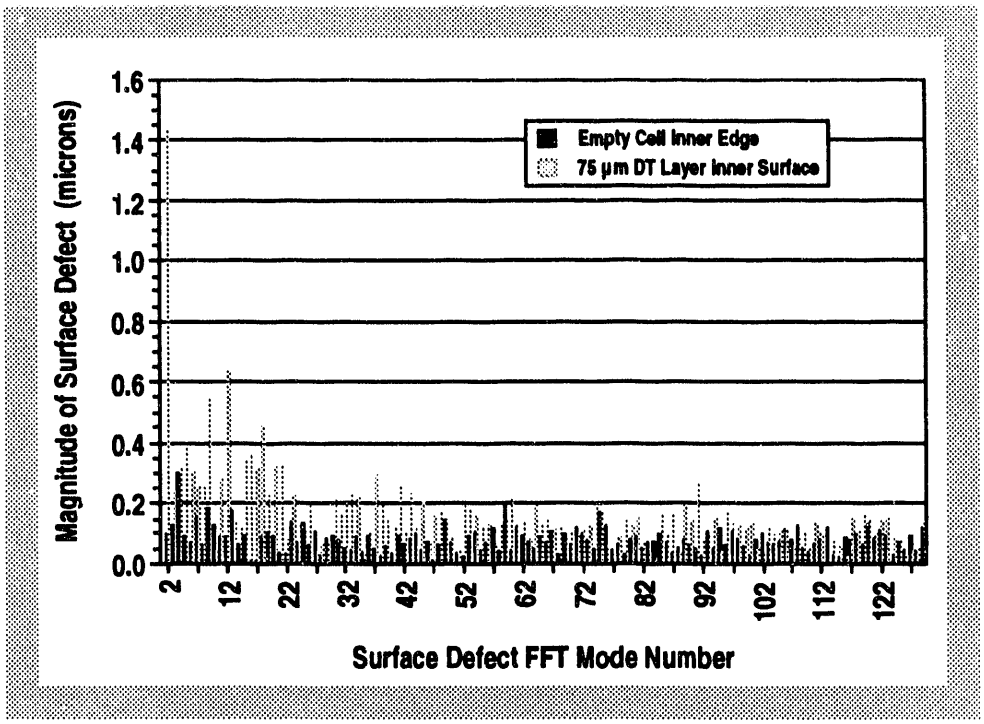

Fig. 3-5. FFT modal analysis of empty cell and DT solid layer.

during ICF target implosions. It is clear from this graph that this layer is extremely smooth for modes above 20, and even the lower order modes present have surface defects only 0.6 µm (0.8%) or less in height. The only significant mode present was the 1.4 µm P1 defect (offset), which was expected because we did not run this experiment to completion.

3.1.5. CONCLUSIONS

This experiment demonstrates that we can produce a thin DT solid layer and measure its surface quality to within 0.2 µm. This work also shows that there are no significant higher order surface defects and that the lower order modes are also quite small (0.8%). All defects may be reducible to the 0.2 µm noise level once we run an experiment to completion. Our next experiment will be an attempt to do just that, possibly followed by an experiment to determine how surface quality varies over time. This could determine the time window for which it is possible to successfully implode future beta-layered DT-filled shells.

For additional information, please contact J. Simpson (LANL).

3.2. CHARACTERIZATION DEVELOPMENT AT LLNL

Jim Sater and Don Bittner of W.J. Schafer Associates (WJSA) performed characterization development activities at LLNL.

3.2.1. CRYOGENIC MICROCALORIMETRY

There is a need in the ICF program for a means of nondestructively determining the amount of fuel contained in an opaque laser fusion target. Several techniques currently exist for determining this parameter in transparent targets. The University of Rochester's Laboratory for Laser Energetics (UR/LLE) uses a Fabry-Perot interferometer to determine the fill gas index of refraction which is related to the pressure. Another approach that exploits the dependence of the gas-liquid or gas-solid phase transition temperature on fuel pressure is used at LLNL by J. Sanchez and R. Upadhye [3-6]. They have constructed an apparatus that determines the transition temperature by slowly ramping the target shell temperature up through the "dew point" while periodically pulsing it with a laser. The apparatus operator uses a TV monitor to watch as the fuel evaporates with each laser pulse and then quickly recondenses. At the dew point, the fuel does not recondense and no change is seen on the TV monitor. The temperature is recorded, and the amount of fuel is calculated.

To meet the requirement of measuring the amount of fuel in an opaque target, we will use a calorimetric technique. Specifically, we will measure the specific heat of an opaque target in the temperature regime where the fuel changes to the gas phase (20 to 30K), by observing the temperature as a function of time while inputting a known heat load. The resultant temperature versus time curve will have a kink at the dew point of the fuel. A model based on the expected typical values produces the curve shown in Fig. 3-6. The heat capacity curve is calculated from the data, and a discontinuity is observed at the dew point (shown in Fig. 3-7 using the same model). Using the temperature of the dew point (the discontinuity in Fig. 3-7), the amount of fuel is calculated using published data [3-7], just as Sanchez and Upadhye have done.

Calorimeter Construction. The design of the calorimeter is crucial to the success of this technique. The calorimeter is operated at temperatures greater than 4.2K by using a dewar insert that is designed to be placed in a standard 60 or 100 liter liquid helium storage dewar. The sample holder is mounted at the end of the dewar insert (Fig. 3-8). Radiative and conductive losses are minimized by using low thermal conductivity materials to support the

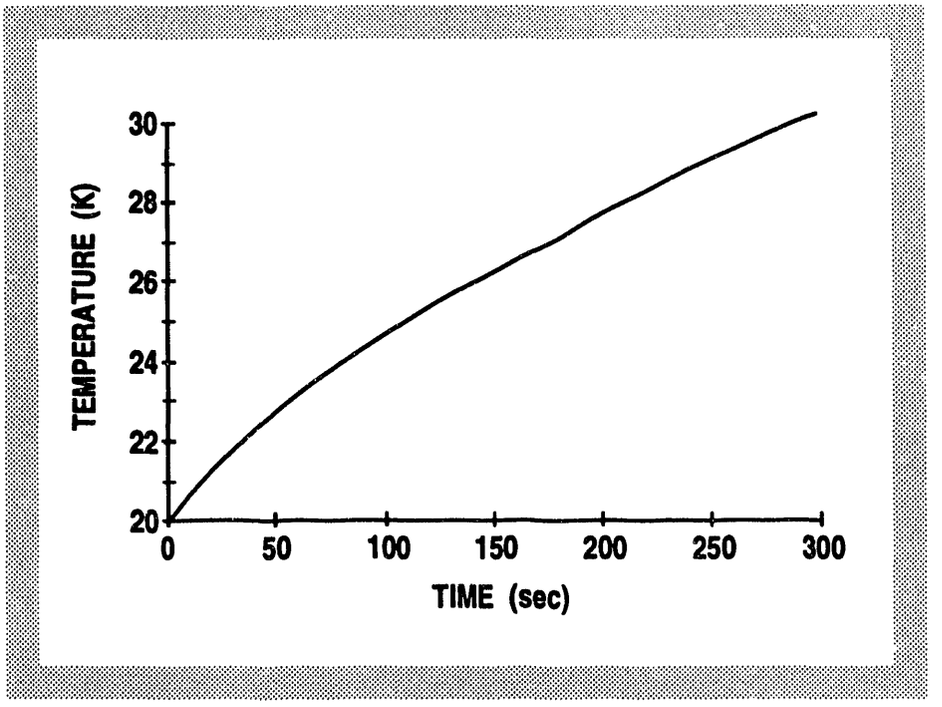

Fig. 3-6. Temperature versus time of the calorimeter for a 1 μW heat load.

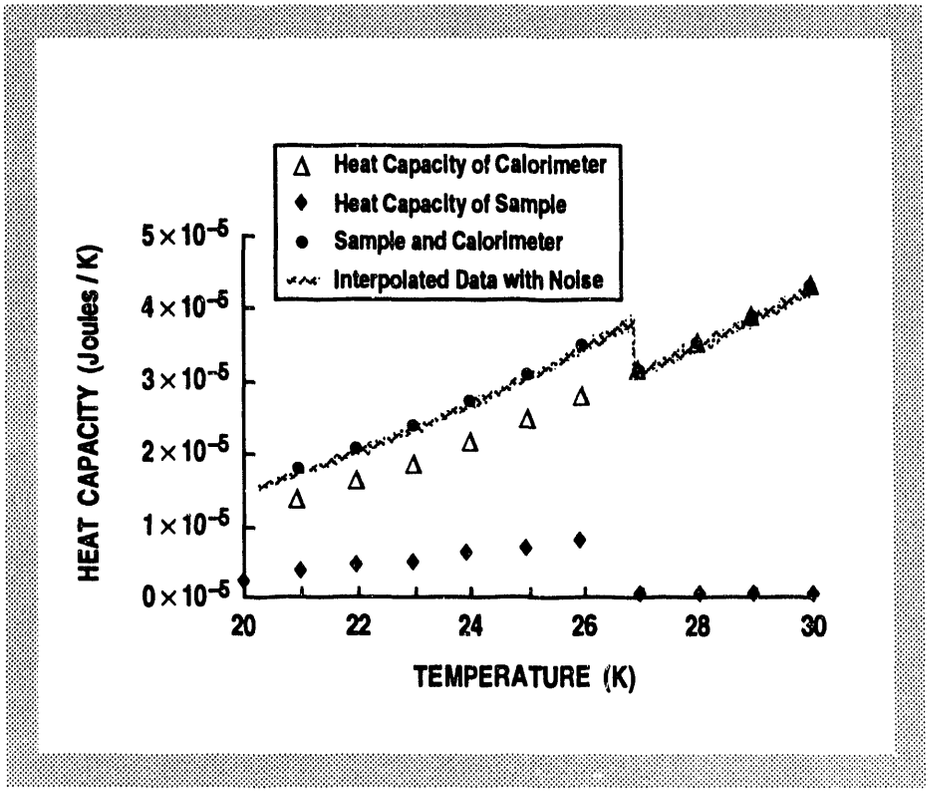

Fig. 3-7. Calculated heat capacities are the discreet points. The solid line shows interpolated "results" with white noise artificially added.

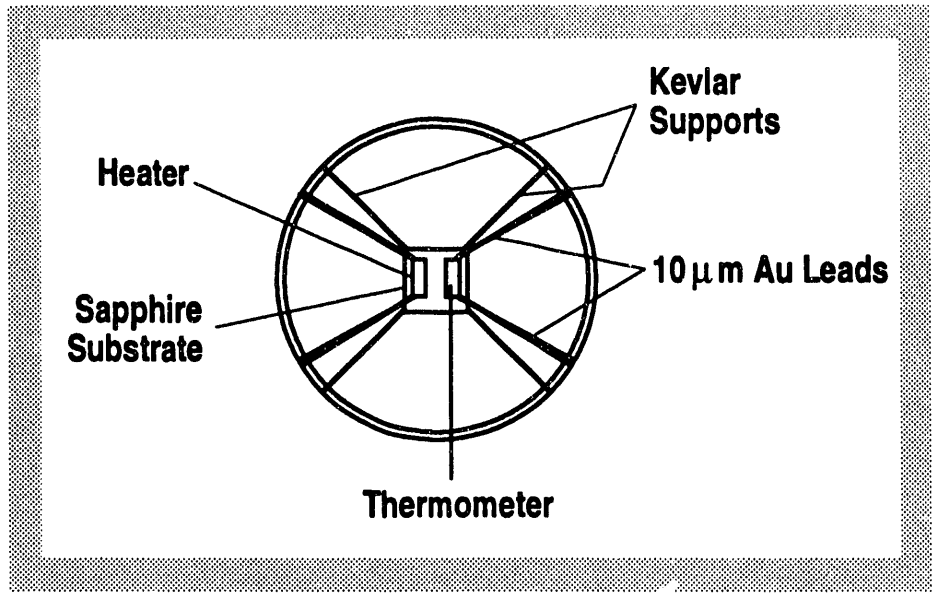

Fig. 3-8. Top view of Cu ring/calorimeter support.

sample holder and by maintaining a temperature regulated shield at the same temperature as the sample holder. The temperature is measured with resistance thermometers and adjusted with electronic temperature controllers.

The sample holder is made out of sapphire because of its desirable characteristics (high thermal conductivity and low heat capacity). This will increase the signal-to-noise ratio for our experiment and decrease the time it takes for the sample and sample holder package to come to equilibrium.

A heater made of nichrome will be vapor deposited on the sample holder and a small resistance thermometer will be glued down. The thermometer and heater contribute less heat capacity to the cell than commercial bulk thermometers and standard heaters.

Expected Sensitivity. We have used published data [3-7] for DT gas and values from standard cryogenic handbooks to look up or calculate heat capacities as a function of temperature for the sample and calorimeter. For some materials, we made a reasonable estimate of their properties based on information from similar materials. Heat leaks were checked to ensure that they were maintained at a tolerable level. We calculated the temperature change as a function of time for a given heat load. We then added a known amount of noise to the "temperature measurement" to see if we could recreate our data with the required accuracy necessary to calculate a fill pressure. The parameters assumed for a typical shell were:

- 25 atmospheres fill pressure.

- 300 μm inner diameter.
- 30 μm thick plastic wall.

The dew point of this shell occurs at 26.9K. The heat capacity of the empty shell was calculated to be 1.42 μJoule/K. The heat capacity of the sample in the filled shell ranged from 3.4 to 6.8 μJoule/K between the triple point and the dew point. It fell off to about 0.25 μJoule/K past the dew point.

The heat capacity of the calorimeter was calculated to be approximately 24.5 μJoule/K at 25K. This included the wires, sapphire substrate, heater, thermometer, and adhesives. A temperature dependence to the third power was assumed for the calorimeter heat capacity.

Heat leak to the sample must be minimized to ensure success of this technique. We use a high vacuum around the sample holder to eliminate gaseous cooling. The major heat leak then is due to the wires from the thermometer and heater pad. For example, the heat leak for 8 to 10 μm diameter Au wire was found to be 6×10^{-6} ΔT W. ΔT is the temperature difference between the sample cell and the point where the wires are thermally anchored. Controlling ΔT is the most critical task for a successful experiment.

If we look at Figs. 3-6 and 3-7, we can see how a 1 mK temperature noise affects our predicted signal. An inflection in Fig. 3-6 is visible at about Time = 180 sec. Figure 3-7 shows the heat capacity of various components. The sum of the heat capacities of the calorimeter and sample is equal to the heat input divided by the first derivative of the curve in Fig. 3-6. The inflection point has now become a discontinuity, and the effect of the noise is more noticeable though not intolerable.

For a relatively large step in the heat capacity, the dew point should be easily observable. If there were no instrumental broadening of the heat capacity transition between the gaseous state and saturated state, we could determine the dew point to within the accuracy of our thermometer. We illustrate this point in Fig. 3-9 which is an expansion of Fig. 3-7 around the dew point. Our data is on about a 10 mK grid and has been filtered by a simple seven-point smoothing algorithm. With this "broadening of our signal," we can still estimate the dew point to within 40 mK giving a 1% accuracy for determination of fill pressure.

For additional information, please contact Dr. J. Sater (WJSA).

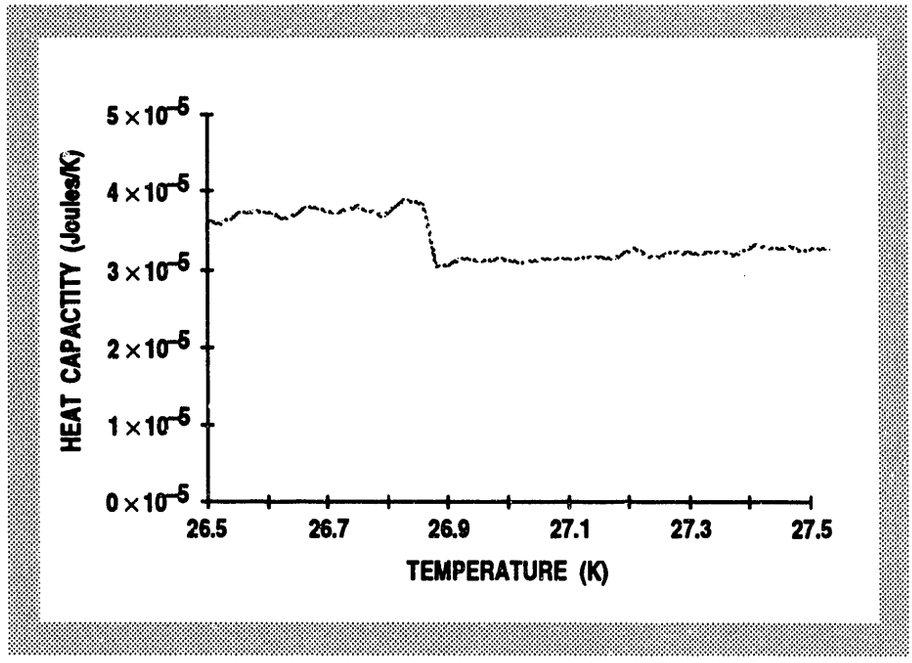

Fig. 3-9. Interpolated data with noise.

3.2.2. AUTOMATIC TARGET SELECTOR (ATS)

Desired Capabilities of an Automatic Target Selector (ATS). The ATS will be used for sorting and roughly characterizing polystyrene mandrels before they have been coated with polyvinyl alcohol. This process is a labor intensive task and is ideal for automation. As a minimum, the ATS must be able to characterize the diameter and circularity of a series of shells randomly placed on a substrate. Circularity is characterized rather than sphericity because the ATS only takes one view. After identifying the shells within a user-specified tolerance, the system must remove the shells to an appropriate container. Additional desirable features include the ability to measure concentricity of the inner and outer surfaces of the shell and to measure the wall thickness.

Measurement Steps for the ATS. The ATS is made up of a microscope, a computer, computer-controlled translation stages, and an interferometer attachment for the microscope. We plan to operate the interferometer in the white light mode with the shells placed on the translation stage at the focal plane. The optical image produced by the microscope is detected by a video camera. A frame grabbing board in the computer converts the video signal into an 8-bit computer image. We use commercially available subroutines and custom code to analyze the image.

The planned operating procedure is to place plastic shells from the drop tower on a flat mirror under the ATS microscope. It is important that the shells be separated from one another since two touching objects will appear to be one object to the computer.

The ATS software is started. The operator enters the required diameter, wall thickness, and uniformity tolerances. The ATS examines the shells for diameter, circularity, concentricity, and wall thickness. Shells that pass will have their position and specifications recorded in a file.

Finally, the ATS will pick up the shells that have passed and put them into a capillary. It will be necessary to have the operator change capillaries when full.

Current Status. Steve Mance of LLNL has worked on the ATS for approximately one and a half years. During this time, the major components of the ATS have been acquired and assembled. The ATS is now capable of scanning the shell sample holder and selecting shells according to size and circularity. It can load these shells into a capillary. This is ideal since shells are typically placed in a capillary for the next coating step anyway.

We still need to implement the methods for measuring wall thickness and concentricity of the inner and outer surfaces of the shell. We also need to do a series of validation runs to determine our error bars.

For additional information, please contact Dr. J. Sater (WJSA).

3.2.3. SURFACE CHARACTERIZATION BY INTERFEROMETRY

We are looking into the use of interferometry as a method to examine the surface finish on capsules. Full-sphere interferometric measurements have been made for large spheres (~1.5 cm o.d.) [3-8]. These optical measurements are based on subaperture optical testing techniques (SOT). With these techniques, large areas can be probed in relatively short periods of time. SOT is a method for measuring the optical path length differences (OPD) of large optical elements without the need for a large, accurate, and expensive reference element. Subregions of the test element are measured separately using a small reference element. The set of subregions is then combined to generate a full surface description.

For this analysis, the sphere is described in terms of low-order spherical harmonics (ℓ–modes). Each subregion is fit to local Zernike polynomials, then the subregions are

combined and the global Zernike fit is converted to spherical harmonics. The full sphere analysis was used to fit the low order ℓ–modes, up to $\ell = 6$.

The data corresponding to higher order modes is not used. This project is an attempt to extend this technique to determine the higher order ℓ–modes. Figure 3-10 is a schematic diagram of the optical system. With this system, one is comparing the capsule surface with the spherical wave front produced by the output lens. We initially set out to look at an assortment of post-mounted capsules. We took an initial qualitative look at several different types of shell surface finishes which included:

- Bumpy — fringes everywhere.
- Transparent/smooth — fringes from multiple reflections.
- Opaque/smooth — few fringes, only one surface.

One set of experiments was run using a precision ball bearing. We expected to produce an OPD plot which was generally flat, indicating a spherical bearing, but with the many high frequency modes indicative of an unpolished surface. The results were as expected. Other experiments were run using coated glass and plastic capsules. The glass capsule

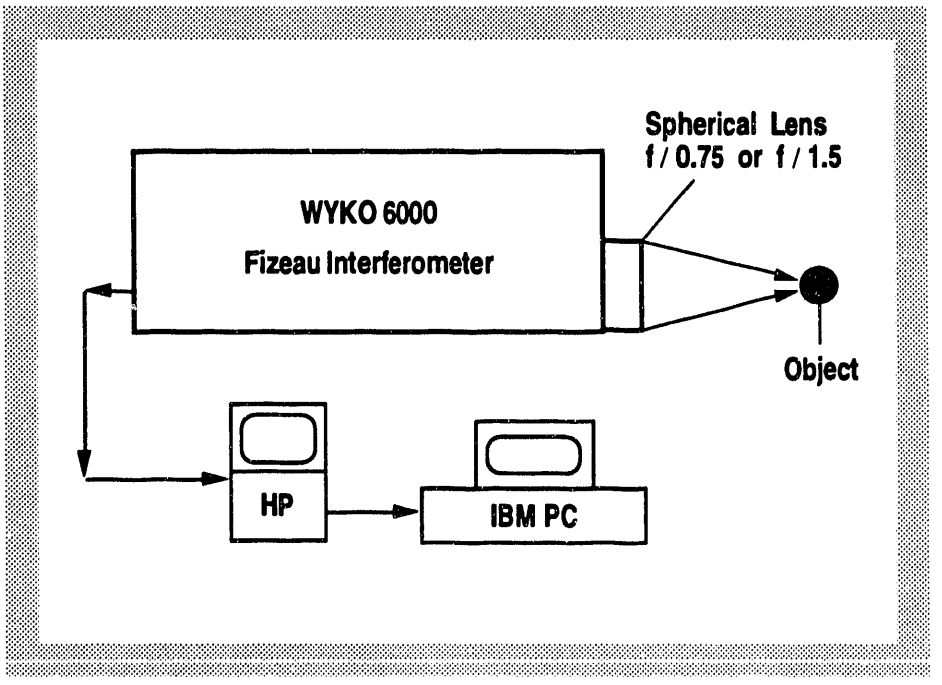

Fig. 3-10. Interferometer system.

produced an OPD plot with a slight saddle shape but the plastic capsule OPD plot had a significant saddle shape. The OPD plot comparing a spherical surface and an elliptical surface would have a saddle shape. A possible cause for this shape is that these capsules are produced in a drop tower. The forces acting on the shells as they form while falling through the tower may produce shells with a slight elliptical shape.

From our initial experiments we have come to the following conclusions:

1. We can generate interferograms of the surface of opaque shells.

2. We will not be able to see features with steep slopes due to limitations of the interferometer system. This is determined by the 256×256 CCD array and the constraint that the maximum height change between pixels is $\lambda/4$. This corresponds to height changes of about 1600Å for ℓ = 6328Å (He-Ne laser).

3. We need to understand the analysis procedure of the interferometer system. Based on what one expects to see in the OPD plots and the results of the glass shell and ball bearing, the plastic sample deviates noticeably from sphericity. We need to confirm that this is, in fact, the case.

4. We need to come up with a suitable test sample. Until now, we have been using samples that were readily available. We need a known system to compare to the interferometric analysis.

For additional information, please contact Dr. D. Bittner (WJSA).

3.3. REFERENCES

[3-1] Martin, A.J., R.J. Simms, and R.B. Jacobs, *J. Vac. Sci. Technol.* **A6** 1885 (1988).

[3-2] Hoffer, J.K., and L.R. Foreman, *Phys. Rev. Lett.* **60** (1988) 1310.

[3-3] Hoffer, J.K., L.R. Foreman, J.D. Simpson, T.R. Pattinson, *Physica B* **165&166** (1990) 163.

[3-4] Simpson, J.D., J.K. Hoffer, and L.R. Foreman, "Beta-Layering of Solid Deuterium-Tritium in a Spherical Polycarbonate Shell," *Fusion Tech.* **21** (1992) 330.

[3-5] Mapoles, E. of LLNL provided image processing software for edge finding and analysis.

[3-6] Sanchez, J.J. and R.S. Upadhye, "A Non-Destructive Method for Measuring the Fill Pressure and Permeability of Plastic Shells," Lawrence Livermore National Laboratory ICF Quarterly Report, Vol. 1, 1 (1990).

[3-7] Souers, P.C., Hydrogen Properties for Fusion Energy, 1st ed., University of California Press, Berkeley, California (1986).

[3-8] Day, R.D. and G.N. Lawrence, *Precision Engineering* **11** (1989) 3 .

SECTION 4

MICROENCAPSULATION PROCESS DEVELOPMENT

4. MICROENCAPSULATION PROCESS DEVELOPMENT

An important goal of our work is to develop improved ICF target fabrication techniques that will facilitate more efficient production of targets. Production of polymer shells is an area targeted for improvement.

4.1. INTRODUCTION

Microencapsulation is one of the two common techniques (the other being drop tower) used to produce polymer shells for ICF target fabrication. Microencapsulated shells have the advantage of being more concentric than those produced in the drop tower. It also appears that the size of microencapsulated shells may not be as limited as the size of drop tower shells. However, the surface finish and wall integrity (presence of vacuoles) of the microencapsulated shells are not as good as the drop tower shells.

Currently, microencapsulated shells are produced via the complex emulsion ("shake and toss") technique. This method produces shells with a broad size distribution. Target quality shells with diameters between 250 and 500 μm are typically harvested from a batch. As the requirement for larger shells increases, it becomes more important to produce these shells in a consistent manner. This need has led to the development of the triple-orifice controlled-mass system.

The objective of this task was to improve the microencapsulation process of polymer shell production; both for the controlled-mass technique and the complex emulsion technique. This goal was accomplished through three efforts. The first was to further our understanding of the fundamental polymer science processes of sphere formation. The second was to use statistical process analysis to identify the most important variables in the microencapsulation technique. The third was to construct a triple-orifice droplet generator and develop the controlled-mass method of microencapsulation.

4.2. POLYMER SCIENCE

Polymer science issues are critical in the production of polymer shells using both the drop tower and the microencapsulation technique. In the microencapsulation technique, polymer solution thermodynamics and phase behavior and phase transition kinetics are just two of the important scientific issues. These two topics address the problems of surface finish and wall integrity. Vacuoles, small voids in the wall of the polystyrene shell, form when the composition of a portion of the wall of the shell reaches a point where maintaining a single, well-mixed phase is energetically unfavorable.

The Gibb's Free Energy for a ternary system containing solvent, non-solvent, and polymer can be described by the following equation.

$$\frac{\Delta G}{RT} = \phi_s \ln\phi_s + \phi_{ns}\ln\phi_{ns} + \frac{\phi_p}{X}\ln\phi_p + \phi_s\phi_{ns}\chi_{s,ns} + \phi_s\phi_p\chi_{s,p} + \phi_p\phi_{ns}\chi_{p,ns}$$

where ϕ_s: Volume fraction of solvent.

ϕ_{ns}: Volume fraction of non-solvent.

ϕ_p: Volume fraction of polymer.

X: Number of segments per polymer chain.

$\chi_{a,b}$: Interaction parameter between a and b.

When the derivative of free energy with respect to composition becomes negative, the free energy of the system can be lowered by separation into two phases: one polymer rich (concentrated polymer), and one polymer poor (very dilute polymer). This process corresponds to the formation of vacuoles.

As the microencapsulated shell "cures" or hardens, the composition of the wall changes with time. This composition change marks out a "cure" trajectory on a ternary phase diagram. When the composition crosses the binodal curve, which we measure as described below in Section 4.4.1, phase separation can occur.

The rate at which phase separation occurs is also important to the formation of vacuoles. After the composition of the wall enters the two-phase region, the system undergoes phase separation at a finite rate, which depends on the extent to which the free energy will be lowered through phase separation. The greater the difference in free energy, the greater the rate. Another important factor in phase separation kinetics is the mobility of the various components (i.e., polymer). As the polymer becomes more concentrated, the mobility of individual polymer chains decreases. If the mobility becomes small enough, it is possible that phase separation will take place so slowly as to be undetectable before the shell is completely hardened. Section 4.4.2 describes the measurement of phase separation kinetics.

4.2.1. PHASE DIAGRAM MEASUREMENTS

The objectives of this portion of the task were to set up the Thermal Optical Analysis (TOA) equipment and to measure the phase diagram of defined polymer/solvent/nonsolvent systems. The TOA equipment consists of a microscope, a Mettler FP900 Thermosystem controller, and an FP82HT Hot Stage. Solutions of known compositions are sealed in glass ampules for measurement. Measurement is performed by heating the sample in the Hot Stage until it becomes a single-phase well-mixed solution. Figure 4-1 shows the raw data for methyl ethyl ketone (MEK)/water/polystyrene. Each data point represents the average result for a single sealed ampule that was measured at least three times. Above the cloud point temperature, the solution is clear. Below this temperature, the solution phase separates, becoming cloudy. Using Fig. 4-1, a ternary phase diagram of the mixture may be calculated at a wide range of temperatures. Figure 4-2 is the phase diagram at 40°C for MEK/water/polystyrene. This temperature was chosen because the triple-orifice system was most often operated at 40°C during FY92 while producing shells. As shown in Fig. 4-2, phase separation occurs at an approximate water concentration of 4% by weight over a range of polystyrene concentrations.

4.2.2. PHASE SEPARATION KINETICS

Phase separation kinetics were measured by laser light scattering (turbidity) through a film of a known composition. The equipment consisted of a HeNe laser, a neutral density filter, a sample cell to hold the film, a photodiode detector, and a computer equipped with a data acquisition board to retrieve the data. The goal of the experiment was to lay down a thin film of a polystyrene solution, contact it with water, and measure the change in turbidity as a

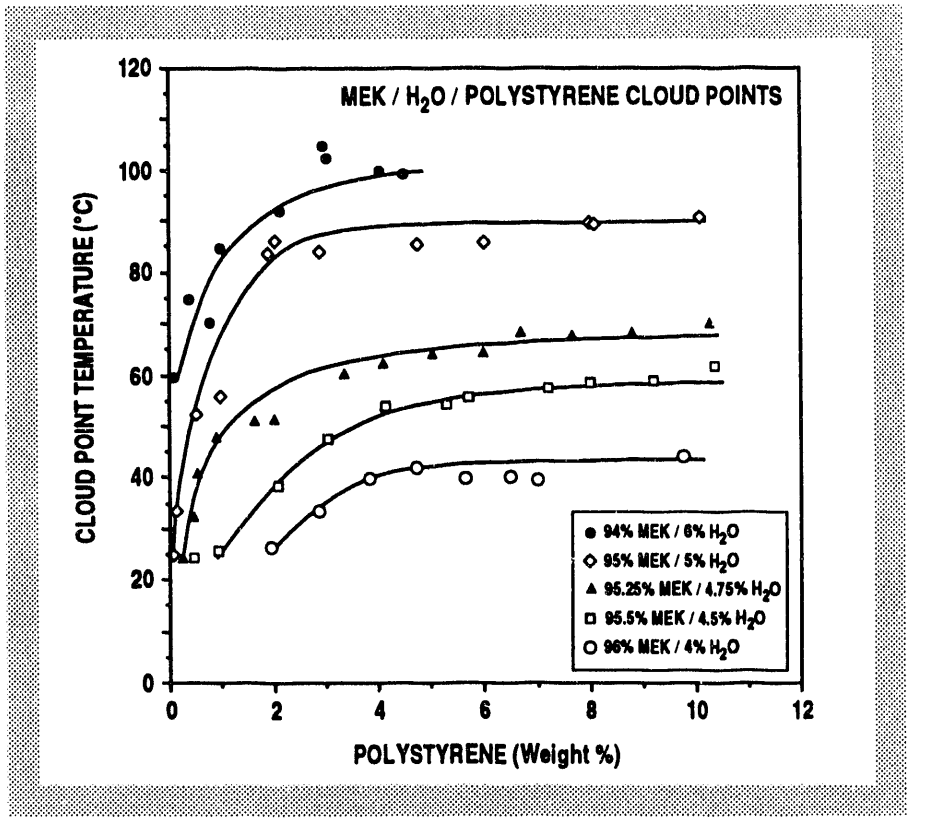

Fig. 4-1. Data from TOA experiments used to determine the phase diagram for MEK, polystyrene, and water. Each data point represents a separate sealed ampule.

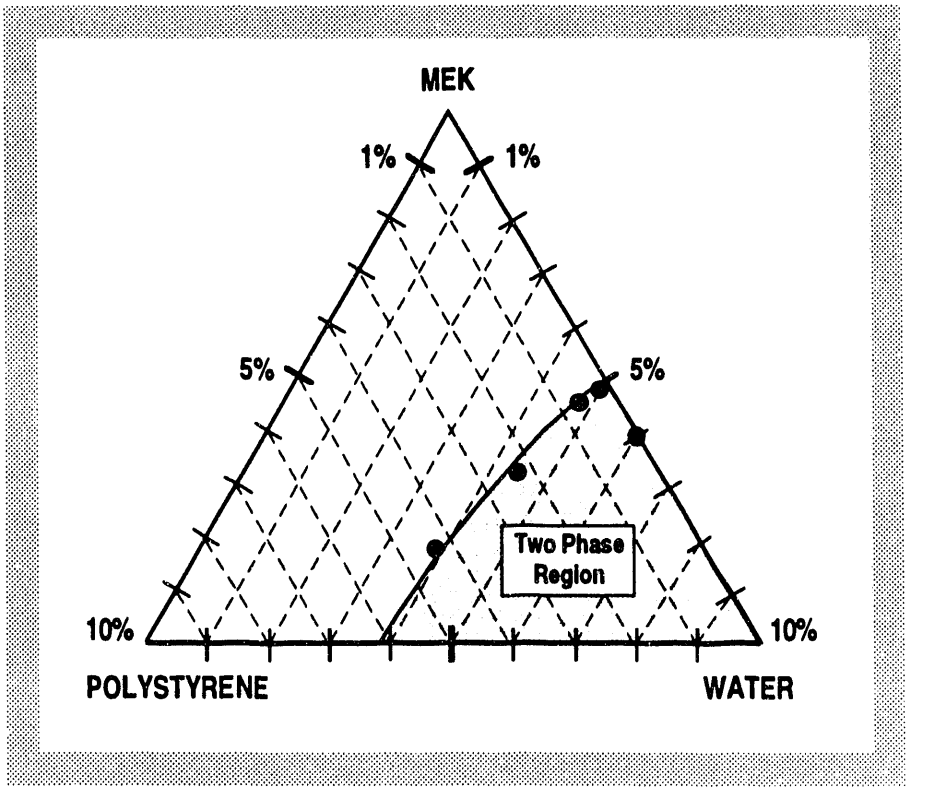

Fig. 4-2. Ternary phase diagram of MEK, polystyrene, and water at 40°C as measured by TOA. Inside the shaded area, the mixture is cloudy (phase separated).

function of time. Because of the low viscosity and hydrophobicity of the polymer solution, it proved to be extremely difficult to obtain meaningful data. After a great deal of effort, a method was developed where the solution was contacted with water between two microscope slides. Figure 4-3 shows the result for one such experiment on a solution of 5% polystyrene in 1,2-dichloroethane and MEK. The result shows that phase separation is occurring within only a few seconds after being contacted with water.

For additional information, please contact Dr. D. Soane or Dr. D. Nelson (STI).

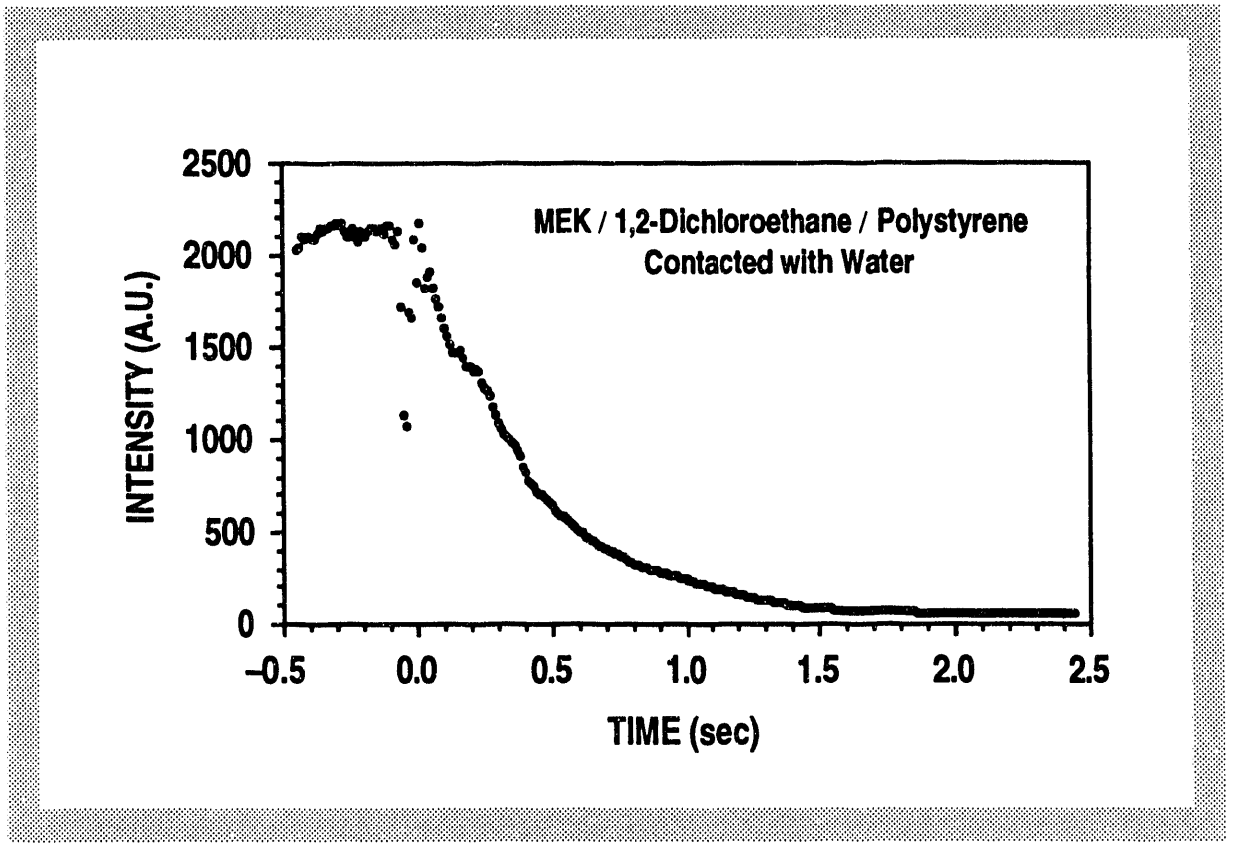

Fig. 4-3. Graph of transmitted intensity versus time for a solution of polystyrene in MEK and 1,2-dichloroethane upon contact with water at time equals zero.The decrease in intensity is due to cloudiness which occurs due to phase separation in the presence of water.

4.3. STATISTICAL PROCESS DEVELOPMENT

4.3.1. INTRODUCTION

We have designed a series of experiments to analyze the complex emulsion microencapsulation process as it was brought from Osaka, Japan [4-1]. The process concept is straightforward: one makes a water-organic solvent-polystyrene emulsion, introduces the emulsion into a stabilizing aqueous solution, and removes the organic solvent from the polystyrene leaving behind a rigid shell. The process makes reasonable shells for current needs but with inconsistent quality. Furthermore, higher quality, larger, thin-walled shells will be needed in the near future. By using statistical experimental design, we endeavored to identify the main factors affecting quality and size and to begin controlling the process.

The results of the experiments were better than expected, especially concerning size range. The average diameter of the shell batches ranged from 0.11 to 1.8 mm with the largest shell being 6.1 mm. The average wall range was from 3.2 to 113 μm. The large ranges indicate a strong probability that the process can be set to produce the proper size. The concern is that the larger shells are of lower quality. Extremely high-quality shells were produced, but not in the larger size range. Further experiments are needed to optimize size and quality simultaneously. Still, the results of this initial experiment are immediately applicable to shell production using the Osaka process and have implications for development of the droplet generator process.

4.3.2. EXPERIMENTAL DESIGN

The Osaka process concept is straightforward, but the actual processing is not. There are polymer/solvent/nonsolvent interactions, viscosity and surfactant effects, and mechanical and thermal processing considerations. We studied microencapsulation literature for similar techniques and decided that 16 independent variables (factors) realistically could be affecting the quality or size (responses) of the final product. Sixteen factors are too many for a complete analysis; they had to be reduced to a smaller number of effective factors. A "fold-over" Plackett-Burman screening design was chosen.

A Plackett-Burman design is based upon a four-trial matrix system [2-2]. Thus, all designs will have a multiple of four as the number of trials (4, 8, 12, 16, 20 . . .). Each design

of N trials can analyze up to N–1 factors for their level of effect. This is a tremendous amount of information for so few runs, but there are two important limitations. First, the results only indicate the strength of the effects. Each factor is run at two levels: high and low. How the effect changes between these levels is totally beyond this experiment. Second, in a standard design, the interactions between factors are not studied. This second limitation was reduced by using a fold-over design. The fold-over design repeats the experiments but with the high and low values reversed. This adds two-factor interactions to the analysis. Thus, our final design for the 16 factors was 2×20 or 40 trials, with each factor run at its low and high limit (see Table 4-1).

The levels of the factors are extremely important. The high and low levels must be different enough to show if a factor does indeed have an effect. However, if a level is set too extreme, no shells will be produced. A missing data point significantly weakens the design. To assure that shells would always be produced, we conducted tests to establish the limits of the ranges. The internal and external solutions were alternately dyed, and the lack of production or destruction of shells was noted. This set the limits of the ranges.

4.3.3. RESULTS

The forty trials were run in random order with the shells characterized en masse only after all the experiments were run. This ensured unbiased results and consistent characterizations. Approximately 30 shells from each trial were individually characterized for diameter, wall thickness, uniformity, and polyvinyl alcohol (PVA) entrapment using a Zeiss interference microscope. PVA entrapment was easily monitored as 1.0% methylene blue had been added to all PVA solutions, regardless of the PVA concentration. Any indication of blue color within the shell was considered entrapment; there was no ranking of degree. The number of colored shells per batch were then totaled to determine the percent contaminated.

Small voids in the shell wall (vacuoles) were determined by scanning the entire batch using a 100X phase contrast objective on a Nikon compound microscope (approximately 1500X total magnification). This generated a relative vacuole density ranking for the batch.

The results per batch were summarized, compiled, and analyzed using the PC program Statgraphics. For ease of visualization, a standardized Pareto plot was made for each response. A Pareto plot is a histogram of the absolute values of the effects divided by the standard error. The chart includes a vertical line at the critical t-value for an $\alpha = 0.05$ (this equals a

TABLE 4-1
FACTORS ANALYZED IN SCREENING EXPERIMENTS

EXPERIMENTAL FACTORS	LOW	HIGH
Polystyrene Concentration	4 wt %	10 wt %
Polystyrene Molecular Weight	22K	200K
Solvent in Organic Solution	Benzene	MEK
Organic Solution in Emulsion	3.0 g	5.0 g
Water in Emulsion	1.0 g	2.5 g
Temperature of Emulsion	25° C	55°C
Mixing of Emulsion	5 sec	20 sec
Polyvinyl Alcohol (PVA) Concentration	0.1 wt %	5.0 wt %
Temperature of Bath	55°C	85°C
Increase Temperature in Bath	No	Yes
Angle of the Stir Blades	45°	90°
Initial Stir Rate	No Vortex	Vortex
Curing Stir Rate	60 rpm	90 rpm
Time of Curing Step	3 hr	6 hr
Temperature of Rinses	25°C	85°C
Solvent Used in Rinses	Water	Isopropanol

95% confidence level). Any bar that exceeds the line will have a statistically significant effect. The Pareto plot for the mean diameter is shown in Fig. 4-4. Table 4-2 summarizes the rest of the results.

In Table 4-2, the first column lists the six responses with arrows indicating the direction we wish to push each response. The remaining columns list the statistically significant factors with arrows indicating which screening level (high or low) had

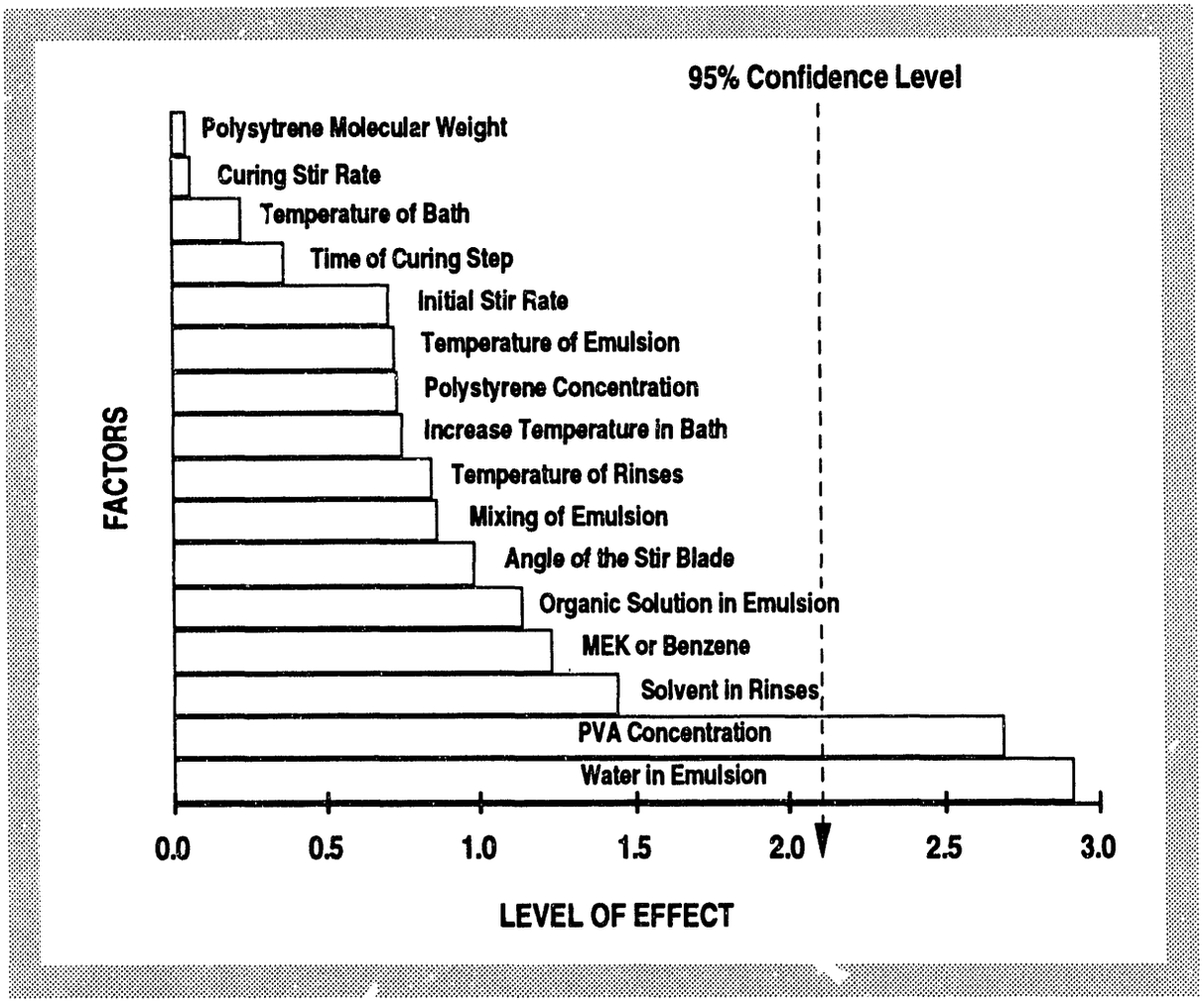

Fig. 4-4. Pareto chart for mean diameter. Only two factors, PVA concentration and water in emulsion, are statistically significant.

the desired response. When all the arrows in a column point in the same direction, all of the indicated responses are improved. The problem occurs when the arrows contradict each other, as in the case of polystyrene molecular weight. To overcome this, there are two options: pick a compromise value, or attempt to negate an effect with other factors.

The mean diameter effects deserve further comment. Strictly speaking, the organic solvent mixture is not statistically significant. This is listed as MEK versus benzene. It refers to the use of a 44 to 56 volume percent MEK and 1,2-dichloroethane or a 50 to 50 volume percent benzene and 1,2-dichloroethane. (The ratios are set to provide a density of 1.05 g/cc to be neutrally buoyant during processing.) Using the standard Osaka conditions, there

TABLE 4-2
SUMMARY OF EFFECTS

SHELL SIZE	MEK VERSUS BENZENE	PS. CONC.	PS MW	GRAMS WATER	PVA CONC.	STIR RATE	RAMP BATH TEMP.	IPA RINSES
Diameter (MEAN) ⇑	(MEK)			⇓	⇓			
Wall Thickness ⇓		⇓			⇑		⇑	
Aspect Ratio ⇑		⇓			⇑	⇑		⇑
Uniformity ⇑	(BENZENE)		⇑		⇑			
Vacuole Density ⇓			⇓	⇑		⇑		⇓
PVA Entrapment ⇓								⇑

are no apparent differences between the two solvent systems. However, as the processing conditions are taken to extremes, the MEK solutions have the potential to make unusually large shells. An MEK solution produced a shell batch whose average diameter was 1.8 mm. (The largest shell was 6.1 mm.) The corresponding benzene solution shell batch had an average diameter of 1.2 mm. (The largest shell was 2.3 mm.)

4.3.4. CONCLUSION

We have completed a screening experiment to determine which factors control the size and quality of microencapsulated shells. A literature search indicated which parameters are typically varied for similar processes. Ranging experiments were done to find the limits for the factors that produce shells. A statistical design was chosen that maximized information while minimizing number of trials. The design was carefully executed, thus keeping the standard error low. This low standard error allowed us to find statistically significant factors for every response monitored.

This experiment was done using the Osaka technique, but the relevance to the droplet generator technique is important. The polymer/solvent/nonsolvent interactions, viscosity and surfactant effects, and the thermal processing considerations are all identical for both techniques. The actual formation of the shell precursor is the only difference. The Osaka technique depends upon the breakdown of an emulsion to form a shell; the droplet generator technique uses measured flows of the various components to set the diameter and wall. Thus, having demonstrated that the Osaka process can cure, wash, and dry shells in the multi-millimeter size range, we are confident that the droplet generator process can also. The droplet generator process holds the additional promise of producing entire shell batches of a desired diameter and wall thickness.

For additional information, please contact D. Schroen–Carey (WJSA).

4.4. DROPLET GENERATOR DEVELOPMENT

The development of the droplet generator involved two efforts. The first was the construction of an improved triple-orifice system and demonstration of polymer shell formation. The second was a parametric analysis to examine the process variables that are important to the production of polymer shells using the controlled-mass microencapsulation technique (triple-orifice).

4.4.1. TRIPLE-ORIFICE CONSTRUCTION

The goal of the triple-orifice is to produce a drop similar to that produced in the shake and toss technique but in a very controlled manner. Each of the orifices has a specific task. The innermost orifice provides the interior water for the shell which ultimately determines the final size of the shell. The annular region between the two inner orifices delivers the polystyrene solution. The outer orifice allows water to flow around the shell forming on the tip of the other two orifices. After the shell reaches a certain size for a given flow rate, it is stripped off into the PVA/water solution. The triple-orifice droplet generator tip is submerged during processing. Thus, the formation of the drop on the generator is analogous to blowing up a balloon.

The original triple-orifice system consisted of the orifice, pressure pots to deliver the fluids, and a 1 liter glass reaction vessel equipped with a stirring blade to provide agitation. Very limited control of flow rates was attainable with the pressure pot delivery system. In

addition, the first system had no heating capabilities. With this system, microencapsulation was demonstrated through the use of a vegetable dye, but no polymer shells were successfully harvested.

To improve the first controlled mass system, several refinements were implemented. First, a new droplet generator with improved flow nozzles was constructed. Second, the vessel was retrofitted with a 3-ft long glass extension tube to allow a greater volume of fluid for solvent removal. Third, the pressure pots for the two inner orifices were replaced with syringe pumps for better flow control. Fourth, a method of heating the vessel fluid was incorporated to facilitate solvent removal from the shells. In addition, various agitation methods were tested, although the optimum has not yet been found. After making these changes, polymer shells (not yet of target quality) were produced and harvested.

4.4.2. PROCESS PARAMETER ANALYSIS

The following four process parameters were tested on the triple-orifice: composition, temperature, flow rates, and forced oscillation. The most important of these was found to be composition.

Several different compositions of polymer solutions were tested. The system most often used, because of its consistent results in producing polymer shells on the order of 1 mm in diameter, was 5% polystrene dissolved in MEK and 1,2-dichloroethane. Although this system was able to produce 1 mm shells, the sphericity of these shells was not good enough to be target quality. Using benzene and 1,2-dichloroethane, shells with greater sphericity were harvested, but they were much smaller in size (~500 μm). As well as these commonly used solvents, 3-chloro-2-butanone was tested as a potential solvent because of its density. The runs with this solvent were unsuccessful because encapsulation was ineffective.

The effect of temperature was studied using the MEK and 1,2-dichloroethane solvent system. 40°C was found to be the best operating temperature between room temperature and 60°C. At 60°C, shells were seen "exploding" shortly after formation at the droplet generator. At room temperature, the shells did not cure quickly enough and were destroyed during agitation. The optimum temperature may be a function of composition, which will be studied in the future.

Flow rates were studied mostly for their effect on overall shell diameter. As expected, the higher the flow rate of the inner water phase, the larger the resulting sphere. Surprisingly, shells of about 1 mm in diameter were easier to produce than smaller shells. Larger flow rates in the polymer solution resulted in greater wall thicknesses. While operating under constant conditions and producing 1 mm shells, size variation was approximately ±10%.

To test forced oscillation as a method to produce controlled, uniformly sized shells, a double-orifice droplet generator was designed and constructed. This was first tested by simply dropping methylene chloride from the inner orifice only. Drops were produced of constant size at a constant rate. After this successful test, shell formation was attempted. This proved to be unsuccessful because the organic phase adhered to the orifice and would not encapsulate properly. This result implies that the outer orifice is necessary to maintain the position of the forming shell. Future systems may include forced oscillation, but a triple-orifice will most likely be required.

For additional information, contact Dr. D. Soane or Dr. D. Nelson (STI).

4.5. REFERENCES

[4-1] Kubo, U., et al., ILE Osaka University, ILE-APZ-79 (1979) **177**.

[4-2] Plackett, R.L. and J.P. Burman, "The Design of Optimum Multifactorial Experiments," *Biometricka* **33** (1946) 305–325.

SECTION 5

FABRICATION OF FILMS AND FILTERS

5. FABRICATION OF FILMS AND FILTERS

The major target component production activity during FY92 was fabrication of flat films and filters for Sandia National Laboratory (SNL).

5.1. SNL FABRICATION REQUESTS

Even though we were validated to fabricate free-standing gold films and free-standing aluminum films had been submitted for validation, SNL fabrication requests to GA/WJSA in FY92 were restricted to Mylar-backed gold foils. These diagnostic foils were of the four types shown in Figs. 5-1 to 5-4. Unless the deposited gold film is nearly stress-free, it can cause wrinkling of the Mylar substrate film, especially when the thickness of the gold film equals or exceeds the thickness of the Mylar film. With other deposition variables held constant, the film stress can be varied by varying the deposition pressure in the sputter deposition process which is being used at GA/WJSA to fabricate films and filters. The optimum pressure for the deposition of nearly stress-free gold films had been established at 15 mtorr in the validation process, and all of the gold films deposited in our fabrication effort were deposited at this pressure.

One hundred and three off-axis targets with Lucite frames (Fig. 5-1) were fabricated and delivered to SNL. The fabrication technique used consisted of mounting the Mylar on a large aluminum ring, characterizing the Mylar thickness using alpha particle attenuation, depositing the gold, cementing the Lucite frame to the Mylar and then cutting it away from the aluminum ring, characterizing the gold thickness using alpha particle attenuation, punching the fiducial hole in the film, and characterizing its position. The aluminum ring was used to support the Mylar during gold deposition because we found that the small stresses imposed by the gold films were sufficient to deform the Lucite frame and cause wrinkling in the film.

Forty-three of the centerline targets I (Fig. 5-2) were fabricated and delivered to SNL. These targets were fabricated by cementing the Mylar film to the titanium frame,

characterizing the Mylar thickness, depositing the gold, characterizing the gold thickness, punching the fiducial holes, and characterizing the fiducial hole positions.

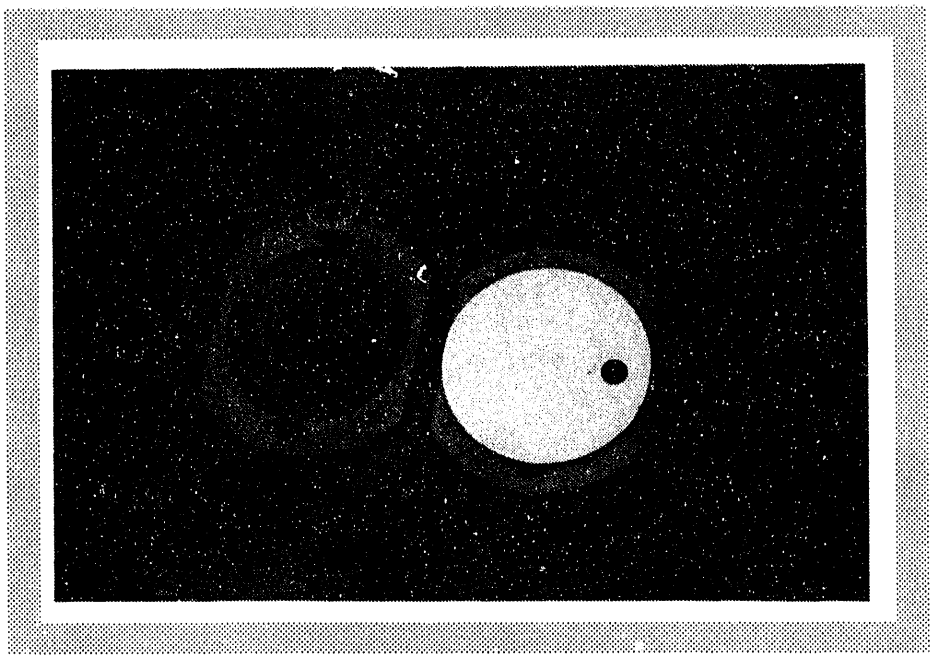

Fig. 5-1. Off-axis target with Lucite Frame.

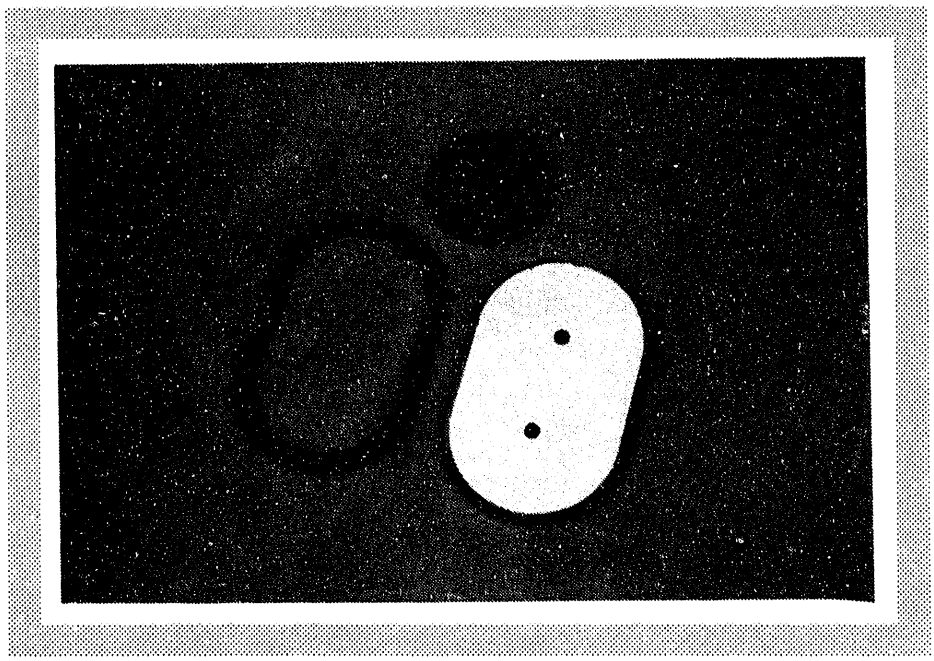

Fig. 5-2. Centerline target I.

Sixty-five of the centerline targets II (Fig. 5-3) were fabricated and delivered to SNL. In the fabrication of these targets, the Mylar was cemented to the titanium frame, the Mylar thickness was characterized, a mask to shield the rectangular fiducial regions from coating was placed on the target, the gold was deposited, the mask was removed, the gold

thickness was characterized, and the dimensions and positions of the uncoated fiducial regions were characterized.

One hundred and forty-nine ultra-compact ion pinhole camera (UCIPC) targets (Fig. 5-4) were fabricated. For these targets, Mylar was mounted on a large aluminum ring,

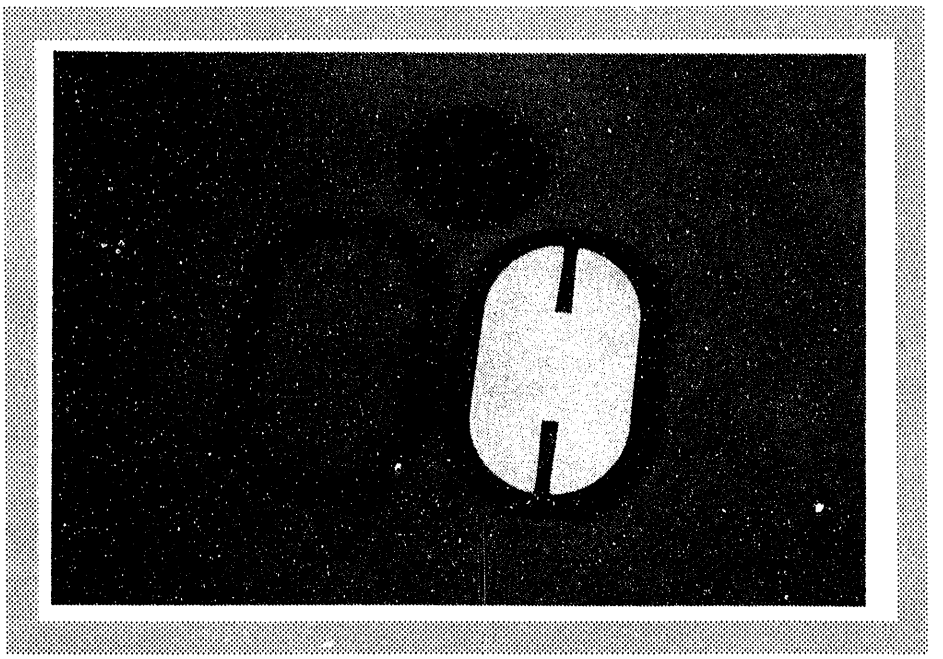

Fig. 5-3. Centerline target II.

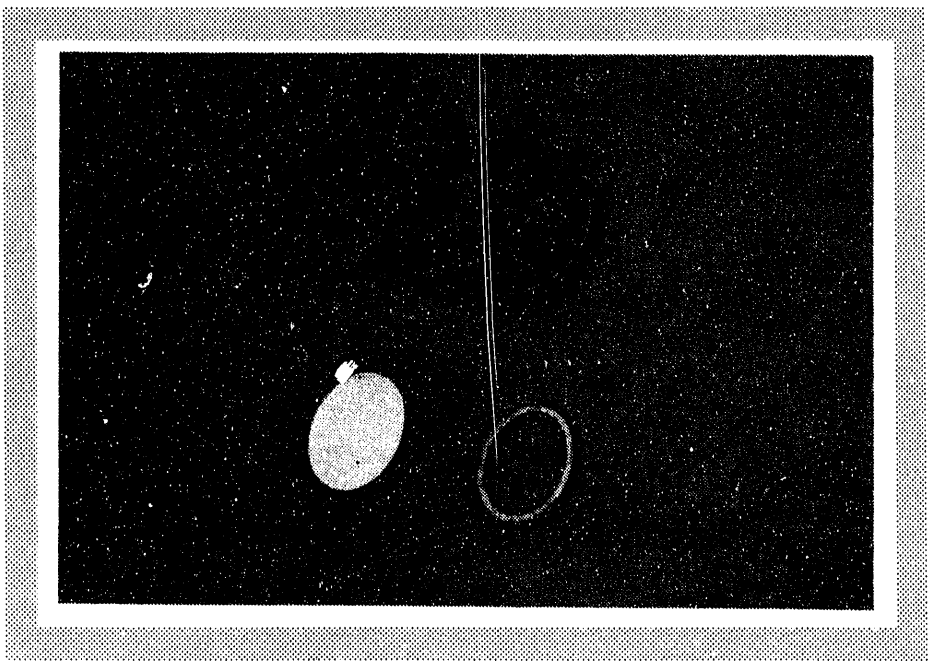

Fig. 5-4. Ultra-Compact Ion pinhole camera (UCIPC).

the Mylar thickness was characterized, gold was deposited on the Mylar, the gold thickness was characterized, as many as 15 of the UCIPC brass frames were cemented to the Mylar within the aluminum ring, and the UCIPC targets were cut free.

5.2. FABRICATION SUPPORT

Flat diagnostic foils were fabricated on location at SNL in support of the PBFA II, SABRE, and Two-Stage facilities. A total of 33 centerline foil targets were fabricated for PBFA II. These foils were fabricated to supply targets for immediate needs incorporating new specifications. A total of 75 UCIPC targets were fabricated to supply the two-stage facility. These foils were made in response to an increase need in target quantities previously unforeseen. A total of 54 foils were fabricated for the SABRE facility. The diagnostics for SABRE are still under development and require frequent changes in foil specifications. Once specifications have been set, production will be transferred to GA.

X-ray filters are also needed for an upcoming shot series on PBFA II. The experiments require a total of 697 foils to be fabricated and assembled into 366 filters. Most of these filters were purchased from vendors, but fabrication and characterization of filters were also carried out on location at SNL using SNL resources. The filters are in the process of final characterization and assembly. A few filter designs are still undergoing development to improve operation.

For additional information, contact Dr. J. Kaae (GA) or T. Alberts (WJSA).

SECTION 6

OMEGA-UPGRADE CRYOGENIC TARGET DELIVERY SYSTEM

6. OMEGA-UPGRADE CRYOGENIC TARGET DELIVERY SYSTEM

An important task in FY92 was development of the conceptual design for a cryogenic target delivery system for the OMEGA-Upgrade facility at the University of Rochester.

6.1. INTRODUCTION

The upgrade of the OMEGA laser at the University of Rochester's Laboratory for Laser Energetics (UR/LLE) will result in a need for millimeter size targets filled with D_2 or deuterium-tritium (DT) and maintained at cryogenic temperatures. This mandates a cryogenic target delivery system capable of filling, layering, characterizing and delivering cryogenic targets to the OMEGA-Upgrade target chamber. The program goal is to design, construct, and test the entire target delivery system by June 1997. When completed, the system will be shipped to Rochester for reassembly and commissioning in time for the OMEGA-Upgrade cryogenic campaign scheduled to start in 1998.

This year, we developed the conceptual design for the cryogenic target delivery system. A design requirements report [6-1] was drawn up to determine the minimum requirements that a cryogenic target delivery system must meet. Once the design requirements were defined, a number of design concepts were considered and the concepts most likely to lead to a successful design selected. The remainder of this section gives a summary of the OMEGA Upgrade cryogenic target delivery system conceptual design. Diagrams and more detailed descriptions of these systems are contained in the conceptual design report [6-2].

6.2. MODULAR APPROACH

The target delivery system can be broken into functional modules: Target Support, Cryogenic Fill Station, Transport, Layering, Characterization and Target Insertion. Each module's function will be designed to integrate with the other modules.

Suitable CH-polymer target shells will be mounted, filled with appropriate fuel gases, cryogenically cooled, and transported into a module that will create a uniform solid fuel layer.

They will then be characterized and transported into the target chamber. A cryogenic storage system will also be developed to allow for transport of filled targets and for inventory purposes.

6.2.1. PHYSICAL CONFIGURATION

To better visualize the actual movement of a target, the schematic layout of the target delivery system is depicted in Fig. 6-1 below:

1. The empty targets are placed in a target rack within the Fill Cryostat, filled and then cooled below the critical point of the fill gas (D_2 or DT).

2. The excess DT is pumped away. The permeation cell (in the Fill Cryostat) is then opened with a cryogenic wrench (not shown).

3. A Cryogenic Transport Mechanism is used to transfer the targets from the Fill Cryostat to the Storage Cryostat (still within the DT fill station glove box).

4. The Storage Cryostat is moved through the air lock of the fill station glove box and on to the room containing the Layering and Characterization Module. This room is located in the basement directly below the OMEGA-Upgrade target chamber.

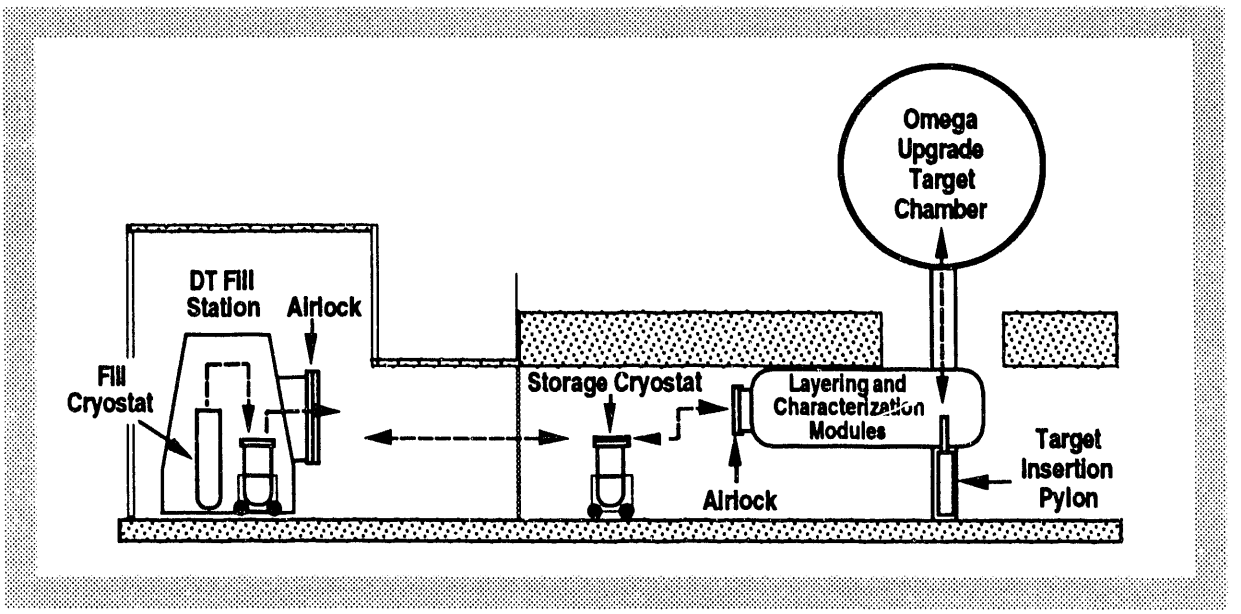

Fig. 6-1. Schematic layout of target delivery system (not to scale).

5. After the Storage Cryostat is moved through an airlock into the Layering and Characterization Module, another cryogenic transport mechanism is used to transfer a single target from the Storage Cryostat into the Layering Module.

6. After the target has been layered and characterized, it is placed at the tip of the Target Insertion Pylon.

7. The Target Insertion Pylon is elevated and positions the target at the center of the OMEGA-Upgrade target chamber.

8. Thermal radiation shrouds surrounding the target are retracted exposing the target to the laser optics. Within ~30 milliseconds after the shrouds are removed, the laser is fired.

6.3. TARGET SUPPORT

The purpose of the target support is to place the filled target at the focus of the OMEGA-Upgrade laser beams and to maintain it during the laser shot. The target will need to be rigidly held and the mounting method must not interfere with the laser beams or associated diagnostics in OMEGA-Upgrade. Additionally, the target mounting method must not cause a major perturbation on surface finish. A tripod mounting technique was chosen as the preferred design. The target support is a stiff, three-legged carbon fiber support that is glued both to the target itself and a (most likely) copper support cylinder (Fig. 6-2). The glue causes the target to be part of the support structure (loaded in compression or shear), further increasing its strength. The use of long-length, small diameter carbon fibers minimizes thermal conduction and contact area to the target and equally important, minimizes the DT dead volume required in the DT fill station permeation cell (<0.1 cc). Additionally, the tripod mount design allows for bottom positioning of the target insertion system in the OMEGA-Upgrade target chamber — a significant design advantage over suspended mounting techniques.

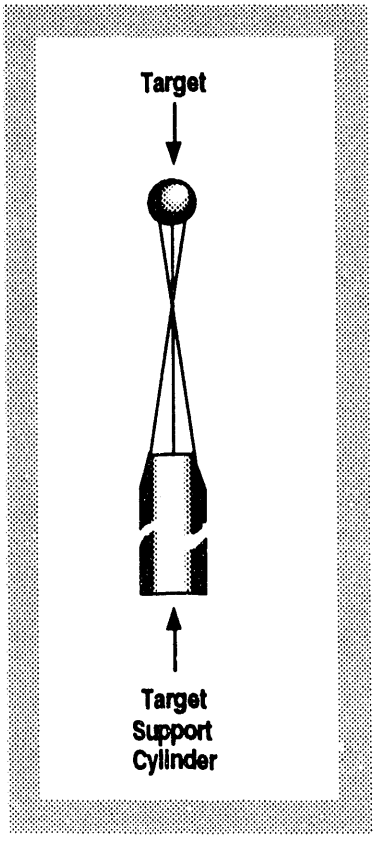

Fig. 6-2. A tripod mount allows accurate positioning and rigidity of the target.

6.4 TRITIUM FILL

The need for thick (100 μm) liquid or solid layers of D_2 or DT fuel requires that the plastic shells be filled to densities as high as 0.16 gm/cc (equivalent to 1500 atmospheres at room temperature). During fills to high pressure, polymer targets have to be filled in steps of less than 10 atmospheres to keep the targets from collapsing. High-pressure fills in polymer shells require maintaining the target(s) at cryogenic temperatures after filling to prevent the shell(s) from bursting. This, combined with the requirement that the gas permeate into the shell, implies that the system must work in a temperature range from room temperature down to as low as liquid helium temperatures. Figure 6-3 shows the high-pressure cryogenic fill station. The cryogenic concentrator, booster pump, and permeation chamber comprise the permeation loop.

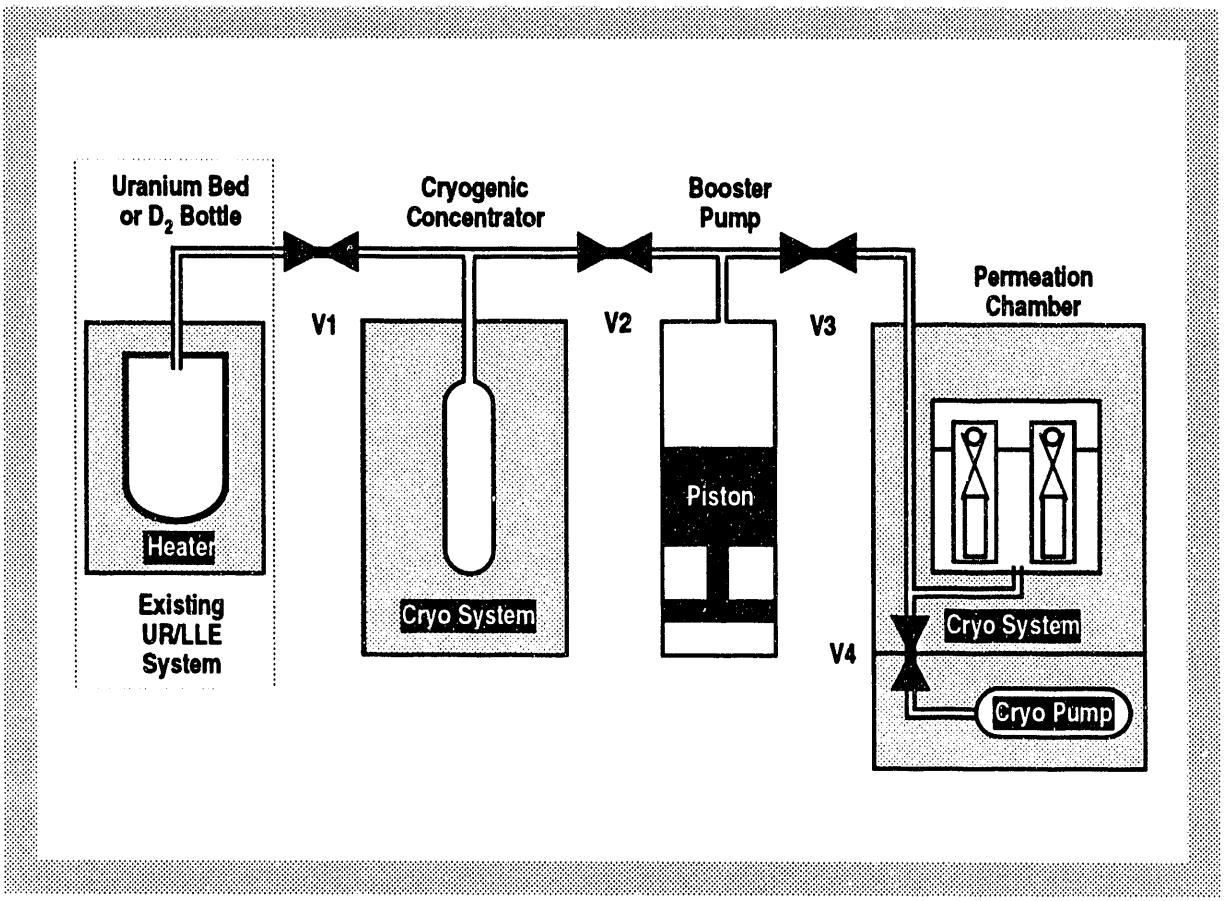

Fig. 6-3. Major components of the cryogenic fill station.

The conceptual design makes use of a permeation chamber that will allow filling of six targets mounted on their supports. While the permeation chamber is heavy walled (28 mm o.d., 10 mm i.d.), its unusable dead volume is small (5 cc including the volume in the line to Valve V3). To accommodate Rochester's site license of 1 g of tritium, cryogenic intensification followed by mechanical intensification is used to obtain DT pressures of up to 1500 atmospheres at room temperature. Closed cycle cryogenic cooling systems are used to cool both the cryogenic concentrator and the permeation chamber. Factors that affect the design of the fill station include requirements for target throughput and tritium inventory capacity. Except for radiological safety constraints, the D_2 system requirements are identical. Both D_2 and DT fill stations will be identical, except that the D_2 fill station will not be located in a triple containment environment, and the D_2 will be supplied from a high-pressure gas bottle rather than from a uranium DT bed.

6.5. TRANSPORT AND STORAGE

The physically separated locations of the DT fill station and the OMEGA-Upgrade target tank necessitates that the modules be physically distinct systems. The transport module's functions are to transfer at cryogenic temperatures a rack of targets from the fill station cryostat to the cold storage cryostat and a single target from the storage cryostat to the layering and characterization cryostat.

The transport system is implemented as a cold transport tube. The transport tube is a low-temperature cryostat that can have its bottom detached when inside another cryostat. To help insure vacuum integrity of the transport tube and to facilitate attaching it to other cryostats, the bottom section of the transport tube is slipped into a vacuum lock. Opening a gate valve at the bottom of the vacuum lock permits the transport tube to be pushed into a receiving cryostat. The targets are cooled with low-pressure helium gas. Thus, the bottom section must attach to the transport tube with cryogenically mountable/demountable seals to prevent compromising the transport tube's vacuum spaces. A mechanical pickup tool at the core of the transport tube is provided for grasping targets.

The procedure for transport of targets from the fill station cryostat to the cold storage cryostat is as follows: the permeation cell in the fill cryostat containing the targets must first be opened. This is done with a long set of coaxial extension socket wrenches. Torque and counter-torque applied to the wrenches opens the cell with no net torque transmitted to the cryostat.

Then, the transport tube is attached to the fill cryostat and pushed into its upper cryogenic chamber. The transport tube's outer walls are allowed to cool and then the bottom section is removed. The lower cryogenic chamber is opened and the transport tube pushed down into it. The target rack is grasped by the transport tube's mechanical pickup tool. The transport tube is raised into the upper cryogenic chamber and the bottom section of the transport tube is reattached, enveloping the target rack. The transport tube is withdrawn from the fill cryostat. Closing the vacuum lock and detaching it from the fill cryostat returns the transport tube to independent operation. This basic process is reversed to deposit the rack of targets into the storage cryostat. Once the storage cryostat is moved to the layering module (Fig. 6-1, Step 5), the same basic process is again used to transfer a single target to the layering cryostat.

6.6. LAYERING AND CHARACTERIZATION

The layering technique will be the cornerstone of the target delivery system. How the target is handled and characterized will be, at least to some extent, determined by the characteristics of the layered target. There are two hydrogenic fuels planned for use in OMEGA-Upgrade cryogenic targets. Most of the targets will be D_2-filled and the remainder will be DT-filled. The layering technique is required to produce uniform and smooth cryogenic fuel layers. There is no clear-cut choice for the layering technique at this time. Target specifications for fuel layer thickness and surface finish go beyond the limits of current target technology.

How well one can determine the efficacy of the layering method depends on the quality of the characterization system. For OMEGA-Upgrade targets, there are more stringent requirements on the targets and, therefore, a need to push the limits of the characterization systems and develop new techniques. The new targets will require uniformity measurements at the 1% level. With the upgraded laser, the roughness of the targets' surfaces has become an issue requiring quantitative measurements.

Typical capsules imploded by UR/LLE's OMEGA laser were on the order of 250 μm in diameter. These capsules were filled with gas at pressures up to about 200 atmospheres. This produces cryogenic fuel layers on the order of a few microns thick. The layering methods previously developed were effective for this category of target. They included:

1. **Fast Refreeze** — One of the early methods which is useful for thin layers where the times for evaporation and condensation are short compared to the

gravity-induced sag time [6-3]. This technique has been used by UR/LLE in their cryogenic campaigns [6-4]. The 100 μm thick layers required by OMEGA–Upgrade targets are too thick for this technique to work.

2. **Thermal Gradient** — Here the distribution of the fuel inside the shell is brought about by an anisotropic thermal environment [6-5]. The temperature gradient across the capsule produces a gradient in the surface tension and evaporation/condensation fluid flow. The fuel can be uniformly distributed inside the capsule by adjusting the temperature profile. This technique, employing helium gas jets to generate a time-dependent thermal gradient, was also developed at UR/LLE [6-6].

3. **Beta-Heating** — This method is a "self layering" technique [6-7] for thick, solid layers of T_2 or DT. The layer must be thick enough so that the energy from the beta-decay of tritium is deposited in the fuel layer. Regions where the fuel is thick will be warmer than areas where the fuel is thin. Fuel on the inner surface will evaporate from thick regions and deposit on thin regions. A steady state will eventually reached where there is a uniformly thick fuel layer. This method is suitable for the DT targets but not for D_2 targets.

Our layering method choice is the Thermal Gradient method with a quick freezing of the fuel to produce a solid layer. It is suitable for layering D_2 as well as DT targets. The layering process uses helium jets above and below the capsule (Fig. 6-4) to generate the thermal gradient necessary to distribute the fuel. The temperature of the helium is controlled by heaters on the jets. When the fuel layer becomes uniform, the heaters on the gas jets are turned off quickly freezing the fuel.

It is important to keep alternative layering methods in mind in case technical difficulties arise with the Thermal Gradient method. Options include:

1. **Liquid Layers** — If a thick, uniform, liquid layer can be produced with a smooth inner surface, an alternative is to keep the layer liquid. The liquid layer would be hard to maintain during transportation to the target chamber and if gas jets are used to maintain the layer, there would be a source of helium gas in the target chamber. One advantage of this method is that the liquid layer should not have the high order ℓ-modes of a solid layer.

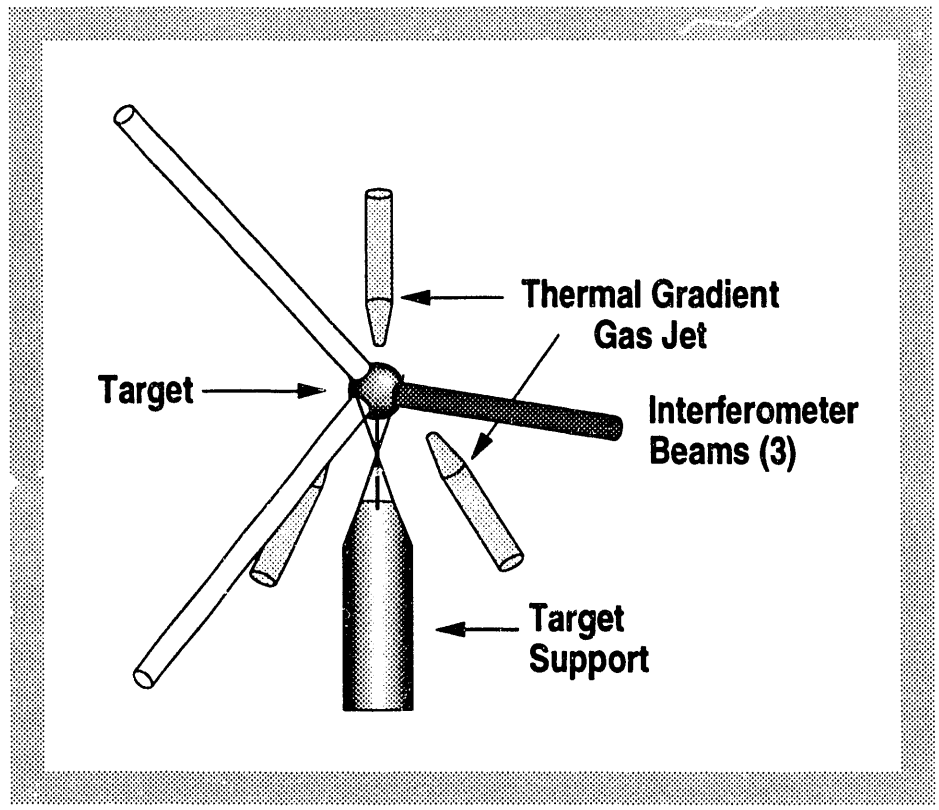

Fig. 6-4. Due to its suitability for layering D_2 as well as DT targets, the thermal gradient method was selected as the layering method.

2. **Pseudo Beta-Heating** — A variation of the beta-heating process has been conjectured, but calculations have yet to be done. This "pseudo beta-heating" process would involve placing beta-decay sources around the target so that beta-particles travel into the fuel and are absorbed. The nontritiated fuel would then redistribute in the same fashion as DT or T_2.

3. **RF Discharge** — This technique, developed at Osaka [6-8], could be used for layering D_2 as well as DT fuels. Here, an rf plasma is used to redistribute the fuel through an evaporation/condensation process. The Japanese have done a proof-of-principle experiment using Krypton as the fuel with liquid nitrogen cooling. However, the desired fuel layer uniformity has not as yet been achieved.

4. **Magnetic Field-Assisted Microgravity** — Magnetic methods are used to induce a magnetic dipole force in the liquid fuel layer that opposes gravity and allows the generation of a uniform liquid layer [6-9].

5. **Foams** — If the fuel cannot support itself in a 100 μm thick layer, then an alternative is to provide a structure for that support. Here, the porous inner wall of a hollow foam capsule would contain (support) the fuel. By overfilling, one avoids problems with the rough inner foam surface. The Japanese have been working on foams most recently [6-10].

Significant effort has been put into characterizing cryogenic targets. Techniques include: direct imaging, classical and holographic interferometry, and different types of methods within each category. Each technique has its own positive and negative attributes, but all require transparent capsules. The characterization choice for OMEGA-Upgrade was based primarily on what UR/LLE has found to be good for them and for which they have experience and confidence. Our characterization choice is the modified Mach-Zehnder interferometer system developed at UR/LLE [6-11]. We will work closely with UR/LLE to set up a system with three orthogonal views (Fig. 6-4). The interferometer will need to be modified to characterize the larger OMEGA-Upgrade capsules.

There has not been as much effort directed towards characterizing opaque capsules. Although not stated as a specific design requirement, the OMEGA-Upgrade targets may be opaque due to a coating of aluminum. This precludes doing on-line characterization with visible light. We are not aware of a characterization technique for opaque capsules with the required resolution. Our plan is to devise a procedure to repeatably layer transparent capsules. If the aluminum layer is not so thick that it affects the thermal gradients, then we will layer and characterize a large number of transparent shells to statistically determine what must be done for "blind" layering of opaque shells.

The Layering and Characterization Module will require a significant amount of work. We do not have a definitive layering method that is assured to produce a uniform thick layer nor to generate a 1000Å surface finish to this specification. There is no characterization method currently in use which can measure the surface finish to this specification. For the DT targets, beta-decay is always going on and should take out any low-order ℓ–mode nonuniformities if the solid layer is maintained near the melting point. However, how smooth the inner surface will be is unresolved. Beta-heating is not an option for the D_2 targets.

6.7. INSERTION

The insertion module's function is to transfer a layered target from the layering cryostat to the center of the OMEGA-Upgrade target chamber in preparation for the laser implosion of the target.

The insertion system cryostat forms an extension of the layering and characterization cryostat. The layering cryostat is located in the basement underneath the OMEGA-Upgrade target tank (Fig. 6-1). After a target is layered, a robot arm in the layering cryostat will transfer the mounted target to the tip of the positioning pylon. The pylon is driven by a series of motors up the cryogenic tower until the target is approximately at tank center. The final drive motor can be geared down for fine vertical positioning. It is also embedded into a two-axis tilt positioner to allow for fine horizontal positioning. Alignment is done optically through gold coated windows of the cryogenic shrouds.

A cryogenic tower extends upward from the layering cryostat until it reaches the tank center. At the tank center, the tower is capped off by two concentric cryogenic shrouds. The outside cryogenic shroud has sufficient size and strength to form a gas tight seal to the tower. This shroud is connected to a fixture at the top of the tank that can retract the shroud slowly (~2 sec) upwards. The inner shroud can be low mass, allowing a linear induction motor in the tower to retract it downwards at high acceleration. Retraction time is tens of milliseconds. This shroud has an open-cylinder configuration. To prevent the target from warming up after the outer shroud has been withdrawn, the outer shroud is retracted only enough to prevent interfering with OMEGA-Upgrade laser beams. The open end of the inner shroud sees direct thermal radiation emanating only from the low-temperature cryogenic shroud. Fins on the inside of the ends of both shrouds minimize the reflected 300K radiation reaching the target. Both shrouds contain gold coated windows to allow positioning of the target-to-tank center.

The dual shroud system minimizes vibration of the target at the time it is shot. The slow retraction of the outer shroud minimizes and allows any shock and vibration associated with breaking the cryogenic seal to the tower to dissipate before the shot. With no complicated opening mechanisms, the inner shroud can be made low mass. The linear motor that retracts the inner shroud is mounted on bellows and these are mounted on a buttress to the building foundation. The acceleration profile of the linear motor can be adjusted to minimize shock to its mount. The target is mounted on a pylon that is independently connected to the floor. Finally, the target can be shot before deceleration of the inner shroud.

Once the target is positioned, the outer shroud retracts. The helium exchange gas cooling the target is diluted by the tank volume to less than 10^{-4} torr and pumped out by the tank vacuum system. Two seconds after the outer shroud is retracted, the inner shroud is retracted and the target shot. Optical interlocks in the target alignment system can warn if the target is out of position prior to the shot so that laser firing can be aborted.

For additional information, contact Dr. R. L. Fagaly (GA) or Dr. D. Bittner (WJSA).

6.8. REFERENCES

[6-1] Fagaly, R.L. and D.N. Bittner, "Design Requirements Report: University of Rochester Cryogenic Target Delivery System," General Atomics Report GA-C20937 (1992).

[6-2] Fagaly, R.L., N.B. Alexander, D.N. Bittner, R.F. Bourque, C. Dahms, C. Hendricks, J. Lindgren, and W.J. Miller, "Conceptual Design Report for the University of Rochester Cryogenic Target Delivery System," General Atomics Report GA-C21093 (1992).

[6-3] Musinski, D.L., et. al., *J. Appl. Phys.* **51** (1980) 1394.

[6-4] Marshall, F.J., et. al., *Phys. Rev. A* **40**, 2547 (1989).

[6-5] Kim, K., and D.L. Krahn, *J. Appl. Phys.* **61** (1987) 2729.

[6-6] Gram, R.Q., et. al., *J. Vac. Sci. Technol. A* **8** (1990) 3319.

[6-7] Hoffer, J. K., and L.R. Foreman, *Phys. Rev. Lett.* **60** (1988) 1310.

[6-8] Chen, C., et. al., "Uniformity of Solid Fuel for ICF Target Can Be Easily Increased by a Microwave Plasma Heating Method," presented at the American Vacuum Society, 39th National Symposium, Chicago, Illinois, November 9-13, 1992..

[6-9] Parks, P.B., and R.L. Fagaly, "Field-Assisted Microgravity for Target Fuel Layering," to be submitted to *J. Appl. Phys.*

[6-10] Norimatsu, T., et. al., *Rev. Sci, Instrum.* **63** (1992) 3378.

[6-11] Kong, H., M.D. Wittman, and H. Kim, *Appl. Phys. Lett.* **55** (1989) 2274.

SECTION 7

POLYMER SYNTHESIS

7. POLYMER SYNTHESIS

This task sought to produce 50 g of each of five polymers, ranked by priority below for the University of Rochester's Laboratory for Laser Energetics (UR/LLE):

- Poly (4-trimethylsilylstyrene)
- Poly (perdeutero-4-trimethylsilylstyrene)
- Poly (4-chlorostyrene)
- The copolymer of styrene and 4-trimethylsilylstyrene
- The copolymer of perdeuterostyrene and perdeutero-4-trimethylsilylstyrene

Each polymer was to have a molecular weight between 100K and 200K, as measured by gel permeation chromatography (GPC) relative to a polystyrene (PS) standard. Because 4-chlorostyrene is readily available commercially, the polychlorostyrene was synthesized first, followed by the trimethylsilylstyrene. The synthesis of the polymers from the monomer could be done by either free radical reagents (benzoyl peroxide) or by cationic means (triphenylcarbonium–$BF4^-$). The initial polymerization of chlorostyrene was done by free radical, in a benzene solution. The appropriate amount of peroxide to obtain a MW = 150K was calculated, based on the kinetics of reaction and the occurrence of chain transfer and termination reactions. Some 15% yield of polymer product (8 g sent to LLE) was obtained at 80°C (refluxing benzene), with a MW = 206K, and a polydispersity of 2.47. A later polymerization reaction using the cationic reagent in dichloromethane resulted in some 80 grams of polymer, but a MW = 26K and a polydispersity of 1.86. We suspect that the solvent acted as a chain transfer agent, shortening the chains. Thus, the first delivery of polychlorostyrene was nominally within the task specifications, but the second batch was far from the specifications.

The synthesis of the trimethylsilylstyrene monomer was done via literature syntheses, starting from 4-chlorostyrene, by making the Grignard reagent and then adding trimethylsilylchloride. The product trimethylsilystyrene is then distilled under vacuum to obtain

pure monomer. The synthesis of this monomer did not proceed smoothly. The Grignard reaction produces a by-product divinyl material. The monomer must be removed from this byproduct before polymerization and the removal is done during the distillation. However, the thermal distillation, even at vacuum around 57°C, risks a thermal polymerization of the material, and the by-product enhances the crosslinking. Twice, the material in the distillation pot polymerized before much if any product could be obtained. In the latter polymerization, we surmised that the distillation should not occur from $CaCl_2$. Apparently, the $CaCl_2$ catalyzes the polymerization in the distillation pot. In a latter run, we decanted the trimethylsilylstyrene from the $CaCl_2$, and had no difficulty with the vacuum distillation. We obtained some 67% overall yield of monomer.

The polymerization of the monomer by benzoyl peroxide in benzene proceeded smoothly, but in low yield. The product had a MW = 239K, with a polydispersity of 2.44. Some 16 g of material were delivered to LLE. A cationic polymerization done in a manner analogous to the chlorostyrene reaction above was performed, and some 10 grams of material (20% yield) was obtained.

All batches of material sent to LLE were first tested at GA, to see whether spheres could be made by the microencapsulation process. If the polymers contained gel, they would be difficult to filter, and few spheres would be made. We had no difficulty producing spheres nor any difficulty filtering the solution.

We did not produce the deuterated materials during FY92 due to several constraints to these syntheses. First, the starting monomer perdeutero-4-chlorostyrene was not commercially available in North America. Custom syntheses involved long lead times, best effort basis, and high cost. The only material commercially available, at reasonable cost, was perdeuterostyrene. We obtained this material and are proceeding with the synthesis. The preferred synthesis involves saturating the double bond to make 2-phenylethanol, brominating the ring, dehydrating to reform the double bond and recover 4-bromostyrene, and then proceed with the Grignard reaction as in the reaction described above. One alternate route, brominating poly (deuterostyrene) and performing the Grignard, was eliminated due to the by-product reaction, which would crosslink the polymer. Other alternate routes to build perdeutero-4-bromostyrene from a variety of deuterated materials were eliminated due to the high cost and/or the lack of commercial availability of the materials.

For additional information, please contact Dr. B. McQuillan (GA)

SECTION 8

MICROMACHINING TRANSITION PLANNING

8. MICROMACHINING TRANSITION PLANNING

A task added late in the year was to prepare a plan for developing micromachining capability.

8.1. INTRODUCTION

Rocky Flats has been doing micromachining of ICF targets for the ICF program for 15 years, under contract from Lawrence Livermore National Laboratory (LLNL) and, to a lesser extent Los Alamos National Laboratory (LANL). A stand-alone ICF micromachining organization at Rocky Flats has evolved to do this work that is supported solely by this ICF activity. The ICF program has grown to rely upon this group to provide ICF target components. The U.S. Department of Energy (DOE) has decided to shut down weapons production activities at Rocky Flats and begin environmental cleanup. This will impact the availability of micromachining support for the ICF program.

GA was tasked to assess this situation and to recommend a plan to ensure that ICF target micromachining support capability is maintained. An initial assessment of the situation at Rocky Flats and its ability to continue to support the ICF production requirements for micromachined target components was made following a fact-finding meeting at Rocky Flats. Attending this meeting were representatives of LLNL, LANL, EG&G/Rocky Flats, GA, and W.J. Schafer Associates (WJSA).

With the cooperation of all participating organizations, information was gathered on the following: Rocky Flats' plans and schedules, the availability of Government-owned micromachining equipment from Rocky Flats and elsewhere, the estimated ICF program requirements for micromachined target components for FY93 and FY94, the equipment required to produce these components, the possibility of stockpiling, the availability of backup support for interim micromachining at LANL, and the facility and security requirements. Possible alternate locations for ICF target micromachining were addressed, along with the requirement for trained personnel, the financial

requirements, and relevant DOE policies/decisions regarding the decontamination and decommissioning (D&D) of the Rocky Flats Plant.

8.2. TRANSITION PLAN SUMMARY

A plan was formulated to effect the transition of the precision micromachining capability now operated by EG&G at Rocky Flats, Colorado, to the GA/WJSA team. Seven options were evaluated:

A. Keep production at Rocky Flats, operated by EG&G.

B. Keep production at Rocky Flats, operated by GA/WJSA.

C. Keep production at Rocky Flats in a new building.

D. Move to another DOE facility (LANL or LLNL).

E. Move to a rented building off the Rocky Flats site, operated by GA/WJSA.

F. Stage the transition to GA/WJSA in California over a one-year period.

G. Transition to GA/WJSA in California immediately.

This list was narrowed down to the three options most attractive from the standpoint of minimizing cost and risk: options B, F, and G, which were evaluated in more detail.

Option B, keeping production at Rocky Flats under GA/WJSA operation for at least the next two to three years, has the advantages of assuring uninterrupted production using some of the same staff and meeting the economic development desires of DOE. However, this option has the greatest number of uncertainties in cost and other factors that will be out of GA/WJSA's control, such as the costs of security and radiological services, rent and utilities, and interface with the local unions. Also, it simply delays the disruption of a move and requires GA/WJSA to operate in another location distant from our California infrastructure.

Option F, staging the transition to GA/WJSA in California within a one-year period to minimize the risks to the production schedule, appears attractive in that production support at Rocky Flats will be continued and ramped down over a transition period while the

capability at GA/WJSA will be ramped up. This is allowed by the fact that there are three high-precision lathes that could be moved in stages, and that many (but not all) precision parts would be stockpiled. While this option maximizes management control and minimizes risk to the Laboratories of loss of production, it has a negative impact on current operation at Rocky Flats.

Option G, transitioning the entire facility to GA/WJSA in California immediately, requires LANL to provide immediate production services during a transitional downtime and may not result in as smooth a transition. It also has the most abrupt negative impact to Rocky Flats personnel.

In all cases, B. Ramer and C. Durbin, who have retired from Rocky Flats, will be retained as consultants to ease the transition. Jobs will be offered (including moving costs, if necessary) to the present Rocky Flats engineers and toolmakers.

The GA/WJSA team recommended a hybrid of Option F and Option G, moving the micromachining capability to California during FY93 in a phased approach as quickly as possible, limited by the practical and programmatic constraints. Rocky Flats and LANL production support will be requested as needed during the transition. This is the least-risk approach and is consistent with the realities of almost certain delays in withdrawing from Rocky Flats due to scheduling of radiological surveys, trade union support for moving the equipment, and the DOE actions necessary to effect the transition. A straw-man transition plan was provided for carrying out this recommended approach, along with a first-order estimate of the costs.

The transition plan was compressed to a six-month time period (see Fig. 8-1). The two-staged plan involves moving the hohlraum production capability during the first few months and moving the equipment used for producing the witness plates and physics packages during the last few months. Production capability that cannot be met by Rocky Flats during this transition will be made up by LANL. It is believed that this two-staged approach will minimize the risks to production rate and quality, provide a smoother transition for all parties, and result in a fully-functional micromachining capability by the end of the six-month transition period. Following the completion of the transition, the ICF program will have this capability entirely within the GA/WJSA team and there will

be no continuing separate costs to LLNL or LANL for micromachined parts.

For additional information, please contact Dr. K. Shillito (WJSA).

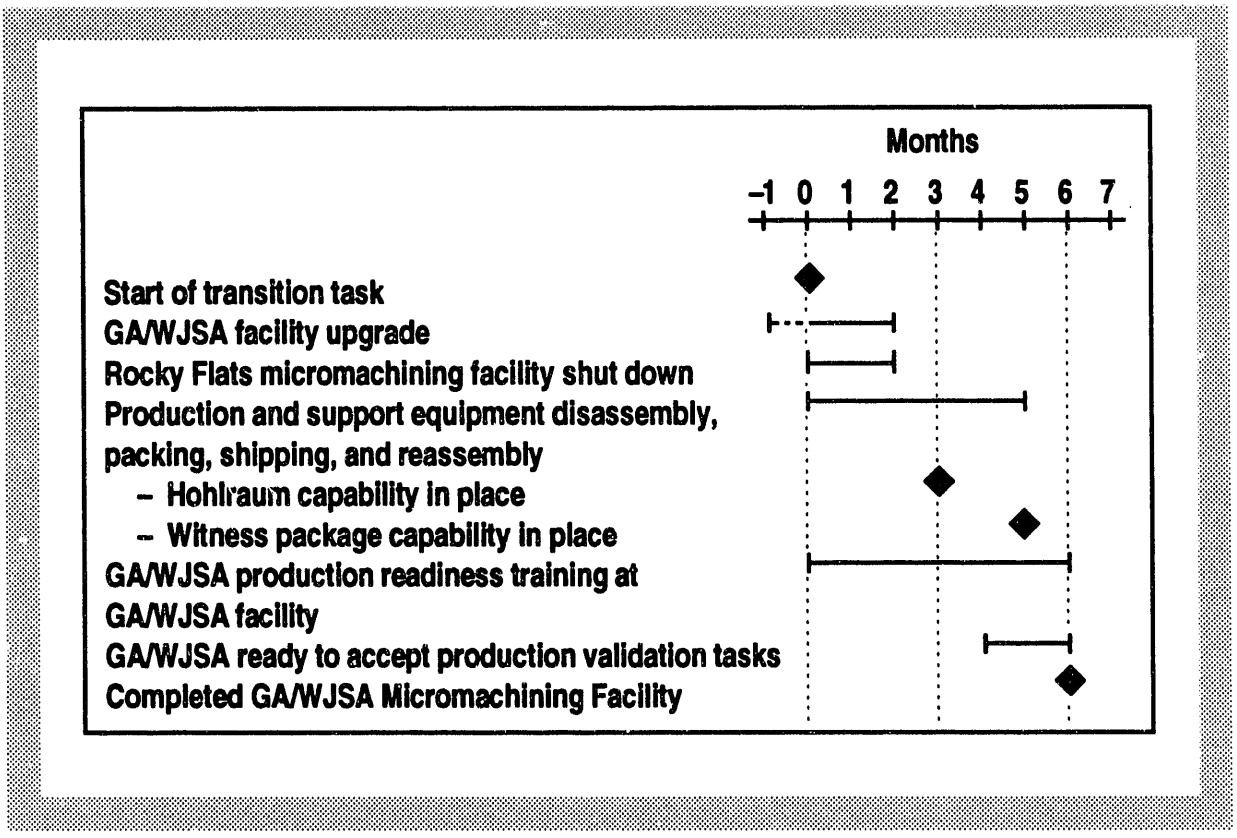

Fig. 8-1. Micromachining Transition Plan Schedule.

SECTION 9

FY92 PUBLICATIONS

9. FY92 PUBLICATIONS

Alexander, N.B., et. al., "The Cryogenic Target Delivery System for OMEGA-Upgrade," Poster session presented at the American Vacuum Society, 39th National Symposium, Chicago, Illinois, November 9–13, 1992.

Fagaly, R.L., and D.N. Bittner, "Design Requirements Report: University of Rochester Cryogenic Target Delivery System," General Atomics Report GA-C20937 (1992).

Fagaly, R.L., N B. Alexander, D.N. Bittner, R.F. Bourque, C. Dahms, C. Hendricks, J. Lindgren, and W.J. Miller, "Conceptual Design Report for the University of Rochester Cryogenic Target Delivery System," General Atomics Report GA-C21093 (1992)

Holland, L., et. al., "Environmental Assessment for the Target Component Fabrication and Technology Development Support of the Inertial Confinement Fusion Program," Report to U.S. Department of Energy, San Francisco Operations Office (1992).

Parks, P.B., and R.L. Fagaly, "Field-Assisted Microgravity for ICF Target Fuel Layering," presented at the American Vacuum Society, 39th National Symposium, Chicago, Illinois, November 9-13, 1992.

END

DATE FILMED

5/25/93